NOTE TO USERS

The original document received by UMI contains pages with slanted print. Pages were microfilmed as received.

This reproduction is the best copy available

UMI

THE UNIVERSITY OF CALGARY

Synthesis, Characterization and Catalytic Testing of Layered Double Hydroxide

Materials Pillared by Heteropoly Oxometalate Anions

by

Mark Robert Weir

A DISSERTATION SUBMITTED TO THE FACULTY OF

GRADUATE STUDIES IN PARTIAL FULFILLMENT

OF THE REQUIREMENTS FOR THE DEGREE OF

DOCTOR OF PHILOSOPHY

DEPARTMENT OF CHEMISTRY

CALGARY, ALBERTA

SEPTEMBER, 1998

0-612-34709-5

Canada

Abstract

Layered double hydroxide (LDH) materials pillared with polyoxometalate (POM) anions were synthesized *via* two routes: the organic anion precursor method and the LDH-OH/LDH-adipate precursor method. Well ordered $[M^{2+}_R M^{3+}(OH)_2][POM] \cdot z H_2O$ (M^{2+} = Mg^{2+} or Zn^{2+}, M^{3+} = Ga^{3+} or Al^{3+}, R = 2, 3, 4 and POM = $H_2W_{12}O_{40}^{6-}$ or $PW_{11}O_{39}^{7-}$) pillared LDH phases were obtained, however significant differences in the chemical composition and microtextural properties of the products were noted. Most notably, pillaring resulted in the creation of accessible internal surface area only for the products synthesized by the LDH-OH/LDH-adipate method. In contrast, the organic anion precursor method produced layered but non-porous products in which the gallery region was completely filled by anions.

Ion exchange of the LDH-adipate precursor produced a series of $Mg_R Al$-$H_2W_{12}O_{40}^{6-}$ materials with final R-values of 1.75, 2.31 and 3.51. The pillared products all had BET-N_2 surface areas in excess of 110 m^2g^{-1} and micropore volumes greater than 0.026 mLg^{-1}. The micropore size distribution plots obtained from argon adsorption isotherms indicate that the micropores become smaller as the surface charge density of the LDH increases; variation of pore size with layer composition has not previously been reported. In addition, the method was also successfully applied for the first time to other layer types, resulting in microporous $Mg_R Ga$-POM and $Zn_R Al$-POM materials with properties similar to their $Mg_R Al$-POM analogues.

The catalytic activity of pillared and unpillared LDH materials prepared *via* the LDH-OH/LDH-adipate method was tested using the decomposition of 2-propanol as a probe reaction. Differences were noted for materials of different chemical composition or for identical samples that had been subjected to different activation conditions. Only acid sites associated with the POM pillars were present after activation at 200°C, resulting in 100% selectivity for dehydration to propene. After activation at 550°C, however, the layers containing Zn^{2+}, and to a lesser degree those containing Ga^{3+}, also became active for dehydrogenation to acetone. Clearly, the strength and number of acid sites may be varied by changing the layer or pillar composition, or by using different activation conditions, suggesting that the LDH-OH/LDH-adipate precursor route offers a great deal of flexibility for synthesizing catalysts with modifiable activity.

Acknowledgments

I wish to acknowledge the following individuals and groups for the contributions that they have made to my research:

- My supervisor, Dr. R. A. Kydd, for his insight and thoughtful discussions.

- Dr. K. B. Brandt, Dr. T. Olorunyolemi and Dr. S. Song.

- Alberta Sulphur Research, for the loan of gas chromatographic supplies.

- Petroleum Recovery Institute, especially Neil DeBree, for the use of an x-ray diffractometer.

- Dr. R Yamdagni, Dorothy Fox and Qiao Wu .

- Dr. A. S. Hinman for his help with the ICP analysis of my samples.

- My parents, Brenda and Bruce Weir.

- Most of all I thank my wife, Jennifer McCann, for the support and encouragement that she has given me throughout my programs of study, both at the graduate and undergraduate level.

I would also like to acknowledge the following agencies for financial support:

- Natural Sciences and Engineering Research Council (NSERC), Killam Trusts, Faculty of Graduate Studies, University Research Services and The Department of Chemistry.

For Jen

and

In loving memory of my father

D. Bruce Weir 1941-1996

Table of Contents

List of Tables

List of Figures

Symbols and Abbreviations

4M2POL	4-methyl-2-pentanol
$\overset{\circ}{A}$	Angstrom (10^{-10}m)
A	absorbance
A^{n-}	unspecified interlayer anion species (e.g. CO_3^{2-}, NO_3^-, $H_2W_{12}O_{40}^{6-}$ etc.)
a,b,c	crystallographic unit cell lengths
adipate	adipate anion ($^-OOC-(CH_2)_4-COO^-$) (i.e. hexanedioate)
β_c	instrument corrected width of the d_{003} x-ray diffraction peak at half-height, expressed in radians
BA	benzoate anion ($C_6H_5-COO^-$) (i.e. benzenecarboxylate)
BET	Brunauer, Emmett and Teller adsorption isotherm equation
c'	1/3 the crystallographic c parameter, $c' = d_{003}$
cm^{-1}	wavenumbers
d_{hkl}	distance between crystallographic hkl planes
d_{00l}	distance between crystallographic 00l planes
D	mean crystallite size ($\overset{\circ}{A}$) along a line normal to the reflecting plane
DTA	differential thermogravimetric analysis
EA	elemental analysis (C, H, N)
E_a	Energy of activation ($kJmol^{-1}$) determined from Arrhenius plot
EXAFS	extended x-ray absorption fine structure spectroscopy

FID	flame ionization detector
FWHM	full width at half maximum
GC	gas chromatography
H_2W_{12}	intact Keggin ion species ($H_2W_{12}O_{40}^{6-}$)
ICP-AES	inductively coupled plasma atomic emission spectroscopy
IR	Infrared (spectroscopy)
λ	wavelength of radiation
LDH	layered double hydroxide
M^{2+}	divalent metal cation (e.g. Mg^{2+}, Zn^{2+} etc.)
M^{3+}	trivalent metal cation (e.g. Al^{3+}, Ga^{3+} etc.)
(m)	medium intensity band in IR spectrum
nm	nanometer (10^{-9} m)
p-HyBA	para-hydroxybenzoate anion ($HO-C_6H_4-COO^-$)
PLS	pillared layered structure
POM	polyoxometalate anion
POXRD	preferred orientation x-ray diffraction
PSD	pore size distribution
PW_{11}	lacunary Keggin ion species ($PW_{11}O_{39}^{7-}$)
r_a	rate of formation of acetone (mmol h^{-1} m^{-2})
r_p	rate of formation of propene (mmol h^{-1} m^{-2})
R	ratio of $M^{2+}:M^{3+}$ in the LDH layers

(s)	strong intensity band in IR spectrum
SA	surface area
(sh)	IR band appearing as the shoulder of a more intense band
TA	terephthalate anion ($^-$OOC-C_6H_4-COO$^-$) (i.e. 1,4-benzenedicarboxylate)
TMCHOL	3,3,5-trimethylcyclohexanol
Torr	units of pressure (mm Hg)
(vs)	very strong intensity band in IR spectrum
x	mole fraction of M^{3+} in LDH layers ($M^{3+}/(M^{2+}+M^{3+})$)
XRD	x-ray diffraction

Chapter 1

Introduction

The term "pillared layered structure (PLS)" is a generic term that is used to describe any inorganic compound consisting of electrically charged 2-dimensional host layers intercalated by bulky ionic species of opposite charge. Host materials capable of permanent expansion include aluminosilicate clays (e.g. smectites[1,2,3] and vermiculites[1,4]), lamellar oxyhalides (e.g. FeOCl)[1], layered metal phosphates (e.g. α-zirconium phosphate)[5,6] and layered silicates (e.g. kanemite and kenyaite)[4,5]. It is important to note that each preceding class of PLS is composed of negatively charged inorganic layers, propped apart by positively charged interlayer cations. Layered double hydroxides (LDHs) intercalated by polyoxometalate (POM) anions constitute yet another important class of pillared layered structures[7,8,9]. LDHs are unique among PLS materials because the distribution of charge is reversed compared to the other classes, i.e. the LDH layers carry a net positive charge that is balanced by interlayer anions.

The development of novel PLS phases has historically been driven by the petroleum industry and the search for new catalysts with larger pore sizes, which are

capable of processing heavier crude oil feedstocks than the zeolite based catalysts that are currently in widespread use. It is therefore somewhat ironic that the anticipated commercialization of PLS based processes will likely occur in the fine chemicals[10] and environmental catalysis industries[1]. The "soft" (low temperature; mild regeneration) catalysis conditions that are typically employed in the manufacture of fine chemicals or in environmental conditioning processes are more compatible with the relatively low thermal and hydrothermal stabilities that are exhibited by many PLS materials.

1.1 Layered Double Hydroxides (LDHs)

1.1.1 The LDH structure

Layered double hydroxides are a class of naturally occurring and synthetic ionic lamellar solids. The general LDH formula is $[M^{2+}_{1-x}M^{3+}_x(OH)_2][A^{n-}_{x/n}] \cdot z\,H_2O$, where M^{2+} is a divalent metal cation such as Mg^{2+}, Zn^{2+}, etc., M^{3+} is a trivalent metal cation such as Al^{3+}, Ga^{3+}, etc., A^{n-} is a simple or complex organic or inorganic anion and x is the ratio $M^{3+}/(M^{2+}+M^{3+})$. The most commonly occurring natural LDH is hydrotalcite, $Mg_6Al_2(OH)_{16}CO_3 \cdot 4\,H_2O$, which occurs in foliated and contorted plates and/or fibrous masses[11]. In order to visualize the hydrotalcite structure, it is convenient to start with that of brucite, $Mg(OH)_2$, shown in polyhedral representation in Fig. 1.1. In brucite, edge-sharing Mg^{2+} octahedra (in which the Mg^{2+} is six-fold coordinated to OH^-) form infinite, two-dimensional layers. Individual layers, which are electrically neutral, are stacked one on top of another and are held together by hydrogen bonding between the layers.
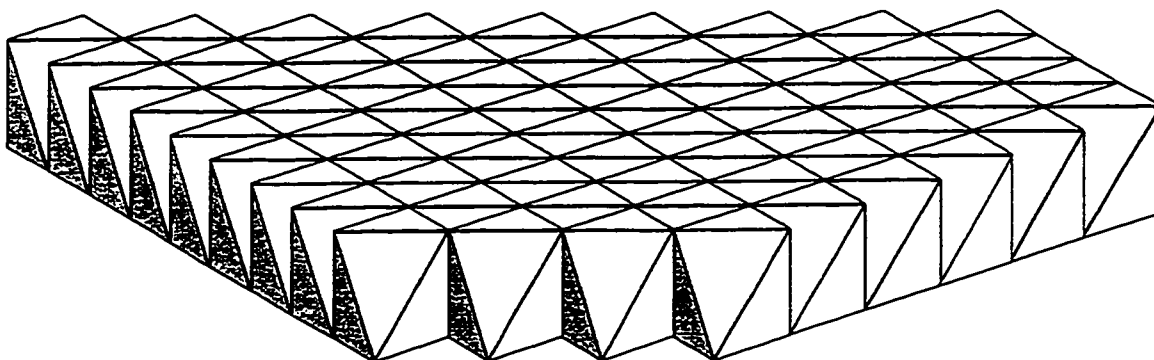
Fig 1.1: Schematic representation of one layer of the $Mg(OH)_2$ (brucite) lattice
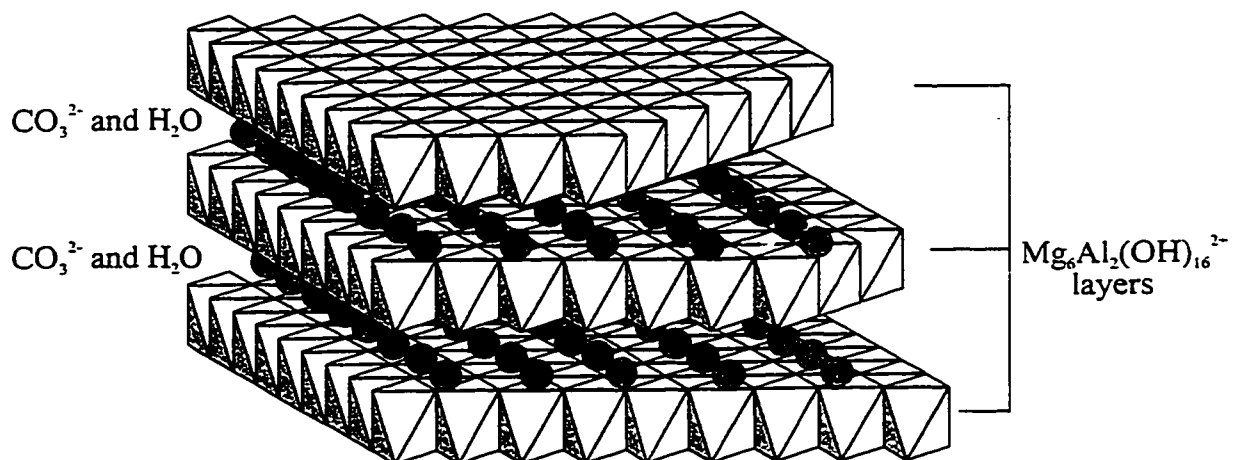
Fig 1.2: Schematic representation of the $Mg_6Al_2(OH)_{16}CO_3$ (hydrotalcite) structure

The hydrotalcite structure (Fig. 1.2) is formed by the isomorphous substitution of some of the Mg^{2+} cations by Al^{3+}. Each Al^{3+} octahedron contributes one unit of positive charge to the layers. Electrostatic repulsion between Al^{3+} ions results in "self avoidance" and an approximately homogeneous surface charge distribution according to the cation avoidance rule[12]. The net positive charge is balanced by hydrated interlayer anions that also serve to prop the layers apart and impose regular layer spacing. Lateral spacing between the anions is determined by both the density of positive charges introduced by the M^{3+} octahedra in the layers, and by the magnitude of the negative charge carried by the anion itself. Thus high surface charge density on the LDH layers and low anion charge favor a close packing arrangement, whereas low surface charge density and high anion charge encourage greater anion separation. In practice, the spaces between the anions are often completely filled with water molecules, which act as bridging species in the hydrogen bonding between the layers and the anions.

Individual LDH layers can stack one on the other with two different symmetries, rhombohedral or hexagonal[11,13]. Minerals such as hydrotalcite crystallize in rhombohedral 3R symmetry (space group R3m), with three LDH layers in the unit cell and a crystallographic c parameter equal to three times the basal spacing. Other minerals, including those of the sjögrenite group, crystallize with hexagonal 2H symmetry (space group $P6_3mmc$), and have two LDH layers per unit cell[11,14]. Some natural minerals of the pyroaurite-sjögrenite group have been listed in Table 1.1, along with the approximate compositions and unit cell parameters. Most naturally occurring LDHs are of

rhombohedral symmetry[15]; the hexagonal polytype may be the high temperature form of the rhombohedral one.

Table 1.1: Natural minerals of the pyroaurite-sjögrenite group[11]

Approximate Composition	Name	
	3R-polytype	2H-polytupe
$Mg_3Fe(OH)_8(CO_3)_{0.5}(H_2O)_2$	pyroaurite	sjögrenite
$Mg_3Al(OH)_8(CO_3)_{0.5}(H_2O)_2$	hydrotalcite	manasseïte
$Mg_3Cr(OH)_8(CO_3)_{0.5}(H_2O)_2$	stichtite	barbertonite
$Ni_3Fe(OH)_8(CO_3)_{0.5}(H_2O)_2$	reevesite	--
$Ni_3Al(OH)_8(CO_3)_{0.5}(H_2O)_2$	eardleyite	--
a^a	3.1Å	3.1 Å
c^a	23.4 Å	15.6 Å

^{a} approximate unit cell parameters

Synthetic LDHs are often characterized by stacking faults as a result of the intergrowth of the rhombohedral and hexagonal polytypes; the severity of these faults depends upon the type and relative amounts of divalent and trivalent metal cations present in the layers[16]. It has been found that Mg/Al LDHs have a preference for the rhombohedral polytype, however the Mg/Ga and Ni/Al containing analogues display a random stacking order, as indicated by the broad and asymmetric (01ℓ) reflections in the X-ray powder diffraction patterns. Since the stacking faults affect only the long range layer-layer interactions and not the local topology of the layer-interlayer bonding, there is no need to take special precautions to prevent the intergrowth of the two polytypes during the synthesis of LDH materials.

1.1.2 The nature of M^{2+} and M^{3+}

A wide variety of M^{2+} and M^{3+} cations have been used to form the LDH structure, the main criterion being that the ionic radius of the M^{2+} or M^{3+} ion is not too different from that of Mg^{2+}. A summary of various metal cations that have been used to form the LDH structure is presented in Table 1.2. LDHs containing Cu^{2+} can only be prepared if a second divalent cation is also present within the layers[11]. Cu^{2+} forms compounds characterized by the presence of a cooperative Jahn-Teller effect; the distortion of the octahedral coordination leads to a gain in energy, and formation of a LDH structure is unfavorable until the Cu/M^{2+} ratio is lower than or equal to one[17,18]. Under these conditions, the second M^{2+} dilutes the Cu^{2+} cations, preventing them from occupying near-lying octahedra, which would lead to the formation of the copper compound with distorted octahedra.

Table 1.2: Ionic radii of some divalent and trivalent metal cations, $\overset{\circ}{A}$[11]

M^{2+}	Mg	Cu	Ni	Co	Zn	Fe	Mn
	0.65	0.69	0.72	0.74	0.74	0.76	0.80
M^{3+}	Al	Ga	Ni	Co	Fe	Mn	Cr
	0.50	0.62	0.62	0.63	0.64	0.66	0.69

The stability of the LDH layers towards pH changes in aqueous media is determined predominantly by the combination of divalent and trivalent metal cations. LDH layers composed of the more acidic M^{2+} and M^{3+} metal cations (e.g. Zn^{2+}, Ni^{2+}, Al^{3+} Cr^{3+})[19] are stable at lower pH, and in some cases significant dissolution does not occur

even at pH values as low as 3.6^{20}. Hydroxides of the more basic metal cations (e.g. Mg^{2+})

become soluble in solution below about pH 8, and significant dissolution from the LDH

layers will occur, resulting in a lowering of the $M^{2+}:M^{3+}$ ratio from that of the desired

value. Stability towards pH changes is a major consideration when choosing an

appropriate pillaring method, and in general, different routes must be used to form

pillared phases depending on the degree of stability exhibited by the layers.

The presence of long-range cation ordering within the LDH layers is still a matter

of debate[21], however evidence of local ordering has been detected by IR spectroscopy[22].

Although cation ordering is expected to occur in LDH materials with $M^{2+}:M^{3+}$ ratios

close to two, it has not been generally observed, except in LDH materials where the radii

of the M^{2+} and M^{3+} cations are similar (i.e. Li/Al[23,24] and Mg/Ga[16]). In general, the

octahedral layers that comprise the LDH materials are compressed vertically and

expanded along the plane, where the compression is limited by the close approach of the

oxygen atoms along the shared octahedral edge[16]. Accompanying this compression is a

counter rotation of the upper and lower oxygen octahedral triads, which shortens the

shared edges and shields the cations from each other. In a Mg/Al LDH with a $M^{2+}:M^{3+}$

ratio of 2:1 the OH-OH distance across shared octahedral edges (obtained from Rietveld

structure refinements) is 2.632Å; this close approach prevents further layer distortions

brought about by the cation ordering process[16]. As previously stated, long range ordering

may only occur if the radii of the M^{2+} and M^{3+} cations are similar. If this criterion is met,

the ordering can proceed without major distortions of the octahedra and thus without any

further decrease of the OH-OH distance. One consequence stemming from the long-range cation ordering in Mg/Ga LDHs is that within each octahedron, the cation-oxygen distances are no longer equal. Two Ga-oxygen distances were observed during an extended x-ray absorption fine structure (EXAFS) study, suggesting that the LDH layers of ordered samples become corrugated or buckled, and thus the layers are no longer planar. Corrugation of the layers increases the distance between adjacent cations and therefore minimizes their repulsion.

1.1.3 The values of x

Further compositional variability may be achieved by altering the mole fraction of the trivalent metal cation (x) in the LDH layers. Increasing the M^{3+} content (increasing x) results in higher surface charge densities on the LDH layers, thus requiring a greater number of charge balancing anions in the interlayer region to achieve electroneutrality. In principle, adjusting the M^{3+} content may allow control over the lateral spacing between the interlayer anions. There is generally a limit to the range of x that will form a pure LDH phase, typically $0.17 \leq x \leq 0.33$, although the exact range is determined by the pH at which coprecipitation is carried out as well as the natures of the metal cations and of the interlayer anions. An x value outside this range may result in several octahedra of the same metal cation coming close together, allowing pure single hydroxides (M^{2+} or M^{3+}) to nucleate and form a separate phase in addition to the desired LDH phase. The chemical composition range of some common M^{2+}/M^{3+} LDH materials containing simple inorganic

anions and prepared at different pH values is presented in Table 1.3. In this table, the layer composition is expressed in terms of the M^{2+}:M^{3+} ratio, R, which is becoming more widely used in the literature. All discussion concerning LDH layer composition throughout this dissertation will use the M^{2+}:M^{3+} notation (R) instead of the M^{3+} mole fraction notation (x).

Table 1.3: Chemical composition range of some common M^{2+}/M^{3+} LDH layer types[11]

M^{2+}/M^{3+}-A^{n-}	Coprecipitation pH	M^{2+}:M^{3+} (R) range
Zn/Al-Cl	7.0	$1.0 \leq R \leq 5.0$
Zn/Al-Cl	10.0	$1.0 \leq R \leq 3.0$
Zn/Al-CO_3	9.0	$1.7 \leq R \leq 2.3$
Ni/Cr-CO_3	13.0	$1.0 \leq R \leq 2.0$
Ni/Cr-Cl	11.5	$1.0 \leq R \leq 3.0$
Mg/Al-CO_3	8.0	$1.0 \leq R \leq 3.0$
Mg/Fe-CO_3	-	$2.7 \leq R \leq 5.6$
Co/Fe-CO_3	9.0	$1.0 \leq R \leq 3.0$

The textural properties of the LDH material depend on the value of R, since altering the M^{2+}:M^{3+} ratio also alters the density of positive charges on the layers, and therefore influences the lateral spacing between the interlayer anions. Porosity in layered double hydroxides may be classified as either intercrystalline or intracrystalline in nature. In the first case, pores are created in the spaces that exist between different LDH crystallites, and tend to be in the large micropore to large mesopore (c.a. 20-300 nm) range, however the exact value depends on the nature of medium in which the materials were prepared[25]. It is primarily the second type of porosity that will be of interest

throughout this dissertation, that which is created within the gallery region between adjacent LDH layers by the process of pillaring with large POM anions. These intracrystalline pores tend to be much smaller than the intercrystalline pores, typically with diameters of 5 Å or less, but their role in determining the physical properties of the pillared LDH is crucial. In addition, it is through these intracrystalline pores that reactant molecules are able to access the catalytically active sites located within the interior of the LDH material.

1.1.4 The nature of the anion

Layered double hydroxides are ionic lamellar solids, and may be thought of as being composed of two discrete building blocks: the LDH layers on the one hand, and the interlamellar anions on the other. The charge balancing anions that are present in the gallery region of the LDH are hydrogen bonded to the LDH layers, and may be exchanged using well established ion exchange techniques. The order of stability (with respect to exchange) of some simple inorganic anions is approximately[26,27,28]

$$F^- > Cl^- > Br^- > NO_3^- > I^-$$

and

$$CO_3^{2-} > SO_4^{2-}$$
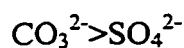
where the divalent anions are more stable to exchange than the monovalent ones. The carbonate anion is strongly retained once it has been incorporated between the LDH layers, effectively reducing the anion exchange capacity of the material and restricting

access by other ions and molecules[29]. For this reason, virtually all naturally occurring LDH materials contain interlayer carbonate anions[11], and most synthetically prepared LDHs are contaminated by carbonate anions to varying degrees. In order to prepare pure LDH phases with anions other than carbonate, it is therefore necessary to work under an inert gas atmosphere and to employ degassed and deionized water to prepare the solutions that are used throughout the entire synthesis.

In addition to balancing the net positive charge on the LDH layers that result from the substitution of Al^{3+} for Mg^{2+}, the interlayer anions also impose a regular separation distance or gallery height between adjacent LDH layers. The values of c' for LDHs containing different inorganic anions are presented in Table 1.4; the c' value given in

Table 1.4: Values of c' for a generic LDH containing some simple inorganic anions[11]

Anion	c' (Å)
OH^-	7.55
CO_3^{2-}	7.65
Cl^-	7.86
NO_3^-	8.79
SO_4^{3-}	8.58
ClO_4^-	9.20

this table is equal to the sum of the interlayer thickness plus the thickness of one LDH layer (4.8 Å), and is obtained directly from the position of the d_{003} x-ray diffraction peak. The number, size, orientation, and strength of the bond between the anion and the hydroxyl groups of the LDH layers determine the thickness of the interlayer. In addition,

the degree of hydration of the LDH material may cause a small variation in the observed

c' parameter, which generally becomes smaller as the LDH is progressively dehydrated.

LDH materials intercalated with simple anions of the type in Table 1.4, or even

with bulky organic anions such as terephthalate, *p*-hydroxybenzoate or *p*-toluene

sulfonate, are not considered to be pillared materials. Low valent anions such as the ones

mentioned above tend to be spaced closely together in the gallery region, with the

remaining space occupied by water molecules. The interlayer region of these materials is

not accessible to molecules that are at least the size of nitrogen (N_2), which is a criterion

that must be satisfied in order for an LDH to be considered truly pillared[15]. Heteropoly

oxometalate anions (discussed in Section 1.2) belong to a class of inorganic anions that

do form pillared-LDH phases, and have been used to produce materials that are

characterized by high surface areas and significant micropore volumes[30].

1.1.5 Thermal stability of the LDH structure

The LDH structure undergoes several stages of decomposition as temperature is

increased. In many cases, the mixed oxides resulting from the complete thermal

decomposition of LDHs are active base catalysts[31,32,33,34,35]. Prior to the complete

decomposition, the natures of the M^{2+} and M^{3+} cations in the layer influence the precise

temperature at which the different transformations occur. For the case of

$Mg_6Al_2(OH)_{16}(CO_3^{2-}) \cdot 4H_2O$, heating to about 200°C results in the loss of the four

interstitial water molecules[36]. Additional heating from 275°C to 450°C results in the

partial dehydroxylation of the inorganic layers and evolution of the interlayer carbonate anions as water and carbon dioxide, respectively[36]. Under these conditions there is a moderate increase in the surface area of the material, from 120 m^2g^{-1} to about 250 m^2g^{-1}, and the overall hexagonal crystal morphology is retained[37,38]. TEM images reveal a distinct cratering of the crystallite surface, which may have been caused by escaping jets of steam and CO_2, indicating that interstitial venting does not occur during LDH decomposition.

Heating LDHs to temperatures not exceeding about 500-600°C results in reversible decomposition of the LDH structure, leaving a residue that analyzes approximately as $Mg_6Al_2O_8(OH)_2$[39,40]. Controlled thermal decomposition of LDHs yields a product that is a fairly strong base ($pK_a \leq 35$) and which is a useful catalyst for reactions such as vapor-phase aldol condensation[39], dehydrogenation of 2-propanol[41], and propylene oxide[42] and β-propiolactone[43] polymerization. It has recently been revealed, however, that the temperature at which complete decarboxylation occurs is dependent upon the layer composition of the LDH material. Within the Mg_RAl-CO_3 series, CO_2 evolution is almost complete at 500°C when R = 3 or 4, which corresponds to LDH layers in which the aluminum content is relatively low[44]. If the aluminum content is high (R = 2) then as much as 20-30% of the carbonate remains after heating to 500°C. Decarbonation is not complete until the material is heated to 900°C, at which point Al^{3+} ions migrate into the MgO, forming spinel ($MgAl_2O_4$) and releasing the remaining

carbonate anions. It was stated that lower charge densities, due to lower Al^{3+} contents, lead to lower amounts of residual carbonate anions[44].

After heating below 600°C, the layered structure can be fully restored by stirring the resulting mixed metal oxide solid solution in water for a period of several days[45]. This is known as the so called "memory effect", and it is an important characteristic of LDHs which has been exploited in some synthesis strategies, as well as when using LDHs as adsorbents or ion scavengers in aqueous and non-aqueous waste streams. Stirring the mixed metal oxide in deionized water will result in the incorporation of interlamellar hydroxyl groups[30], however, any anionic species could be added to the suspension and be preferentially incorporated. In this way, LDHs containing carbonate, chloride, nitrate, organic anions or even polyoxometalate anions have been formed. Finally, heating the LDH above 600°C causes an additional and irreversible dehydroxylation of the LDH layers to form a mixture of MgO and $MgAl_2O_4$ (spinel), as evidenced by the XRD powder pattern.

1.1.6 Synthesis of LDHs

LDH materials are generally synthesized via a coprecipitation reaction after the method of Miyata[46]. Although there are several variations on this general approach, the most typical conditions involve the addition of a mixed metal salt solution, which contains both the M^{2+} and M^{3+} cations, into a reaction flask with vigorous stirring and the coaddition of a base solution to maintain constant pH. The choice of base solution varies

depending on the desired interlayer anion species; in the case of carbonate a mixed

$NaOH/Na_2CO_3$ solution is used. If the desired anion is NO_3^- or Cl^-, then a mixed metal

nitrate or mixed metal chloride solution is used, and the pH is maintained by the addition

of NaOH only. Finally, if an organic anion is desired in the interlayer region[8,47,48], then

the mixed metal salt solution (nitrate or chloride) is added to a solution containing the

corresponding organic acid dissolved in water, and again, pH is maintained at a constant

value by the addition of NaOH.

There are limits to the usefulness of the coprecipitation method, however, since

many anions of particular interest cannot be incorporated between the LDH layers directly

by this route. For example, POM anions are generally not stable at typical coprecipitation

pH values, and thus only hydrolysis byproducts are obtained by this method, except in the

case of a few of the more acidic LDH layer types[19,49,50]. In general it is necessary to

prepare the LDH-POM materials by a more indirect route. In a typical procedure an

intermediate LDH species is synthesized by a coprecipitation reaction, and then

subsequently modified to form the desired product, making use of one or both of the

following characteristics of the LDH: anion exchange[48,51,52,53,54] or memory effect[30,55]

after careful calcination below 600°C.

In addition to considering the LDH layer and pillar compositions, it is also

necessary to carefully control the microstructural properties of the LDH/POM in order to

produce materials that are characterized by large surface areas, accessible and well

defined micropores and high thermal stability. Several workers have noted that these

properties are very sensitive to the synthesis conditions, and great care must be taken in order to control both the composition and structure of the hybrid materials. In addition, those synthesis methods that work well for acidic LDH layers seldom work well for the basic LDH analogues as well.

1.1.7 Base catalysts derived from LDH precursors

As was mentioned in Section 1.1.5 the LDH layers decompose upon heating to 500-600°C to form partially dehydroxylated mixed metal oxides[56]. The active surface sites are believed to include residual surface hydroxyl groups[31] as well as a range of O^{2-} M^{n+} acid-base pairs. The number and strength of basic sites depends on the chemical composition of the precursor and on the activation conditions[37].

In the case of Mg/Al-CO_3 LDHs, calcination at 500°C results in a product that has an x-ray powder diffraction pattern corresponding to poorly crystallized MgO, but with a lattice constant slightly smaller than that of pure MgO. One explanation is that Al^{3+} replaces Mg^{2+} in the mixed oxide as well as in the LDH layers, which results in the generation of a net positive charge. The excess positive charge of the mixed oxide could be compensated by the presence of two types of defects: cationic vacancies or inclusion of interstitial oxygen ions in the structure. ^{27}Al MAS-NMR studies have detected the presence of tetrahedral aluminum in mixed oxides formed by calcining Mg/Al LDH materials; it has been suggested that at least some of the tetrahedral aluminum is located at tetrahedral positions in the MgO lattice, which could give rise to the formation of

clusters of Mg-Al inverse spinel[57,58]. The Al^{3+} located at the tetrahedral or octahedral

sites produces the defect of Mg^{2+} or Al^{3+} in the framework in order to compensate the

positive charge generated. The O^{2-} ions adjacent to the Mg^{2+}/Al^{3+} defects become

coordinatively unsaturated and could provide strong basic sites[41].

1.2 Polyoxometalate (POM) anions

Polyoxometalate anions constitute a very large class of structurally distinct

polymeric inorganic compounds. These complexes may be classified as either

isopolyanions, represented by the formula $[M_mO_y]^{p-}$, or as heteropolyanions, $[X_xM_mO_y]^{q-}$

$(x \leq m)$. One special case is the metatungstate anion, $H_2W_{12}O_{40}^{6-}$, which is classified as

an isopolyanion[59], but in fact is isomorphous with the heteropolyanions[60,61].

The first systematic survey of the chemistry of heteropoly oxometalate anions was

carried out by Wu[62] in the early part of this century. Even at that time, heteropoly anions

had been widely used in biological chemistry as protein precipitants and in the

colourimetric determination of uric acid[63], cholesterol[64], adrenaline and phenol for many

years, however the complex solution chemistry of the anions was poorly understood. Wu

identified two distinct series of complex phospho-acids of molybdenum and tungsten, and

reported the conditions necessary to obtain the free acids and salts of the anions of

different stoichiometries. In the ensuing years the advent of spectroscopic techniques,

including FT-IR[65,66,67], Raman[66-68,69,70,71] and multi-nuclear solution NMR[67,72,73], as well

as polarographic and voltammetric methods[74,75,76], has permitted the *in situ* analysis of solutions containing heteropoly oxometalate anions.

1.2.1 α-12-Heteropoly oxometalate anions: the Keggin structure

The structure of an α-12-heteropoly oxometalate anion is shown in Fig. 1.3 in an atom-and-bond representation. This structure was first proposed by Keggin[77,78] in 1933 for 12-tungstophosphoric acid, and is now commonly referred to as the Keggin structure. The general Keggin ion formula is $[XM_{12}O_{40}]^{n-}$, where the *addenda atom* M is usually molybdenum or tungsten in its highest (d^0, d^1) oxidation state[59]. Up to six addenda atoms may be replaced by another element, e.g. vanadium, titanium, chromium etc., to form mixed addenda anions. The central *hetero atom*, X, is shown in Fig. 1.4 as a shaded tetrahedron in which an oxygen atom (O_a) occupies a position at each vertex. The central tetrahedron is bonded to four M_3O_{13} triad ligands, one of which is shown in Fig. 1.4, through the O_a atoms. Within the triads, there are three additional types of oxygen atoms present: O_t are terminal atoms bonded only to a single M atom; O_b are bridging M-O-M atoms that connect the corners of adjacent triads; and O_c are bridging M-O-M atoms that connect metal atoms within the same triad.

The T_d symmetry of the central XO_4 tetrahedron is preserved in the overall intact α-Keggin structure of the heteropoly tungstates. The α-Keggin structure is the thermodynamically stable isomer, however, a β-Keggin isomer is also known for several heteropoly tungstates (X = B, Si, Ge, H$_2$) and molybdates (X = Si, Ge, P, As). In the β-
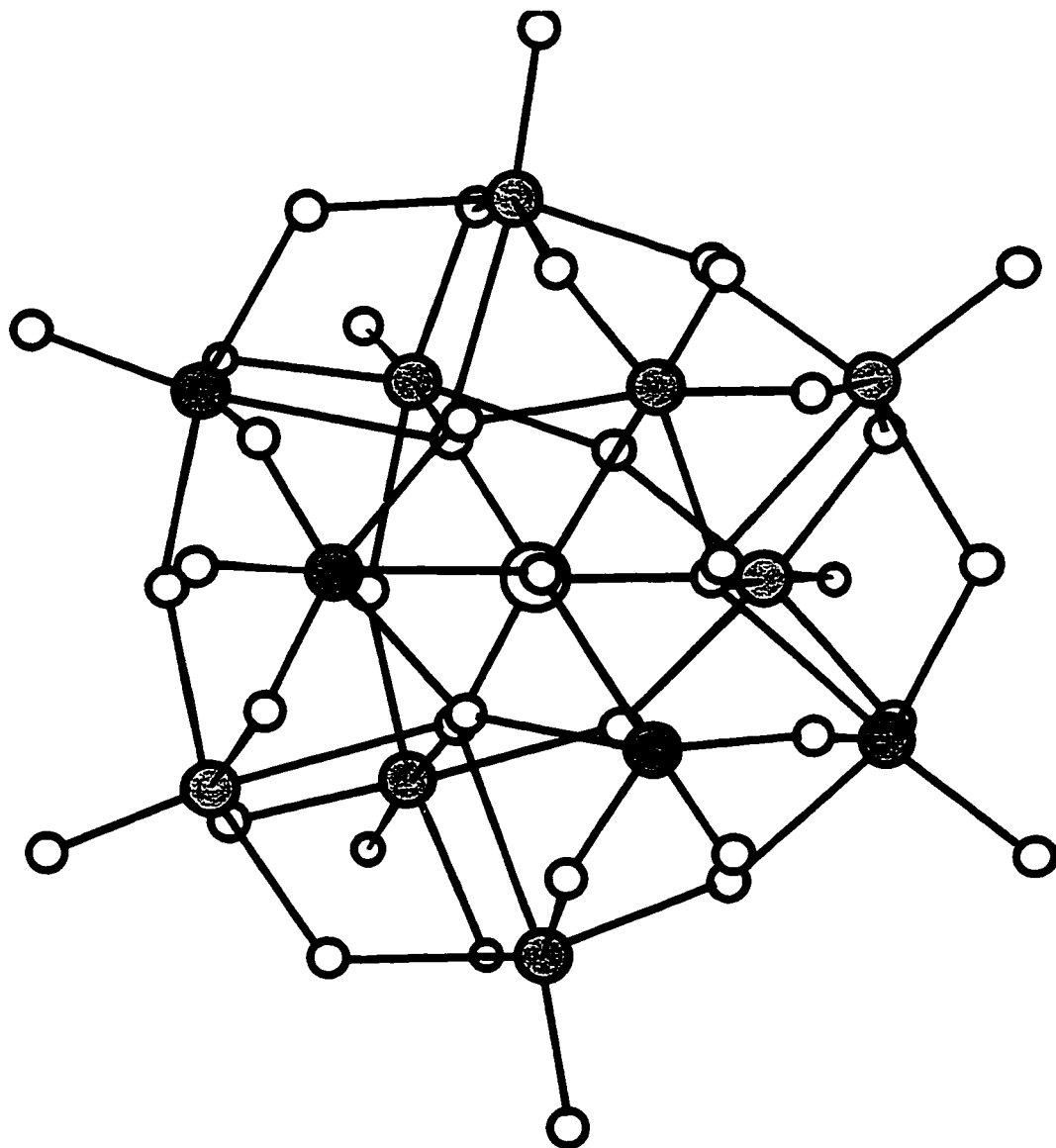
Fig. 1.3: Atom-and-bond representation of the α-$[XM_{12}O_{40}]^{n-}$ structure. Small open white circles represent oxygen atoms, large central open white circle represents hetero atom and shaded circles represent metal atoms.
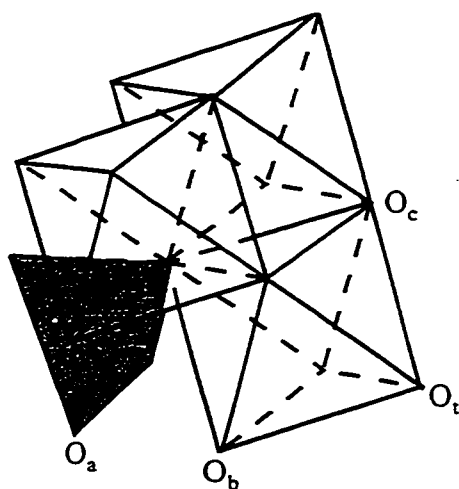
Fig. 1.4: Central tetrahedron and one M_3O_{13} triad
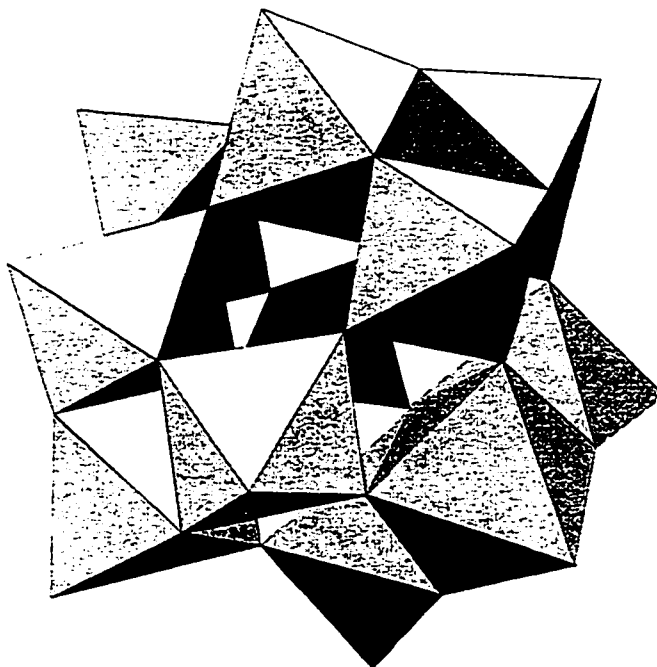
Fig. 1.5: Polyhedral representation of the keggin structure (note: the triad on the rear face has been omitted for improved clarity)

Keggin isomer one of the M_3O_{13} triads of the α-structure shown in Fig. 1.5 is rotated by 60°, thereby reducing the overall symmetry from T_d to C_{3v}. Several other isomers, the so-called γ-, δ-, and ε-structures, may be obtained by the rotation of an additional one, two or three M_3O_{13} triads by 60°, respectively, but are not of significance under normal conditions and therefore will not be discussed further.

1.2.2 Influence of hetero- and addenda-atom on pH stability of the Keggin structure

Heteropoly oxometalate anions undergo a series of rapid but reversible decomposition reactions in solution as the pH is increased, which has led to considerable confusion in the literature over the years due to incomplete characterization of the solution species being studied. The exact sequence of the decomposition steps, as well as the pH at which decomposition occurs, depends on the combination of the hetero- and addenda-atoms that make up the Keggin ion. In general, the 12-heteropolymolybdates are less stable than the 12-heteropolytungstates. With respect to the hetero-atom, the order of stability is roughly $Si > (Zr, Ti) > Ge > P > As$[79]. That is to say, the pH range of stability extends highest for the 12-tungstosilicate anion, which decomposes above pH ca. 5 to form the lacunary (defect) Keggin structure α-$SiW_{11}O_{39}^{8-}$. Since the oxygen atoms are shared between polyhedra, the removal of the first WO_6 octahedron results in the stoichiometric loss of a single MO^{n+} group from the intact Keggin structure.

The corresponding 12-tungstophosphate anion (abbreviated as PW_{12}) undergoes an analogous decomposition to form α-$PW_{11}O_{39}^{7-}$ (or simply PW_{11}), albeit at a

considerably lower pH value of about 1.5 - 2.0. Fig. 1.6 illustrates the complete series of

decomposition reactions known for the α-PW$_{12}$ ion[59], which was one of two Keggin ions

used as pillaring species throughout this work. It should be noted in particular that the β-

PW$_{12}$ does not exist, and that the β-PW$_{11}$ is not stable[59]; it has been assumed that only the

α-PW$_{11}$ ion was present in solution under the conditions that were employed during the

POM exchange reactions throughout this work.

$$\text{H}^+, \text{WO}_4^{2-}$$

$$\beta\text{-PW}_9 \longrightarrow [\beta\text{-PW}_{11}\text{O}_{39}]^{7-}$$

$$\text{PO}_4^{3-} \text{ WO}_4^{2-}$$

rapid

$$\alpha\text{-PW}_9 \overset{?}{\rightleftharpoons} [\text{P}_2\text{W}_{19}\text{O}_{68}]^{14-} \rightleftharpoons [\alpha\text{-PW}_{11}\text{O}_{39}]^{7-}$$

$$[\text{P}_2\text{W}_{21}\text{O}_{71}]^{6-}$$

$$\text{OH}^-$$
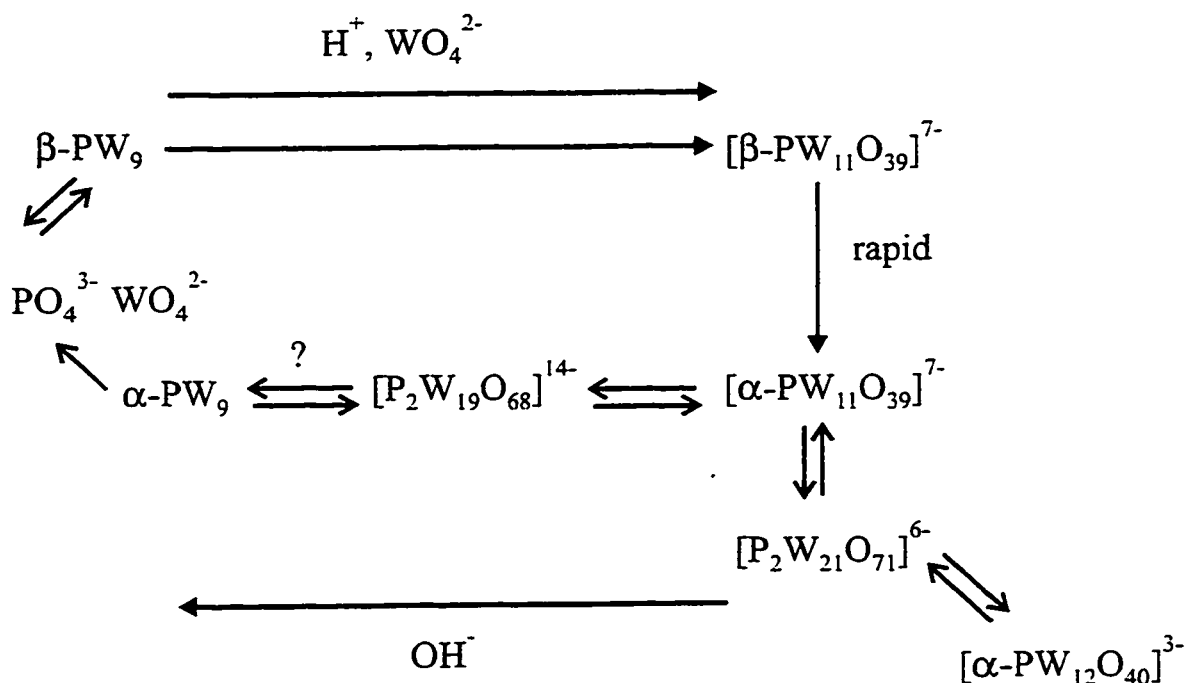
$$[\alpha\text{-PW}_{12}\text{O}_{40}]^{3-}$$

Fig. 1.6: Summary of the tungstophosphate hydrolysis reactions in solution[59]

Another Keggin ion used to pillar LDH materials was the metatungstate anion

α-H$_2$W$_{12}$O$_{40}{}^{6-}$ (H$_2$W$_{12}$), which is formally an isopoly oxometalate anion in which the two

protons play the role of the tetrahedrally coordinated hetero atom at the center of the ion. It is known that the metatungstate anion is isomorphous with the corresponding heteropoly oxometalates, and in fact it behaves as a heteropoly anion of the Keggin series in all respects. Since the α-H_2W_{12} species is the thermodynamically stable product, and the H_2W_{11} lacunary ion has been observed only as a ligand, a discussion of the rather complex aqueous tungstate polymerization will not be provided here.

1.2.3 Thermal stability of α-12-heteropoly oxometalate anions

One of the properties that a potential pillar must display is high thermal stability. This allows the structure and catalytic properties of the pillar to be retained after high temperature pretreatment or prolonged reaction times at high temperature. Decomposition temperatures for a variety of heteropoly oxometalate anions have been reported in the literature, however they must be viewed with skepticism since the solubility of the residue, which is considered to be a more precise criterion for determining the extent of decomposition, was infrequently studied. In many cases, the Keggin structure is believed to be stable upon heating to at least 200-250°C, and possibly as high as 350°C for members of the molybdophosphate series[79]. Decomposition begins with a partial reduction and distortion of the Keggin unit, followed by a complete and irreversible collapse of the structure with the formation of MoO_3[80]. In addition, IR studies have indicated a large stabilizing effect for silica supported 12-molybdo-phosphoric acid, which retained the Keggin structure after heating to 700°C[81].

The corresponding tungstophosphate anion appears to be considerably more stable with respect to thermal treatment, with DTA data suggesting that the heteropoly structure of 12-tungstophosphoric acid decomposes at about 600°C[82]. Prior to complete decomposition, however, several additional stages of weight loss were observed. The first stage was attributed to the removal of zeolitic water to give the 4-5 hydrate, followed by the formation of the anhydrous acid at 350-450°C. The powder x-ray diffraction pattern changed upon heating the material to about 450°C, with the reflections becoming more broad and decreasing in intensity, but still showed evidence for retention of the Keggin structure. The final stage of weight loss was presumed to be loss of phosphorus by sublimation of P_2O_5, leaving a residue described as approximately 12 WO_3. More recent results indicate that the decomposition of the Keggin structure may start as low as 500°C in the case of prolonged heating.[83] It is unknown whether a thermal stabilization effect similar to that observed[81] for PMo_{12} also occurs for supported PW_{12} anions.

The metatungstate H_2W_{12} anion appears to be of intermediate stability compared to the above two examples. Anhydrous metatungstate was obtained after heating below 200°C[84], but rapidly decomposed to a material of variable composition above 250°C. The material that was formed above 250°C could not be identified as any of the known oxides of tungsten. Decomposition of metatungstate to tungsten trioxide was complete at 450°C. It was found that the water molecules are zeolitic, that is the water content varied continuously with temperature, whereas the ammonium content remained almost constant to a temperature of about 250°C, after which there was a rapid loss of $NH_3(g)$.

1.2.4 POM anions as homogeneous and heterogeneous catalysts

Many POM anions are currently used in industrial processes as homogeneous or heterogeneous catalysts, and several review articles discussing their applications have recently appeared[85,86,87]. One feature that makes heteropoly compounds particularly well suited for catalyst design is that their acidic and redox properties may be controlled by choosing appropriate hetero- and polyatoms (addenda atoms). The heteropoly tungstates make excellent acid catalysts (see Table 1.5), whereas the heteropoly molybdates generally function as efficient oxidation catalysts (see Table 1.6). In addition, the acid strengths for the heteroatoms decreases in the order $P^{5+} > Si^{4+} > Ge^{4+}$, and in the solid state the acidity can be further controlled by the salt composition[85].

The Keggin structure has been previously described in Section 1.2.1 and a polyhedral representation of the structure appeared in Fig. 1.5 (where one triad was omitted for the sake of clarity). Although it is not immediately obvious, the individual Keggin ion units are close packed structures and thus are completely non-porous. In fact, the surface areas of the solid heteropoly tungstic and heteropoly molybdic acids are very small, generally not exceeding about 10 m^2g^{-1}. More specifically, the specific surface area of calcined 12-tungstophosphoric acid[83] was found to be only 4-5 m^2g^{-1}. This value is considerably lower than one would expect based on the crystal structure of the free acid, in which $PW_{12}O_{40}^{3-}$ and bridging proton/water units, usually represented as $H_3 \cdot 29 H_2O$, occur alternately at the corners of the body-centered cubic lattice[88]. This

Table 1.5: Acid-catalyzed reactions by heteropoly compounds
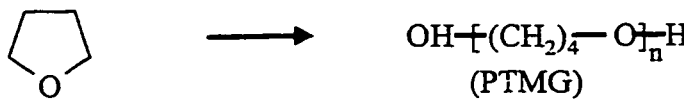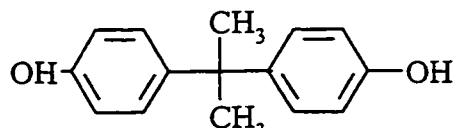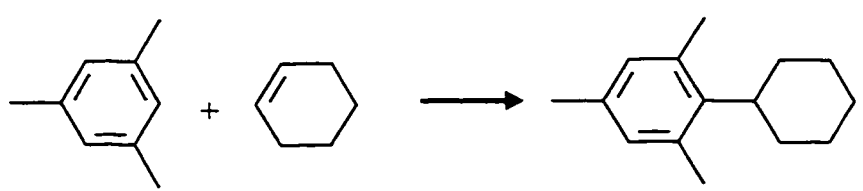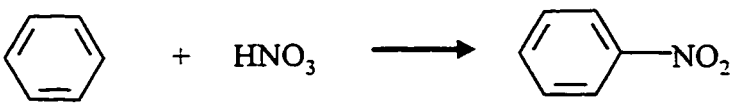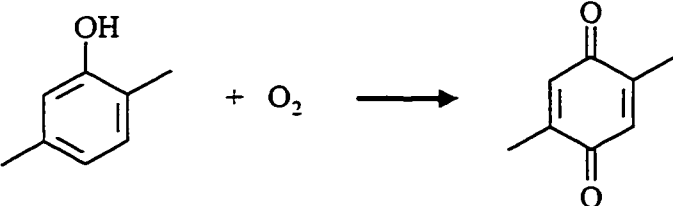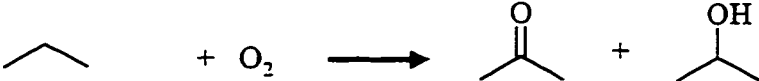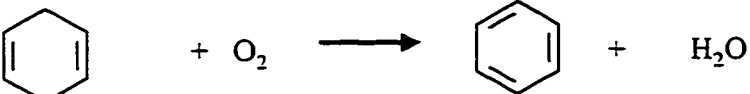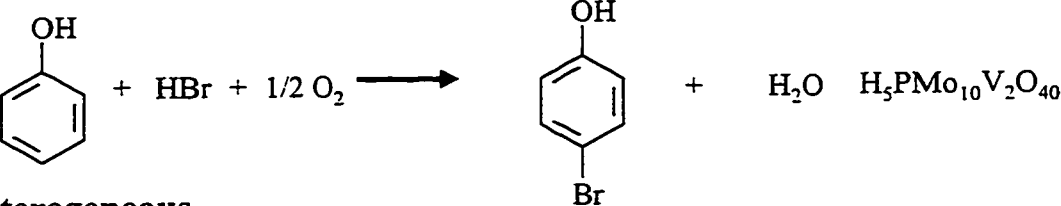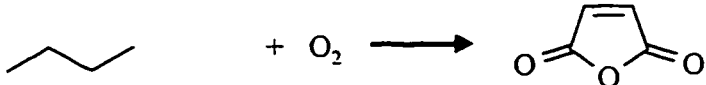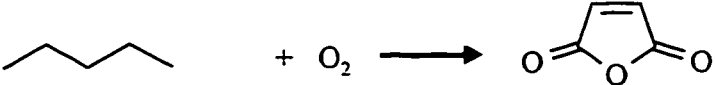
Reaction	Catalyst

Homogeneous

$H_2C=CHCH_3 + H_2O \longrightarrow CH_3CHOHCH_3$ $H_3PM_{12}O_{40}$
$(M=W,Mo)$

(tetrahydrofuran) $\longrightarrow$ $OH-[(CH_2)_4-O]_n-H$ $H_3PW_{12}O_{40}$
(PTMG)

2 (phenol)$-OH + CH_3COCH_3$

$\longrightarrow$ $OH-C_6H_4-C(CH_3)_2-C_6H_4-OH$ $H_3PW_{12}O_{40}$

Heterogeneous

(trimethylbenzene) $+$ (cyclohexene) $\longrightarrow$ (dimethyl-cyclohexyl-benzene) $Cs_{2.5}H_{0.5}PW_{12}O_{40}$

(benzene) $+ HNO_3 \longrightarrow$ (benzene)$-NO_2$ $Cs_{1.5}H_{1.5}PW_{12}O_{40}$

$CH_3COOH + C_2H_5OH \longrightarrow CH_3COOC_2H_5 + H_2O$ $H_3PW_{12}O_{40}$

CH_3OH (or CH_3OCH_3) $\longrightarrow$ $C_1 \sim C_6$ Hydrocarbons $H_3PW_{12}O_{40}$
$Cs_{2.5}H_{0.5}PW_{12}O_{40}$

Table 1.6: Oxidation reactions by molecular oxygen catalyzed by heteropoly compounds

Reaction	Catalyst

Homogeneous

2,5-dimethylphenol $+ O_2 \longrightarrow$ 2,5-dimethyl-1,4-benzoquinone $H_5PMo_{10}V_2O_{40}$

propane $+ O_2 \longrightarrow$ acetone $+$ isopropanol $H_7PW_9Fe_2NiO_{37}$

cyclohexene $+ O_2 \longrightarrow$ benzene $+ H_2O$ $H_5PMo_{10}V_2O_{40}$

phenol $+ HBr + 1/2\, O_2 \longrightarrow$ 4-bromophenol $+ H_2O$ $H_5PMo_{10}V_2O_{40}$

Heterogeneous

$CH_2=C(CH_3)CHO + O_2 \longrightarrow CH_2=C(CH_3)COOH$ $CsH_3PMo_{11}VO_{40}$

$CH_3CHO + O_2 \longrightarrow CH_3COOH$ $Cs_xH_{3-x}PMo_{12}O_{40}$

$CH_3CH(CH_3)COOH + O_2 \longrightarrow CH_2=C(CH_3)COOH$ $H_5PMo_{10}V_2O_{40}$

butene $+ O_2 \longrightarrow$ maleic anhydride $BiPMo_{12}O_x + VO^{2+}$

pentene $+ O_2 \longrightarrow$ maleic anhydride $H_5PMo_{10}V_2O_{40}$

structure would be expected to result in zeolite-like channels through the interior of the solid acid, which would be accessible to large molecules after the removal of water molecules. It appears, however, that in the free acid the removal of zeolitic water molecules results in collapse or shrinkage of the pores, thus preventing access to the interior and lowering the surface area.

Some heteropoly oxometalate salts, however, have been found to have very high specific surface areas. As shown in Table 1.7[89], for each of the heteropoly anions SiW_{12}, PMo_{12}, PW_{12} and AsW_{12}, the specific surface area of the parent acid as well as the salts of sodium and silver are all very low. With the exception of $K_4SiW_{12}O_{40}$, the potassium, ammonium, rubidium and cesium salts have larger surface areas[89], and the materials were found to be microporous with average pore radii in the range of $9 - 14$ Å. Due to the dependence of the surface area and microporous structure on the nature of the counter cation, most catalytic applications of the solid heteropoly compounds make use of the ammonium, alkylammonium or divalent metal salts.

Table 1.7: Effect of the counter-cation on the specific surface area (m^2g^{-1}) of α-12-heteropoly oxometalates[89]

Cation	Anion			
	$SiW_{12}O_{40}^{4-}$	$PMo_{12}O_{40}^{3-}$	$PW_{12}O_{40}^{3-}$	$AsW_{12}O_{40}^{3-}$
H	3.2	8	8	6.5
Na	1.3	3.5	3.7	-
Ag	-	-	3.0	-
K	3.3	39.9	90.0	46.0
NH_4	116.9	193.4	128.2	82.1
Rb	116.3	-	-	101.4
Cs	153.4	145.5	162.9	65.4

1.3 POM Pillared Layered Double Hydroxides (LDH-POM)

1.3.1 Potential advantages offered by LDH-POMs

Several advantages that could enhance the physical and or catalytic properties of the hybrid materials may potentially be realized by pillaring LDH materials with polyoxometalate anions. The unpillared LDH layers are intrinsically basic materials after calcination, however they tend to be completely non-active after low temperature treatment. The main reason for this lack of activity stems from the presence of water molecules in the interlayer region, and the relatively small size of carbonate or nitrate etc. anions, which limits reactant molecule accessibility to the gallery region. Incorporating large POM anions into the interlayer region would increase the gallery height by a factor of two, thus greatly increasing accessibility even after thermal treatment at only 125°C. However, lateral spacing between adjacent pillars may be small, and therefore the observed pore sizes seldom agree with the expected value based on the spherical size of the pillar.

One particularly exciting consequence of using catalytically active LDH-POM materials is that the microporous structure may allow shape or size selective processes to occur at the interior active sites. Thus, in the same way that the microporous structure of alumino-silicate zeolites increases product selectivity by preventing branching or specific types of substitution on cyclic products, the potential also exists to conduct selective reactions within the highly constrained space of the LDH interlayer region. Unfortunately, current methods of LDH-POM synthesis do not allow rigorous control of

the layer composition, and thus the anion distribution cannot be varied in a predictable manner. To date only one study has reported shape selectivity for an LDH-POM catalytic reaction[90]. The more highly microporous materials that have recently been synthesized using multi-step synthetic methods[30,91] may hold greater promise as potential shape selective catalysts.

Finally, the opportunity exists to introduce different types of catalytic activity by incorporating pillars into the interlayer region. Thus acid or redox activity may be imparted to the hybrid material by selecting an appropriate pillaring species. Subsequent thermal treatment of the hybrid material may then be performed at low temperatures leaving the LDH layers intact, or at higher temperatures resulting in the decomposition of the layered structure and the formation of strong base sites that are characteristic of calcined LDHs. As was previously mentioned, supporting $PMo_{12}O_{40}$ on silica resulted in a large stabilization of the Keggin structure, raising the decomposition temperature by 350°C from 350°C to 700°C. Although a similar stabilization effect has not yet been reported for the LDH-POM materials, the possibility that it may occur provides an additional incentive to pursue this research.

1.3.2 Synthetic difficulties

The main synthetic difficulty in making LDH-POM materials is caused by the vastly different pH stability displayed by both the layers and the pillaring anions, which is illustrated in Fig. 1.7. Considering the Mg/Al LDH layers again, it is apparent from
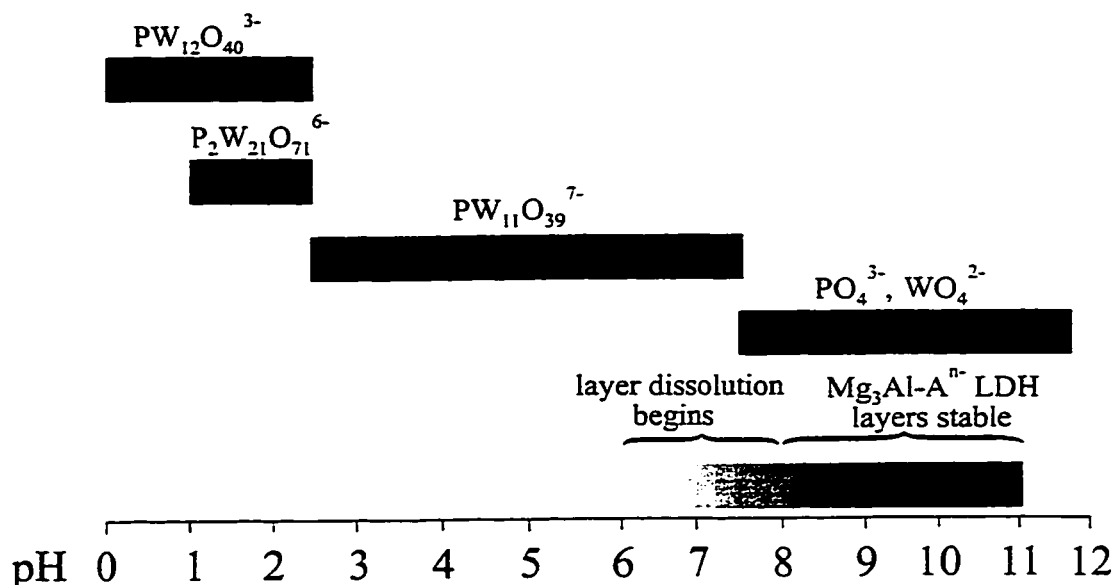
Fig. 1.7: Regions of pH stability for Mg_3Al LDH layers and solution species associated with the α-12-tungstophosphate anion

Fig. 1.7 that the LDH layers are stable only above pH 8. Below pH 8 dissolution of Mg^{2+} from the layers will occur. In general, most LDH layers are stable only in neutral to basic solution, with the major exceptions being the Zn/Al and Ni/Al analogues, which are quite stable in solution even at pH 3.6[20]. Conversely, the Keggin structure of the PW_{12} pillar is fully intact only below pH ca. 2.5, and between pH 1.0 and 2.5 other species co-exist in solution[73]. As shown in Fig. 1.7 the only species in solution between pH 2.5 to 7.5 is the lacunary PW_{11} ion, which ultimately decomposes to the tetrahedral species by pH 8.0.

For the above stated reasons it is generally necessary to choose an intermediate pH value, typically around pH 6, which lies within the upper limit of the Keggin ion (or lacunary Keggin ion in this case) stability range, as well as being within the extreme

lower limit of LDH layer stability. Attempting to pillar LDH materials with POM anions under these conditions, however, is usually complicated by two factors. Firstly, the LDH layers partially dissolve resulting in the desired $M^{2+}:M^{3+}$ ratio being lost; usually the $M^{2+}:M^{3+}$ ratio is lowered due to increased solubility of the divalent metal hydroxide. Secondly, an impurity phase, which is thought to be a mixed M^{2+}/M^{3+}-salt of the partially hydrolyzed POM anion, is formed[30]. The exact nature of this salt phase is unknown, but it is characterized by a broad X-ray diffraction peak centered on 11 Å. This salt phase is believed to be a low surface area material that is deposited on the surface of the LDH crystallites.

1.3.3 Catalysis by LDH-POMs

The use of LDH-POMs in catalysis is a relatively new area of interest. In fact most papers dealing with the topic have appeared only within the last 5 years. The first demonstration of catalysis by LDH-POM materials was for the photooxidation of 2-propanol to acetone over $Zn_2Al-V_{10}O_{28}$[92]. Since the time of this initial study, numerous papers have appeared examining the catalytic oxidation of cyclohexene over Mg/Al-POMs[93], olefin oxidation over Zn/Al-POMs[94], the acid catalyzed esterification of acetic acid with n-butanol over Zn/Al-POMs[54], etc.

Catalysis may also occur over vanadium, tungsten or molybdenum oxides formed by polyanion pillar decomposition or by impregnation, which are supported on the calcined LDH material after high temperature treatment. The conversion of n-butane was

studied over calcined Mg/Al LDHs impregnated with different vanadium loadings[95], but

this still remains a relatively unexplored area of research. The obvious disadvantage to

this approach is that the layered structure of the LDH is not retained after pretreatment,

and thus there is no opportunity to perform size or shape selective catalysis. Regardless

of the loss of the microtextural properties, it is possible that different active sites may be

formed as a result of the interaction between the cations in the mixed metal oxide matrix

and the supported metal oxide. In addition, interesting effects may arise due to the

presence of strong base sites in the mixed oxide and acidic or redox sites on the supported

metal oxide, which could result in different activities or different product distributions.

1.4 Thesis Overview

Section 1.3.2 outlines some of the synthetic difficulties that must be contended

with during the synthesis of LDH-POM hybrid materials. Due to the different ranges of

pH values over which the LDH layer structure and POM anion Keggin structure are

stable, most previous attempts at pillaring LDH materials with POM anions have resulted

in non-microporous products with low accessible surface areas. Therefore, one of the

main challenges addressed in the current work was to optimize synthesis conditions in

order to obtain hybrid materials with acceptable physical and chemical properties for use

in catalytic studies. Furthermore, it was hoped that a single synthesis method could be

adapted for the synthesis of LDH-POM materials with a wide range of layer compositions

and pillar types, perhaps with minor modifications to the general method.

In Chapter 2 the two methods that were used to synthesize POM-pillared LDH materials will be described in detail. In addition, the various physical and spectroscopic techniques used in the characterization of the final products and intermediates will be described. The final section of the chapter addresses the issue of reproducibility of the syntheses and the precision of the characterization techniques.

In Chapter 3 of this Dissertation the results of a study involving the synthesis of Mg_RAl-POM, Mg_RGa-POM and Zn_RAl-POM materials using the organic anion precursor route[8] will be presented. A significant part of the chapter focuses on the similarity and differences of Mg_RAl and Mg_RGa LDH materials. Particular emphasis is on the $M^{2+}:M^{3+}$ ratio in the LDH layers following coprecipitation at different pH values and using mixed metal salt solutions of different compositions. The Zn_RAl series was included primarily in order to examine the usefulness of the method for preparing LDH materials known to be stable over a range of pH values that coincides with the range of Keggin ion stability.

In Chapter 4 discussion focuses on a series of LDH-POM materials with compositions similar to the ones discussed in Chapter 3, but which were prepared via the LDH-OH/LDH-adipate precursor route[30]. The decision to adapt this new synthesis method was based on previous reports of exceptionally well ordered, high surface area LDH-POM materials being achievable by this method. Although the LDH-OH/LDH-adipate method had not previously been applied for the synthesis of pillared materials with acidic LDH layer types, the literature contained examples where several of the individual steps had been demonstrated for Zn_RAl and other acidic layer types. Thus, it

was anticipated that the overall method might also allow the synthesis of Zn_RAl-POM hybrid materials with high surface area and well defined micropore structure.

In Chapter 5 the catalytic properties of the LDH-POM materials prepared using the LDH-OH/LDH-adipate precursor method will be examined. Chapter 5 focuses on the activity of LDH-POM materials after activation at either 200°C or 550°C for the catalytic decomposition of 2-propanol to either propene (dehydration) or acetone (dehydrogenation).

In summary, the major objectives in this project were to:

i. Synthesize POM pillared LDH materials by optimizing existing methods. In particular, the organic anion precursor method of Drezdzon[8] and the LDH-OH/LDH-adipate method of Yun and Pinnavaia[30] were studied extensively. One of the major objectives of the project was to adopt a single method of synthesis for both "acidic" and "basic" pillared-LDH materials.

ii. Extend the synthesis to include LDH materials containing different metal cations, especially Ga^{3+}. The substitution of Al^{3+} by Ga^{3+} has previously been shown to affect the catalytic properties of inorganic oxide materials.

iii. Control the physical properties of the hybrid materials, for example surface area and pore size distribution, by varying the $M^{2+}:M^{3+}$ ratio.

No previous reports have claimed a systematic variation of the micropore structure with changing layer composition.

iv. Test the LDH-POMs for catalytic activity. The effect of altering the chemical composition of the LDH layers and/or POM pillars on the acid/base character of the hybrid material was of primary interest.

Chapter 2

Experimental Methods

2.1 Synthesis of LDH-POMs

As was previously stated in Section 1.3.2, the layered structure of LDH materials and the Keggin structure of POM anions are not generally stable over the same range of pH values. For this reason, the direct coprecipitation of a mixed metal salt solution in the presence of POM anions is not generally a feasible option for preparing LDH-POM materials, except in the case of a limited number of the more acidic (i.e. Zn/Al, Ni/Al) layer types[19,49,50]. A variety of multiple step synthesis methods for the preparation of polyoxometalate-pillared layered double hydroxides have recently appeared in the literature[7,8,30,91]. Two of these methods have been evaluated over the course of this project: the organic anion precursor route of Drezdzon[8] which is the focus of Chapter 3, and the LDH-OH/LDH-adipate precursor route of Yun and Pinnavaia[30] which is covered in Chapter 4.

In the following sections a detailed description of the organic anion precursor route and of the LDH-OH/LDH-adipate precursor route has been provided. The conditions described below are those that have been optimized for the formation of

Mg$_R$Ga pillared LDH phases. Any modifications to the experimental conditions that were necessary in order to accommodate the different layer compositions will be discussed in the appropriate section of the relevant chapter. Although the first step in each synthesis is formation of the LDH layers by coprecipitation of M^{2+} and M^{3+} from a mixed metal salt solution, the conditions that are used in each case are sufficiently different to justify a separate description at the beginning of each section.

2.1.1 Materials used

The reagents NaOH (BDH Assured), MgCl$_2$•6H$_2$O (BDH Assured), AlCl$_3$•xH$_2$O (BDH Assured) and terephthalic (1,4-benzenedicarboxylic) acid (Aldrich, 98%) were used as obtained without additional purification to prepare the materials described in the organic anion precursor section. An aqueous solution of GaCl$_3$ was used in the synthesis of all gallium containing species. LDH precursors described in the LDH-OH/LDH-adipate section were prepared using the reagents Mg(NO$_3$)$_2$•6H$_2$O (BDH Assured), Al(NO$_3$)$_3$•9H$_2$O (MCB Reagents, A.C.S. reagent), NaOH (BDH Assured), Na$_2$CO$_3$ (BDH AnalR), adipic (hexanedioic) acid (Aldrich, 99%), also without additional purification.

Ammonium metatungstate was prepared according to a literature method[84]. 90.8 g tungstic acid (Aldrich, 99%) in 250 mL distilled, degassed (DDI) water was heated to 80-90°C, and 10.5 mL 28% ammonium hydroxide solution (BDH Assured) was added at this temperature. Following complete addition, the mixture was stirred for an additional two hours at the addition temperature. Crystals of (NH$_4$)$_6$(α-H$_2$W$_{12}$O$_{40}$) were obtained by

evaporating the filtrate to dryness overnight at 90°C. The sodium salt of the heteropoly acid $H_3PW_{12}O_{40}$ was prepared by reaction of the parent acid with a stoichiometric amount of sodium carbonate in DDI water at 50°C. After complete addition of the sodium carbonate solution, the sodium salt of the heteropoly acid was obtained by evaporating the solution to dryness overnight at 90°C.

2.1.2 Organic anion precursor route

The synthesis of $Mg_6Ga_2(OH)_{16}TA\bullet zH_2O$ ($TA=C_8H_4O_4^{2-}$, terephthalate anion) at pH 10.0 is described here. LDH-TA precursors with different $Mg^{2+}:Ga^{3+}$ ratios were synthesized under similar conditions; the amount of $GaCl_3$ was kept constant, but the quantity of $MgCl_2$ was adjusted to give the desired $Mg^{2+}:Ga^{3+}$ ratio in the mixed metal chloride solution.

A 1-L, four-neck, round bottom flask was fitted with a 250 mL pressure equalized addition funnel with a ground glass joint, a thermometer inserted through a Teflon™ collar tapered to fit a 24/40 ground glass joint, a pH probe inserted through a similar collar and a suba-seal septum. Syringe needle tips inserted through the septum were used to permit the flow of nitrogen into and out of the system. The flask was placed into a heating mantle and the heating rate was controlled by adjusting a Variac variable transformer. Prior to the beginning of each synthesis the flask was flushed with nitrogen for several minutes to remove any traces of carbon dioxide, which would otherwise be incorporated into the LDH as interlayer carbonate anions. All subsequent additions to the

flask were performed as quickly as possible and with continuous nitrogen flow in order to minimize the introduction of CO_2.

The flask was charged with 250 mL of fresh DDI water and 2.82g of terephthalic acid. NaOH solution (2 M) was added via a syringe needle inserted through the septum to the vigorously stirred mixture until a final pH of 12.7 was obtained, and the terephthalic acid had completely dissolved. The amount of terephthalic acid that was used represents a 100% excess of terephthalate anions, based on the assumption that the acid is doubly deprotonated. In a separate flask, a solution containing 100 mL DDI water, 2.00 mL of 8.44 M $GaCl_3$ and 10.31g $MgCl_2 \cdot 6H_2O$ was prepared and thoroughly mixed. The mixed-metal chloride salt solution was added dropwise to the stirred terephthalate solution at room temperature via the addition funnel, resulting in the immediate formation of a white precipitate accompanied by a decrease in pH of the terephthalate solution. Simultaneous addition of NaOH solution through the septum was manually performed to maintain a constant pH of 10.0 ($\pm$0.2) over the course of the 30 minute addition period. Following the complete addition of the mixed-metal salt solution, the thick suspension was stirred at room temperature for an additional 2 hours, and then aged at 70°C ($\pm$5°C) for approximately 18 hours. Once the suspension had cooled to 28°C, the final pH was 9.7. The crystals were washed by repeatedly centrifuging, decanting the supernatant and shaking in fresh DDI water until most of the chloride had been removed (as judged by the addition of $AgNO_3$). The final product was stored under DDI water in a sealed Nalgene™ bottle until needed.

The terephthalate anions were replaced with polyoxometalate anions in order to obtain the desired LDH-POM product. All anion exchange reactions were performed under nitrogen in order to avoid contamination by atmospheric CO_2. A typical procedure involved the addition of 15.3g of moist $Mg_6Ga_2(OH)_{16}TA$ (corresponding to approximately 2.8g dried weight) to 250 mL DDI water, followed by sufficient stirring to produce a homogeneous suspension of the LDH-TA precursor. The pH of the LDH slurry was then adjusted to about 5.5 by the addition of 20% HNO_3. Approximately 7.13 g of $Na_7PW_{11}O_{39}$ was dissolved in 100 mL of DDI water and then added dropwise to the LDH slurry with co-addition of nitric acid to maintain a constant pH value of about 5.5-6.0. After complete addition, the slurry was stirred at room temperature for 2 hours, and then at 70 °C for an additional 18 hours in order to improve the crystallinity of the final product. The product was washed several times by repeatedly centrifuging, decanting and resuspending in fresh DDI water. After the final decanting step, the product was air dried overnight at room temperature, and was stored in vials.

2.1.3 LDH-OH/LDH-adipate precursor route

The synthesis described here is for a Mg_3Ga-carbonate precursor (Mg_3Ga-CO_3). LDH-carbonate precursors with different Mg^{2+}:Ga^{3+} ratios, or different M^{2+} or M^{3+} cations in the layers, were synthesized under similar conditions. In the initial step of this synthetic route the desired interlayer anion species is the carbonate anion, therefore

reactions were conducted in a vessel that was open to the atmosphere since contamination by atmospheric CO_2 was not a problem.

A 2-L, three-neck round bottom flask was equipped with a pH probe and an addition funnel. The flask was charged with 600 mL of fresh DDI water, and the pH was adjusted to 10.0 by the addition of 2 M NaOH. A mixed metal nitrate solution (16.07 g $Ga(NO_3)_3 \cdot 9\,H_2O$ and 48.15 g $Mg(NO_3)_2 \cdot 6\,H_2O$ in 390 mL DDI water) was added dropwise with vigorous stirring at a constant temperature of 40°C. The pH was maintained at 10.0, first by the co-addition of a mixed Na_2CO_3/NaOH base solution (final CO_3:Ga ratio was 1.5) and then by the co-addition of 2 M NaOH solution. After complete addition of the mixed metal nitrate solution, the resulting thick white suspension was allowed to stir for 2 hours at 40°C, and then for an additional 40 hours at 70°C. The final product was washed by repeated cycles of centrifuging and shaking in fresh DDI water (three cycles), and then dried overnight in air at 90°C.

From this point on, all reactions were performed under flowing nitrogen in order to minimize competing reactions with carbonate anions from atmospheric CO_2 sources. The first step in preparing the LDH-hydroxide precursor was to decompose the above LDH-CO_3 precursor by heating at 500°C in a quartz tube furnace under flowing nitrogen for 5 hours. After cooling to room temperature under flowing nitrogen, 1.0 g of the resulting mixed oxide solid solution was quickly transferred to a sealed 1 L round bottom flask and stirred at room temperature in 100 mL of fresh DDI water under flowing

nitrogen for 5 days. The product, which is denoted Mg₃Ga-OH, was not isolated or washed; the slurry was kept under nitrogen and was immediately used in the next step of the synthesis. The temperature of the slurry was increased to 55°C and a 200% excess of adipic acid (0.96 g) dissolved in 100 mL of slightly warmed DDI water was added all at once, and then stirred at 55°C under flowing nitrogen for one hour. The Mg₃Ga-adipate precursor was also used directly in a subsequent step of the synthesis, and therefore was not isolated or washed.

After stirring for one hour at 55°C, the magnetic stirrer was turned off, and the above LDH-adipate slurry was allowed to settle. Once the solid material had formed a separate layer at the bottom of the flask, approximately 50 mL of the clear liquid was removed. Stirring was resumed and the temperature was increased to approximately 94°C (2 degrees below the boiling point in Calgary) and an additional 100 mL of boiling DDI water was added all at once. Boiling POM solution (i.e. 1.65 g $(NH_4)_6H_2W_{12}O_{40}$ in 50 mL DDI water) was placed in a pressure equalized addition funnel above the flask, and was added rapidly but dropwise at ambient pH to the vigorously stirred LDH-adipate slurry. An additional period of aging, lasting between five minutes and two hours at near-reflux temperature, was performed after the complete addition of the POM solution in order to improve the crystallinity of the product. The suspension containing the product was then quickly cooled in an ice bath, was centrifuged, and was washed two times with fresh DDI water. Crystals of the final product were air dried at room temperature, ground, sieved (60-80 and 80-100 mesh size) and stored in separate vials until needed.

2.2 Catalyst Characterization

2.2.1 Powder X-ray diffraction studies

Powder X-ray diffraction patterns were obtained with a Scintag XDS 2000™ diffractometer using Cu K_α radiation (λ = 1.540562 Å). Samples were step-scanned either from 3 to 30° 2θ or 3 to 65° 2θ in 0.025° steps with a stepping time of 1 second. Preferred orientation x-ray diffraction (POXRD) patterns were recorded at room temperature. The oriented film specimens were prepared by evaporating to dryness an aqueous suspension of the sample on glass slides. Random powder mounts were prepared for all mixed oxide solid solutions by grinding the calcined material and transferring to an aluminum sample holder prior to measuring the diffraction pattern at room temperature. Thermal stability studies were conducted by heating oriented samples on glass slides in a tube furnace for one hour at the indicated temperature under flowing nitrogen, followed by measurement of the XRD pattern at room temperature.

2.2.2 Infrared spectroscopic studies

Infrared (IR) spectra of the samples pressed in KBr pellets were obtained at a resolution of 2 cm^{-1} between 4000 and 350 cm^{-1}. Spectra were collected using either a Mattson Instruments 4030 Galaxy Series FT-IR spectrometer, using 500 sample scans and 124 background scans, or a Mattson Instruments Genesis Series FT-IR using 32 sample scans and 32 background scans. In each case the sample was referenced against air.

2.2.3 Inductively coupled plasma-atomic emission spectroscopy (ICP-AES)

Chemical analysis for Mg, Zn, Ga, Al and W was performed using a Thermo Jarrell Ash Atom Scan 16 ICP spectrometer. Approximately 2 mg of sample (60-80 mesh) was dissolved in 100 mL of 5% HNO_3. The following wavelengths were used for the analysis: Mg (279.5 nm), Ga (294.364 nm), Al (396.1 nm), Zn (213.8 nm) and W (239.7 nm). Concentrations were obtained from calibration curves that were prepared using commercially available standard solutions and the reagent blank.

2.2.4 Magic angle spinning solid state NMR (MAS-NMR)

^{27}Al and ^{71}Ga MAS-NMR spectra were obtained at 78.2 MHz and 91.5 MHz, respectively, on a Bruker AXM2-300 NMR spectrometer under an external magnetic field of 7T. Rotors containing the packed samples were spun at the magic angle (54° 44' relative to the external magnetic field) at a spinning rate of 10 kHz or 14 kHz for the ^{27}Al or ^{71}Ga samples, respectively. Typical acquisition parameters were 7000 scans with a 0.7 μs excitation pulse and 1 s delay for the ^{27}Al NMR spectra and 120 000 scans with a 0.8 μs pulse and 0.5 s delay for the ^{71}Ga NMR spectra.

2.2.5 Surface area measurements

Surface area measurements were made using the BET method on an ASDI RXM 100 instrument at an adsorption temperature of 77 K, after pretreating the 60-80 mesh or 60-100 mesh sample under high vacuum at 125°C or 200°C for two hours, or at 550°C for four hours, depending on the purpose of the experiment. The mass of sample used in

each case was chosen such that approximately 4 m^2 of total sample surface area was present in the sample tube. Four data points were collected using initial pressures of nitrogen that were chosen in order to yield final P/P_o values of 0.02, 0.04, 0.08 and 0.16, which are approximately evenly spaced along the linear portion of the BET adsorption isotherm. The dry weight of the sample, as measured after the adsorption experiment, was used to obtain the final value of the specific surface area.

2.2.6 Elemental analysis

Analysis for carbon, nitrogen and hydrogen was performed using a Control Equipment Corporation 440 Elemental Analyzer using approximately 2 mg of sample. The instrument had an absolute precision of ± 0.3%.

2.2.7 Micropore size distributions

Micropore size distributions were derived from argon adsorption isotherms obtained at 87 K, after pretreating the 60-80 mesh sample at 125°C for two hours under high vacuum. The mass of sample used in each case was governed by the specific surface area (SA) of the particular LDH-POM (as determined above), in order to provide a total surface area of 17 m^2. Thus the amount of sample used was equal to 17m^2/SA. The software used to analyze the argon adsorption data was based on the Saito-Foley model for cylindrical pores[96], making use of the physical parameters listed in Table 1.7. A cylindrical pore model represents the structure of the micropores that are present in pillared LDH materials better than alternative models that assume slit-like pore geometry.

Table 2.1: Physical parameters of argon and the oxide anion used in the Saito-Foley model for micropore size determinations

physical parameter	oxide anion	argon
diameter	0.276 nm	0.336 nm
surface density	1.31×10^{15} molec/cm^2	8.52×10^{14} molec/cm^2
magnetic susceptibility	1.3×10^{-29} cm^3	3.25×10^{-29} cm^3
polarizability	2.5×10^{-24} cm^3	1.63×10^{-24} cm^3

2.3 Catalytic work - Model compound studies

2.3.1 Model reaction: conversion of 2-propanol

Selectivity in the decomposition reaction of 2-propanol has previously been used as a means of investigating the acid-base properties of the catalytic sites of metal oxide surfaces[97]. The dehydration of 2-propanol to form propene is assumed to be catalyzed by acid sites, whereas acetone is formed by dehydrogenation of 2-propanol via a concerted mechanism involving both acid and basic sites[97,98]. The rate of formation of propene (r_p) may be regarded as a measure of the acidity of the active sites, whereas the ratio of the dehydrogenation rate (r_a) to the dehydration rate (i.e. r_a/r_p) is a measure of the basicity.

2.3.2 Experimental setup

A quartz tube, continuous flow, fixed bed microreactor was used to carry out the catalytic conversion of 2-propanol. Approximately 150.0 mg of 60-100 mesh LDH-POM material was placed on a quartz frit at the center of a quartz reactor tube; the frit was

positioned within the reactor tube such that the sample was supported at the center of the

furnace. A smaller mass of each LDH-CO$_3$ material was used, generally about 35-40 mg,

which yielded a catalyst bed of approximately the same thickness that was used for the

LDH-POM materials. A flow diagram of the reactor system is illustrated in Fig. 2.1.
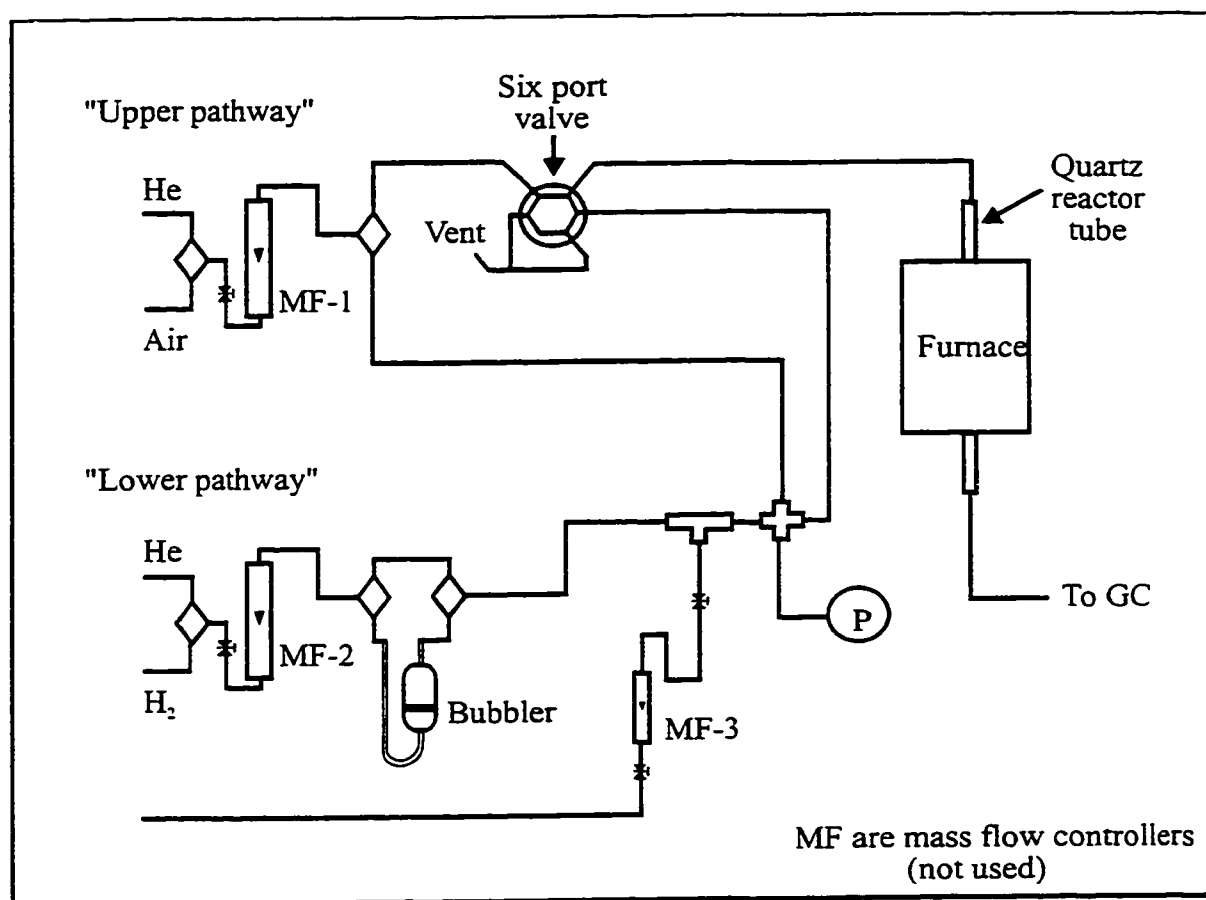
Fig. 2.1: Flow diagram of the reactor used for the catalytic conversion of 2-propanol.

During pretreatment, helium from the upper pathway was passed through the six

port valve and then directly into the quartz reactor tube. Pretreatment of the catalyst

samples was carried out either at 200°C for two hours or at 550°C for four hours. The

catalyst was then cooled to the initial reaction temperature under flowing helium. In order to start the reaction the six port valve was switched to allow the helium to carry the 2-propanol out of the bubbler and directly into the reactor tube. The bubbler was thermostated at 22°C with a constant He flow rate of 22 mL/min, resulting in a constant feed rate of 2.582 mmol 2-propanol per hour.

The reaction proceeded for six minutes before the first of the data points was collected, thus allowing the system to reach a steady state and to ensure that the temperature of the reactor was stable. Analysis of the products was accomplished by on-line gas chromatographic separation using a Hewlett Packard HP 5890 gas chromatograph equipped with a stainless steel column (3 mm o.d., 3 m long) packed with Poropak Q (80-100 mesh). During the reaction the effluent from the reactor was continuously passed through a sample loop, which was automatically sampled every 15 minutes. The oven was held at a constant temperature of 160°C, and detection was achieved using a hydrogen flame ionization detector (FID) at 180°C. The retention times and relative sensitivity[99] for each component are listed in Table 2.2.

Table 2.2: Retention times and relative sensitivity data for 2-propanol and the expected reaction products

molecule	retention time (min)	relative mass sensitivity
propene	2.30	1.0
acetone	9.83	0.49
2-propanol	11.08	0.53

2.3.3 Data interpretation

The raw intensity (area under the GC peak) for each compound was corrected by dividing by the relative mass sensitivity (rs) listed in Table 2.2, and then was used to calculate the mass percent of each compound present in the reactor effluent according to Eq. (1).

$$\text{mass \% A} = \frac{(\text{Area A}) / (\text{rs})}{\Sigma_i \, [(\text{Area})_i / (\text{rs})_i]} \times 100\% \tag{1}$$

The mass percent value was then converted into a mole percent (or % yield) after taking into account the formula weight of each compound. The rate of formation of propene r_p and of acetone r_a were calculated by multiplying the mole percent of each product by the feed rate of 2-propanol (2.582 mmol/h). To facilitate direct comparison, the rates were normalized on a unit area basis by multiplying by the mass of catalyst after pretreatment (m) and dividing by the surface area of the catalyst after pretreatment (SA).

$$\text{rate of formation of A} = \frac{(\text{mole \% A}) * (2.582 \text{ mmol 2-propanol/h})}{(\text{SA}) * m} \tag{2}$$

Selectivity was defined as the mole percent of a particular product divided by the total mole percent of acetone and propene.

$$\text{Selectivity to A} = \frac{\text{mole \% of product A}}{\text{mole \% of propene} + \text{mole \% of acetone}} \times 100\% \tag{3}$$

These calculations can be justified on the basis that the only products observed were propene and acetone, and that one molecule of 2-propanol is converted to either one molecule of propene or one molecule of acetone. Deactivation data for the catalyst samples were calculated according to equation (4).

$$\text{Deactivation} = \frac{(\text{conversion after 6 minutes}) - (\text{conversion after 2 hours})}{(\text{conversion after 6 minutes})} \qquad (4)$$

2.4 Reproducibility of results

Layered double hydroxides are non-stoichiometric materials that are capable of forming with variable chemical compositions. The general LDH formula was discussed in Section 1.1.1, and it was stated that the properties of the LDH product could be altered by varying the identities and/or mole fraction of the M^{2+} or M^{3+} metal cations in the LDH layers. In addition the number of steps involved in the complex syntheses used to produce LDH-POM materials, some of which are performed by hand and are therefore difficult to replicate from one synthesis to another, result in additional minor compositional and textural variations arising in the different samples. Thus, it is unrealistic to expect absolute reproducibility in the chemical and physical properties of different synthetic samples.

Despite these difficulties, however, successive syntheses of similar LDH materials in which slight modifications to the synthesis conditions were made have indicated that the general trends observed for the individual layer types are reproducible. Therefore,

while the observations and conclusions described in this thesis are valid, the exact numerical values (e.g. precise chemical composition, specific surface area, micropore volumes, etc.) may not be perfectly reproducible in future syntheses.

Some of the techniques used to characterize the various LDH-POM products and intermediate products are qualitative in nature (i.e. POXRD, infrared spectroscopy and MAS-NMR spectroscopy). Samples characterized by these techniques were selected randomly from the bulk sample and were assumed to be representative of the composition of the bulk. Since these techniques were used only to detect the presence of specific chemical species, and a quantitative measurement was not desired, special precautions to ensure complete homogeneity of the overall product were not necessary. Reasonable effort was exercised to ensure that similar quantities of sample were present in all analyses involving absorbance or diffraction of radiation, in order to avoid the usual difficulties associated with the specific phenomena.

Quantitative results were reported for the BET-N_2 surface area measurements, micropore size distribution experiments, ICP-AES analyses and elemental analyses (CHN). The repeatability of each method was ascertained initially by performing duplicate analyses of several samples, and was confirmed periodically by repeating the analysis of randomly selected samples, or by analyzing a different sample of a specific product that produced an unusual result. A discussion of the individual techniques follows, with emphasis on the specific factors that could affect the reproducibility of each type of measurement.

BET-N_2 surface area measurements are sensitive to the pretreatment conditions and drying history of the LDH sample. Thus, an effort was made to reproduce, as closely as possible, the heating rate, maximum pretreatment temperature and the length of pretreatment from one measurement to the next. The system was calibrated prior to every measurement using helium gas, and four data points on the BET isotherm were collected during the N_2 adsorption step. Repeat measurements of the same sample, when performed, deviated by less than 5%.

The micropore size distribution measurements are also expected to be sensitive to the pretreatment history of the samples, as was previously discussed for the BET-N_2 surface area experiments. The effect of different pretreatment temperature on the pore sizes and pore volumes is likely to be quite dramatic, therefore consistent pretreatment procedures were used for all samples. The accuracy of the instrument used to determine the micropore size distributions was tested using zeolite Na-Y as a standard, and was found to reliably display a narrow distribution centered very near 7 Å, as expected.

ICP-AES measurements of 2-10 mg of LDH material dissolved in dilute HNO_3 were initially performed using two wavelengths whenever possible, to ensure that there was no interference from other elements in solution. In addition, three individual measurements of each sample were performed at each wavelength, and the average concentration value was utilized. It was anticipated that errors associated with the accuracy of measuring 2-10 mg of sample would not affect the results of the analysis since it was only the *ratio* of the concentration of two species in solution that was of

interest. A two point calibration curve was prepared prior to the analysis of each set of samples, using the sample blank (5% HNO_3) and a multi-element standard that contained each element (commercial standards diluted to 40 ppm concentration) as the zero and high concentration solution, respectively. Elemental analysis for carbon, hydrogen and nitrogen content was generally required only for semi-quantitative or qualitative purposes, therefore a single analysis was performed for each sample

The reproducibility of the catalytic results appearing in Chapter 5 was confirmed by performing numerous duplicate experiments in the early stages of the study. Duplicate catalytic runs were performed following the standard activation procedure, using either a fresh sample of an LDH-POM prepared in the same synthesis, or an LDH-POM of similar composition from a different synthesis. Excellent reproducibility of the catalytic data was observed, as discussed in Chapter 5, thus the remaining LDH-POM catalyst samples were tested only once. As a further precaution, the reactor temperature was changed in a random manner in order to prevent a systematic influence of deactivation phenomena. Furthermore, after collecting data for the final reaction temperature, the reactor was returned to the initial reaction temperature in order to establish that the same steady state conversion was achieved at the beginning and at the end of the experiment; in all cases this was found to be true.

Chapter 3

The Organic Anion Precursor Route

3.1 Overview

Prior to 1988 the standard method for preparing LDH materials with isopoly- or heteropoly oxometalate anions as the interlayer species was by anion exchange of the chloride or nitrate containing LDH precursor[92,100]. Both precursors were readily obtained in high yield by coprecipitation of the appropriate salts of the desired M^{2+} and M^{3+} metal cations from aqueous solution under a nitrogen atmosphere[30]. The final LDH-POM product was subsequently obtained by the addition of an excess amount of the POM anion to an acidified suspension of the precursor LDH, followed by aging at elevated temperature and washing. In this way, multi-hundred gram quantities of LDH-POM materials could be obtained in less than three days without the need for specialized glassware or equipment.

More recent investigations have indicated that there are severe limitations to the usefulness of the above synthesis method[51,52]. In general the high layer charge densities that are typical of LDH materials result in strong interactions between the LDH layers and the interlayer anions, thus reducing the ease with which the anions are displaced. It has

been shown that anion exchange reactions of LDH proceed with greater difficulty as the charge density of the material increases (i.e. as R becomes smaller)[101]. In addition, the relatively small gallery height imposed by the chloride or nitrate anions physically impedes the entrance of the much larger POM anions into the interlayer space[8].

One promising method for the synthesis of LDH-POM materials was proposed by Drezdzon[8]. In this method an LDH precursor containing a large organic anion was initially prepared via a slightly modified version of the standard coprecipitation method[30]. The choice of organic anion should result in a precursor gallery height that is close to the value expected in the final LDH-POM, and thus the layers are essentially swollen apart by the organic anions, and so the interlayer space becomes more readily accessible to the POM anions. It was found that the addition of nitric acid or hydrochloric acid to a suspension of the organic anion intercalated LDH material resulted in the formation of the chloride- or nitrate-containing phase. The author suggested that as the suspension was acidified, the organic anions became protonated and thus the electrostatic attractions between the LDH layers and the interlayer anions were weakened and anion exchange occurred.

Based on the encouraging results of the acidification study, attempts were made to incorporate isopoly oxometalate anions between the layers via an ion exchange reaction. In the original paper, the polymeric heptamolybdate (Mo_7O_{24}) or decavanadate ($V_{10}O_{28}$) species were generated _in situ_ by the addition of an aqueous solution containing either Na_2MoO_4 or $NaVO_3$ followed by acidification of the reaction mixture with HNO_3.

Lowering the pH of the reaction mixture had the two-fold effect of allowing the isopoly oxometalate anions to form and to protonate the interlayer anions and thus facilitate the displacement of the organic anions by the POMs.

The organic anion precursor method for preparing LDH-POMs has more recently been applied to Zn_RAl layers[50], however no other layer types have been reported. In addition, the anion exchange properties of LDH materials intercalated with benzoate[47], p-methylbenzoate[50] and p-hydroxybenzoate[50] anions have been investigated. It was determined that a wide variety of organic anions are capable of swelling the LDH interlayer region and thus facilitating the incorporation of POM anions.

3.2 LDH layers containing basic cations: the Mg_RAl and Mg_RGa series

The vast majority of LDH-POM materials reported in the literature contain Al^{3+} as the trivalent metal cation in the LDH layers. Based on the successful implementation of this method for the synthesis of well ordered pillared LDH phases of various compositions, the decision was made to extend the method further in order to include the synthesis of gallium containing LDHs. Reports of LDHs containing Ga^{3+} as the trivalent metal cation prior to undertaking this work were limited to the carbonate containing materials[16,102]. The substitution of Ga^{3+} for Al^{3+} has been shown in other cases to affect the catalytic properties of inorganic oxide materials. For example, Ga-H-ZSM-5 has previously been shown to promote the conversion of light paraffins to aromatics via the

Cyclar process[103], and gallium containing pillar interlayered clay minerals (PILCs) are known to be active for the dehydrogenation of propane to propene[104].

3.2.1 Analysis of LDH materials by POXRD: Relevant theory and background

Preferred orientation x-ray diffraction (POXRD) spectroscopy is one of the most widely used techniques for characterizing layered materials. The experimentally measured parameter is the angle of diffraction (θ) of a beam of x-rays by atom planes within the LDH structure. The layer repeat distance (d) is related to the angle of diffraction through Bragg's law, $n\lambda = 2d\sin\theta$, where n is the order of diffraction and λ is the x-ray wavelength. The d_{003} diffraction peak is the first order reflection arising from the separation between adjacent layers, as shown in Fig. 3.1, and is generally observed as the peak at the lowest value of 2θ in the powder pattern (see Fig. 3.2). Higher order diffraction lines, corresponding to n = 2, 3 etc. (i.e. d_{006}, d_{009}), appear as equally spaced lines at larger 2θ values. As was discussed in Section 1.1.4, the gallery height may be obtained by subtracting the thickness of one layer (4.8Å) from the d_{003} spacing.

In addition to providing information on the gallery height, the degree of crystallinity (size in the z-direction) of the sample may also be inferred from the d_{003} reflection since there is an inverse relationship between the width of this peak and the degree of crystallinity. Assuming that the anions within the interlayer region are well ordered, the particle-size broadening effect is expressed quantitatively by the Scherrer equation, $D = 0.9\ \lambda/(\beta_c\cos\theta)$, where D is the mean crystallite size (Å) along a line normal

to the reflecting plane, λ is the x-ray wavelength, β_c is the instrument corrected width of

the d_{003} harmonic at half-height expressed in radians and θ is the diffraction angle[105].
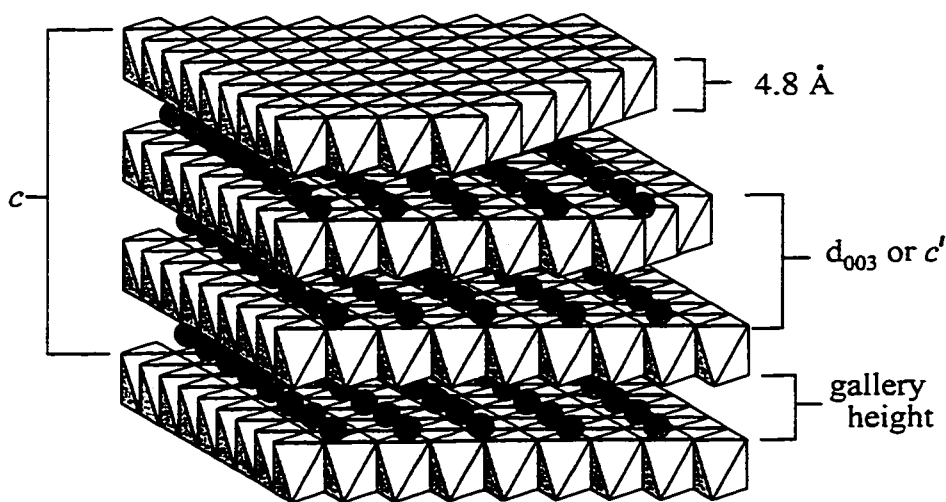
Fig 3.1: Definition of the crystallographic c parameter and d_{003} (c') values

The ordering of LDH crystallites that occurs when an aqueous LDH suspension

is evaporated to dryness on a smooth substrate results in the selective enhancement of the

$d_{00\ell}$ reflections, while those reflections that are due to the ordering of cations within the

layers are not enhanced. X-ray diffraction analysis of oriented samples allows a better

discrimination between the basal (00ℓ) reflections (the intense and sharp lines at high

values of 2θ) and the non-basal lines, and facilitates their discrimination from the

reflections due to impurities[106,107,108].

Unfortunately, preferred orientation samples do not display theoretical peak

intensities, which only occur in completely random samples, and therefore it is not

possible to obtain quantitative information. As an example, an x-ray diffraction pattern

that was obtained from an oriented film sample of Zn_4Al-TA appears in Fig. 3.2a, and the

pattern obtained from the same material as a random powder mount of coarsely ground

particles is shown in Fig. 3.2b. In the pattern obtained from an oriented sample the $d_{00\ell}$
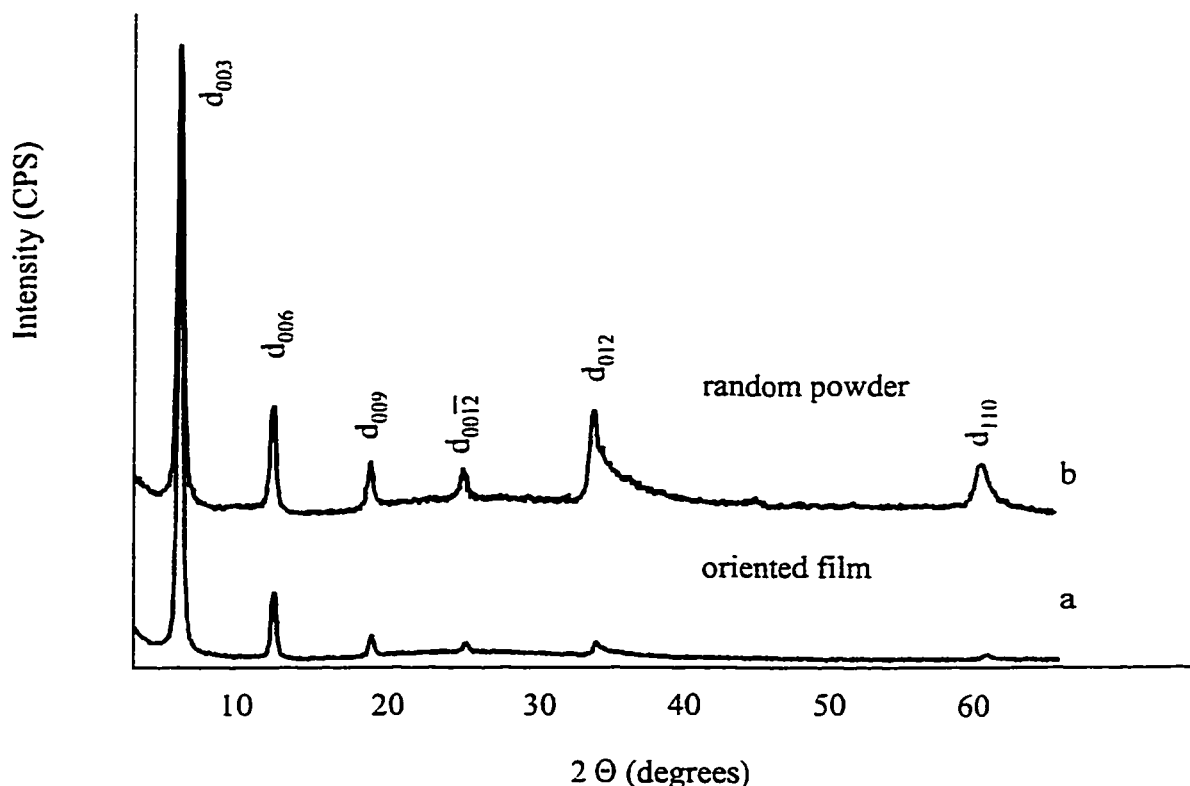
Fig. 3.2: X-ray diffraction patterns of Zn_4Al-TA as a) an oriented film and
b) a random powder mount

reflections are significantly enhanced relative to the d_{110} and d_{012} reflections. The

selective enhancement of the $d_{00\ell}$ harmonics is due to the basal planes in an oriented

sample being preferentially exposed to the incident x-ray beam. Thus, although an

oriented film and a random powder may contain the same total number of diffraction centers, the observed x-ray intensity will differ depending upon how many of the centers are properly aligned to diffract the x-rays at the Bragg angle.

Furthermore, the relative intensities of the reflections arising from different phases present in the oriented film are sensitive to the manner in which the ordered sample was prepared. For example, an aqueous suspension of Zn_3Al-TA was centrifuged at 200 rpm for 2 minutes. Under these conditions, the LDH crystallites did not completely settle to the bottom of the test tube, but instead a gradient was created in which the particle size and particle number density increased from top to bottom. Thus, in Fig. 3.3 the POXRD pattern of the sample prepared from the top portion (Fig. 3.3a) appears to have a relatively smaller amount of the impurity phase (denoted by the asterisk, *) compared to the sample prepared from the bottom portion (Fig. 3.3b). In fact the difference may be attributed to the better orientation obtained in the film composed of fewer and smaller LDH crystallites[94], and to the lack of preferential orientation in the rather amorphous impurity phase. For the above stated reasons any attempt to quantify the relative amounts of POM pillared phases and impurity phases based on the diffraction patterns of oriented samples is meaningless, and therefore has not been discussed.

3.2.2 Comparative POXRD study of Mg_RGa-TA and Mg_RAl-TA precursors

A series of twelve Mg/Ga containing LDHs was prepared by coprecipitation of mixed metal chloride salt solutions with initial Mg:Ga ratios of 2:1, 3:1 or 4:1 at constant
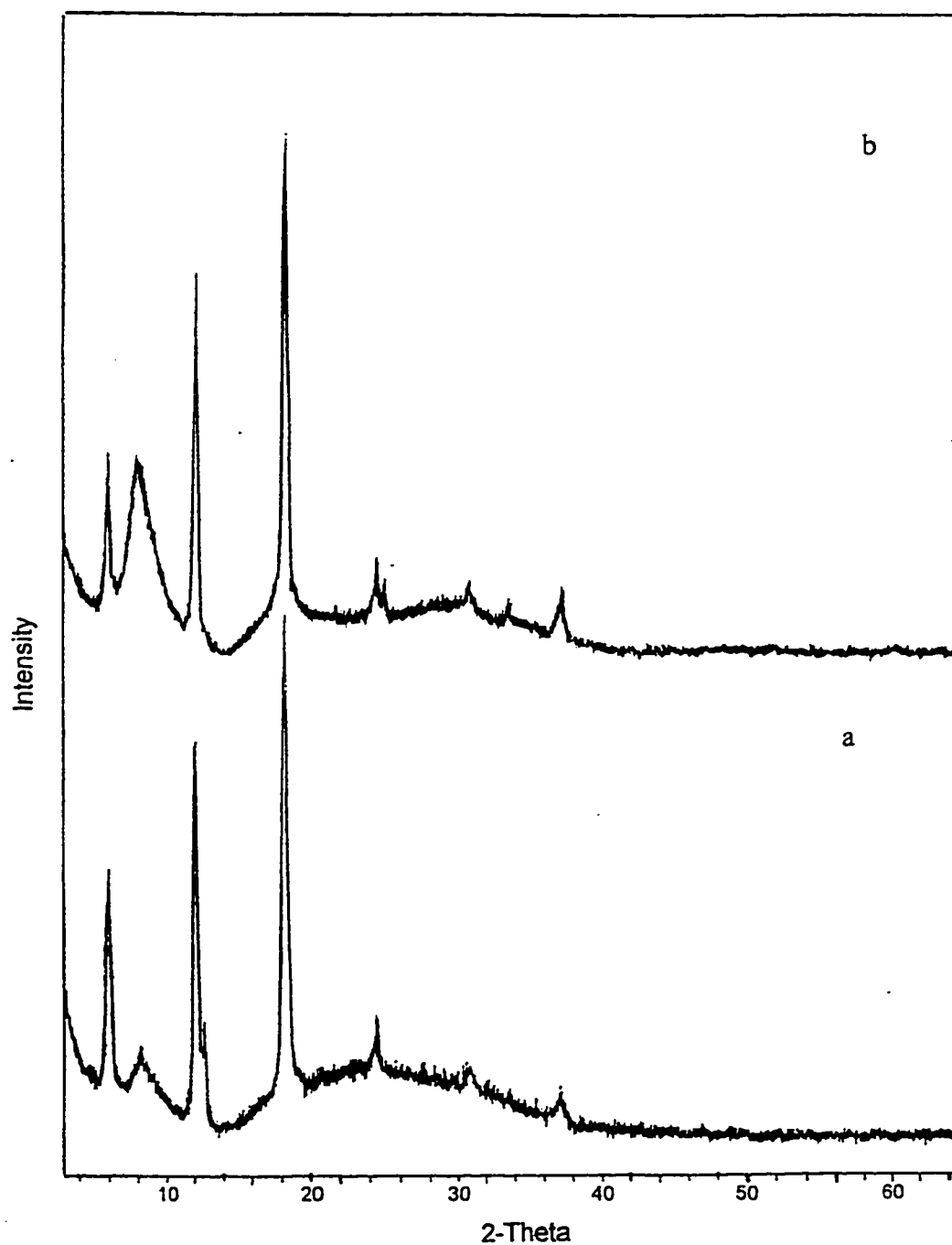
Fig. 3.3: POXRD patterns of Zn₃Al-H₂W₁₂ prepared using the a) top and b) bottom portion of the centrifuged sample

Fig. 3.3: POXRD patterns of $Zn_3Al-H_2W_{12}$ prepared using the a) top and b) bottom portion of the centrifuged sample

pH values of 10.0, 8.6, 7.7, or 6.8, in the presence of a two-fold excess of terephthalate

anions. Aluminum containing analogues were synthesized under similar experimental

conditions for comparison. The resulting products have been abbreviated $M^{2+}_R M^{3+}$-A^{n-},

where R is the M^{2+}:M^{3+} ratio in the initial mixed metal salt solution and A^{n-} is the desired

interlamellar anion (but not necessarily the anion that was actually incorporated).

POXRD patterns corresponding to Mg_RGa-TA products coprecipitated at pH 10.0, 8.6,

7.7 and 6.8 are presented in Figs. 3.4, 3.5, 3.6 and 3.7, respectively. The corresponding

patterns for the Mg_RAl-TA analogues are presented in Figs. 3.8, 3.9, 3.10 and 3.11. The

d_{003} reflection values and BET-N_2 surface areas have been summarized in Table 3.1.

Table 3.1: d_{003} spacing and BET-N_2 surface area of Mg_RGa-TA and Mg_RAl-TA layered double hydroxides coprecipitated at various pH

M^{2+}:M^{3+} molar ratio, R, in synthesis mixture	Coprecipitation pH							
	6.8		7.7		8.6		10.0	
	d_{003}/Å	Area/ m^2g^{-1}	d_{003}/Å	Area/ m^2g^{-1}	d_{003}/Å	Area/ m^2g^{-1}	d_{003}/Å	Area/ m^2g^{-1}
Mg:Ga=4	14.13	32	14.02	35	7.946	40	8.13	61
Mg:Ga=3	14.13[a]	70	14.19	39	14.19	41	7.91	39
Mg:Ga=2	[a]	96	14.14	45	14.28	19	14.31	27
Mg:Al=4	14.08	5	14.03	22	14.07	0.1[b]	8.07	-
Mg:Al=3	14.13	68	14.09	62	14.16	0.1[b]	7.93	8
Mg:Al=2	14.23	35	14.09	68	14.30	38	14.25	34

[a] strong presence of gallium oxide hydroxide.
[b] diffuse POXRD pattern.
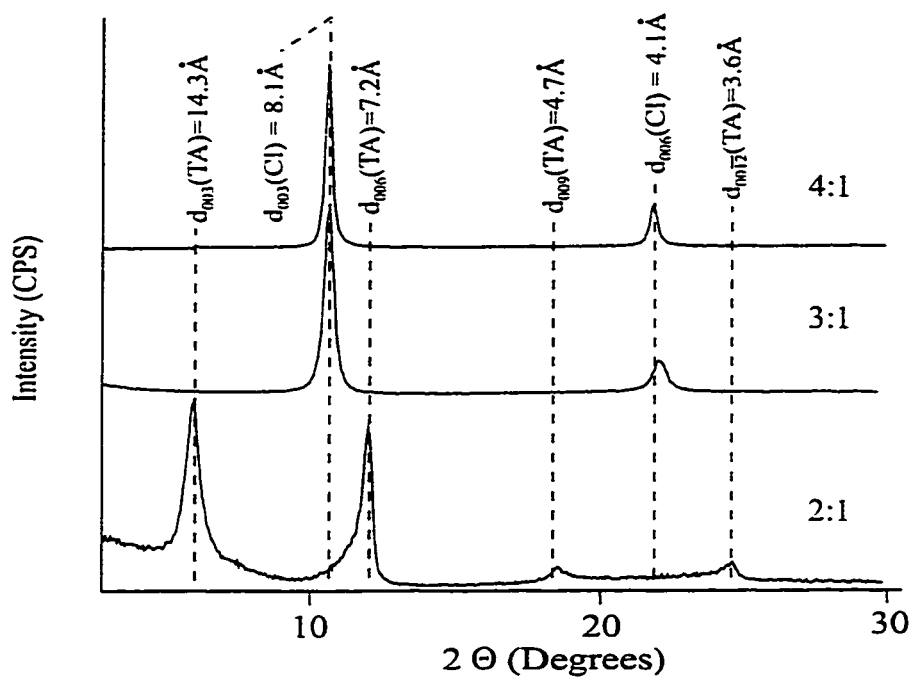
Fig. 3.4: POXRD patterns of Mg$_R$Ga-TA products obtained at pH 10.0
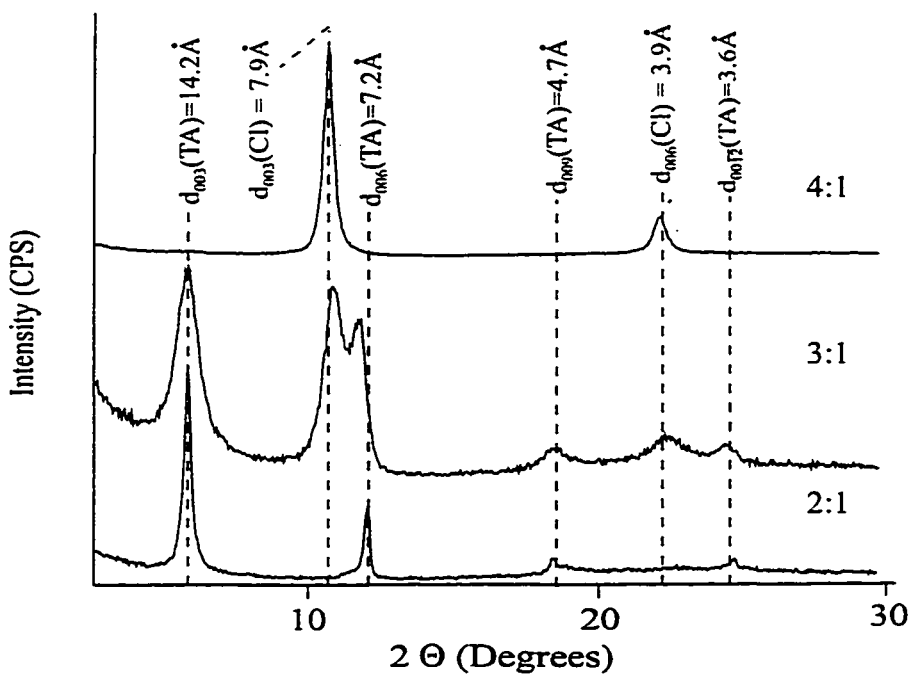
Fig. 3.5: POXRD patterns of Mg$_R$Ga-TA products obtained at pH 8.6
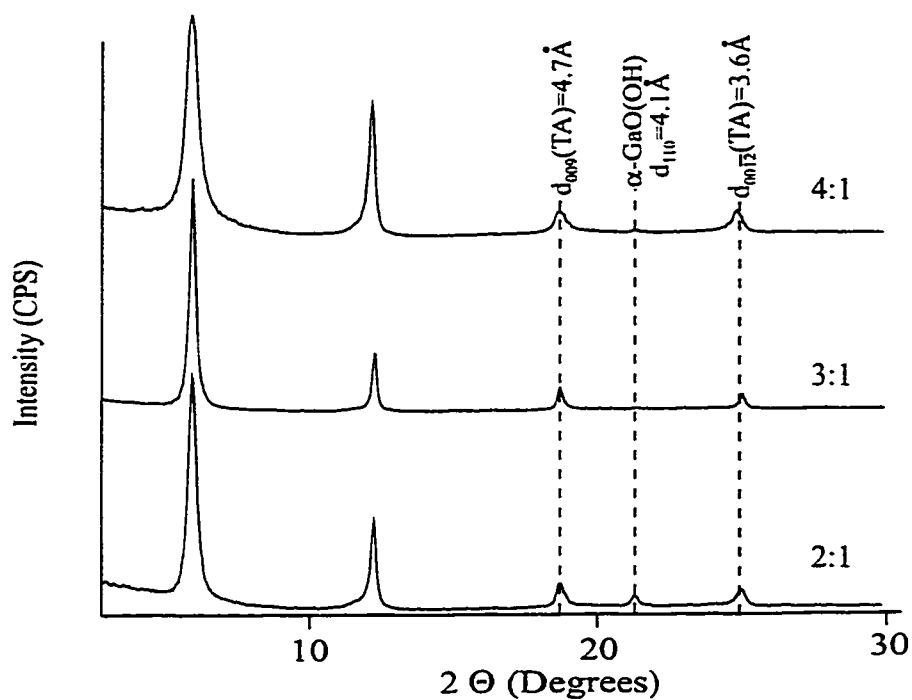
Fig. 3.6: POXRD patterns of Mg$_R$Ga-TA products obtained at pH 7.7
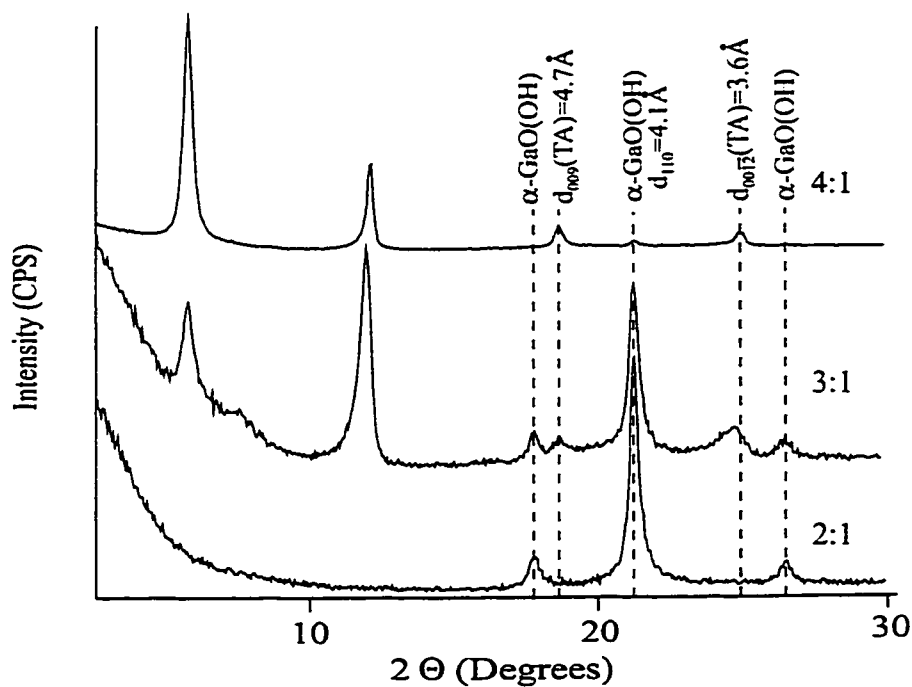
Fig. 3.7: POXRD patterns of Mg$_R$Ga-TA products obtained at pH 6.8
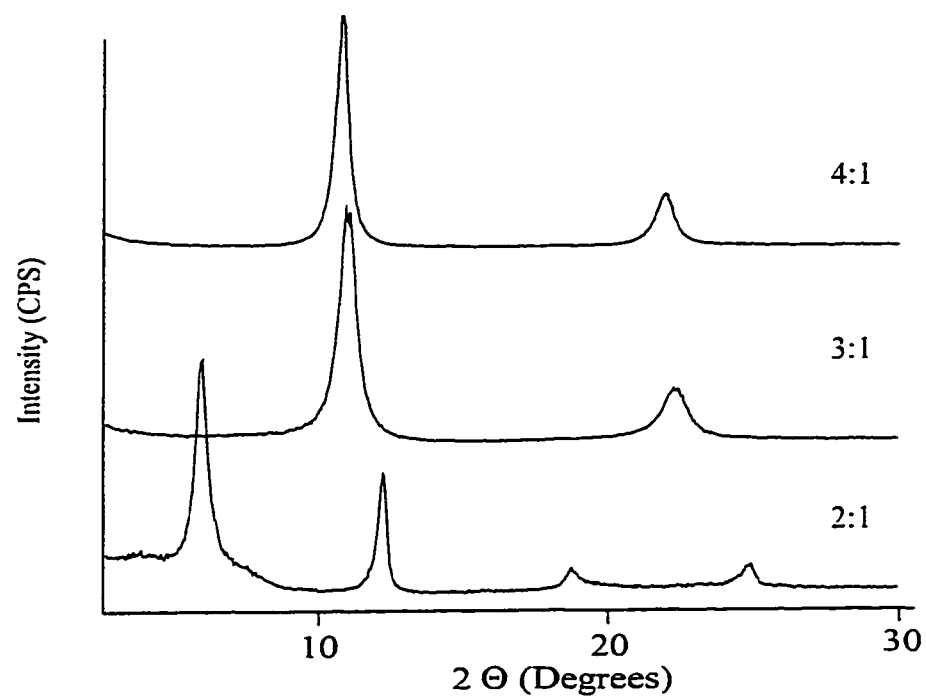
Fig. 3.8: POXRD patterns of Mg$_R$Al-TA products obtained at pH 10.0
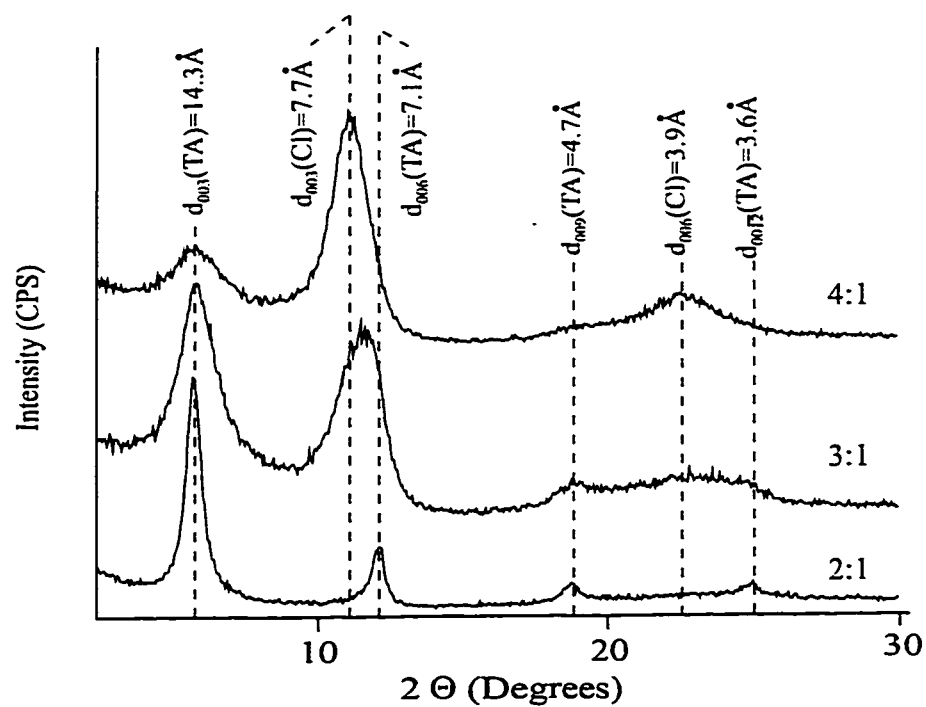
Fig. 3.9: POXRD patterns of Mg$_R$Al-TA products obtained at pH 8.6
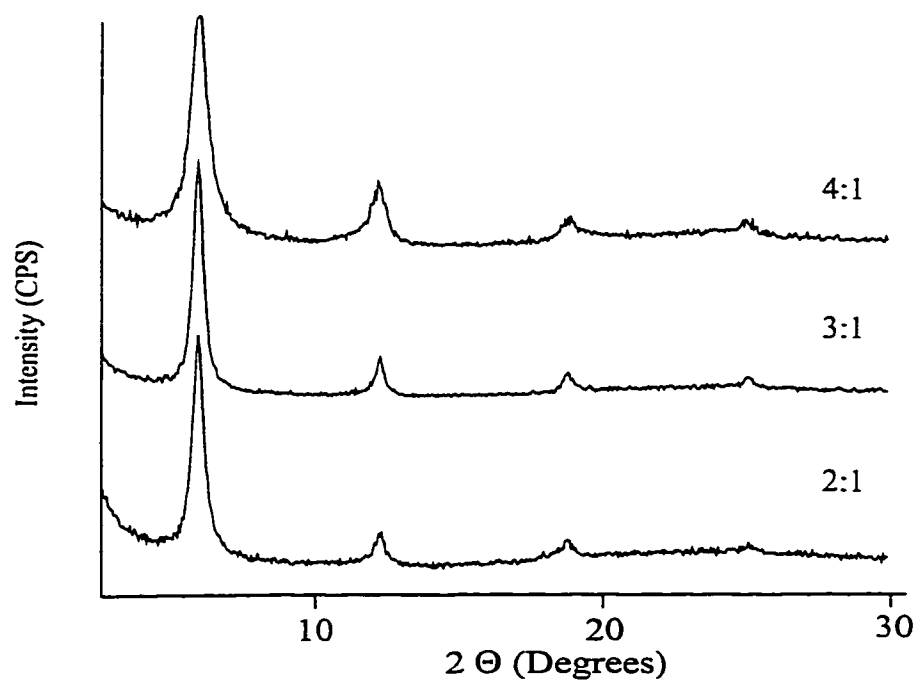
Fig. 3.10: POXRD patterns of Mg$_R$Al-TA products obtained at pH 7.7
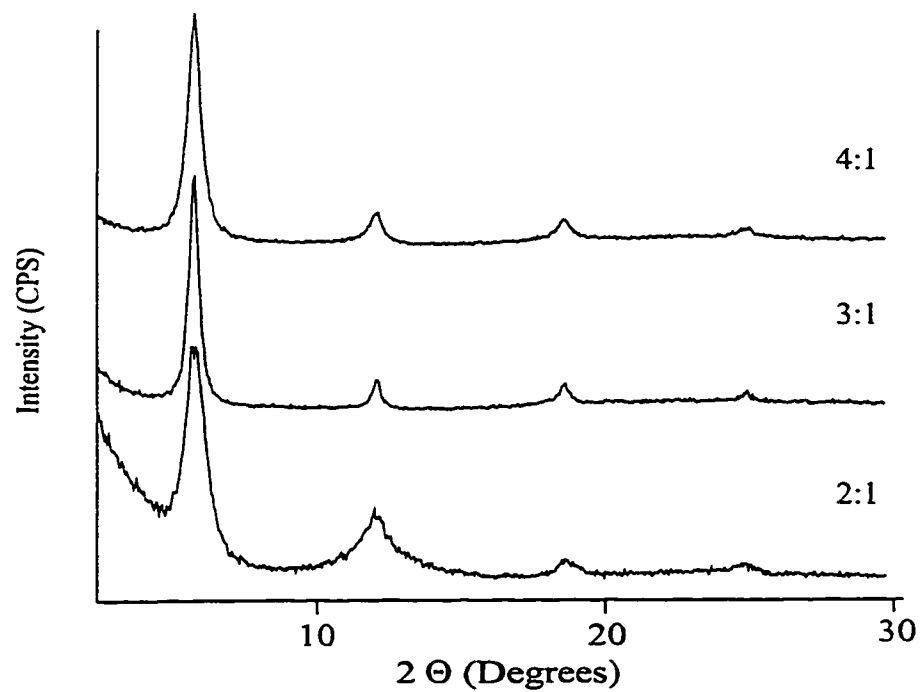
Fig. 3.11: POXRD patterns of Mg$_R$Al-TA products obtained at pH 6.8

The first attempts at synthesizing layered double hydroxides of the series Mg_RGa-TA and Mg_RAl-TA were performed at pH 10.0. This pH value was chosen because true coprecipitation conditions exist only at about pH 10 and above. Below pH 10 precipitation of the trivalent metal hydroxide occurs first, followed by reaction with Mg^{2+} cations remaining in solution[15]. ICP-AES analysis of the products revealed that in each case the $M^{2+}:M^{3+}$ ratio was nearly identical to the ratio that was initially present in the mixed metal salt solution (see Table 3.2). The noticeable exception to this trend was the Mg_2Ga-TA sample, which was determined to have the composition $Mg_{2.3}Ga$-TA. The magnesium enrichment in the Mg_2Ga-TA sample is probably attributed to the partial loss of Ga^{3+} due to the formation of soluble $Ga(OH)_4^-$, which forms at about pH 9^{109}. Analysis of the layer composition for the corresponding Mg/Al analogues yielded virtually identical results, confirming that nearly complete incorporation of M^{2+} and M^{3+} was achieved under the synthesis conditions.

Table 3.2: $M^{2+}:M^{3+}$ **molar ratios of** Mg_RGa-TA **and** Mg_RAl-TA **layered double hydroxides coprecipitated at various pH measured by ICP**

$M^{2+}:M^3$ molar ratio, R, in synthesis mixture	coprecipitation pH			
	6.8	7.7	8.6	10.0
Mg:Ga=4	1.2_3	1.3_3	3.0_0	4.0_0
Mg:Ga=3	0.5_4	1.2_5	2.5_3	2.9_9
Mg:Ga=2	0.2_0	0.9_6	1.8_8	2.2_9
Mg:Al=4	1.0_9	1.9_8	2.8_0	-
Mg:Al=3	1.1_6	1.6_3	2.5_1	3.0_8
Mg:Al=2	0.6_3	1.4_4	2.0_4	2.1_4

The powder diffraction patterns shown in Fig. 3.4, however, indicate that terephthalate-intercalated LDH materials (d_{003}=14.3Å, 2θ=6.17°)[13,20] are formed at pH 10.0 only if the Mg:Ga ratio in the layers is about 2:1 (lower pattern). Furthermore, the $d_{00\ell}$ reflections for this sample are broad and asymmetric, indicating that the product is poorly crystallized and that the anions in the gallery region are partially disordered. LDHs with larger Mg:Ga ratios, specifically Mg_3Ga-TA (middle pattern) and Mg_4Ga-TA (upper pattern), display d_{003} reflections that are characteristic of an LDH-chloride phase (d_{003}=8.1Å, 2θ=10.88°)[46]. The chloride containing phases appear to be more highly crystalline than the Mg_2Ga-TA product, i.e. *D* (mean crystallite dimension along a line normal to the reflecting plane) was calculated from the d_{003} reflections to be 135 Å and 265 Å for Mg_2Ga-TA and Mg_4Ga-TA, respectively. The behavior of Mg_2Al-TA, Mg_3Al-TA and Mg_4Al-TA precipitated at pH=10.0, as shown in Fig. 3.8, is virtually identical to that described for the corresponding Mg_RGa-TA.

The IR spectrum of an LDH-Cl contains only those bands that arise from the hydroxyl groups and metal-oxygen bonds in the inorganic layers. In order to confirm that the chloride anion was preferentially incorporated by the R = 3 and R = 4 LDHs, it was necessary to attempt the synthesis of a separate 'Mg_4Ga-TA' material under conditions identical to the ones described for the Mg_4Ga-Cl, with the exception that $Mg(NO_3)_2$ and $Ga(NO_3)_3$ were used in place of the chloride salts. The presence of the v_3 absorption band of nitrate near 1384 cm^{-1} would provide an unambiguous probe for identifying the

gallery species. In fact, the product obtained from a 4:1 $Mg(NO_3)_2/Ga(NO_3)_3$ mixed

metal salt solution at pH 10.0 displayed a POXRD pattern (not shown) that was very

similar to the upper pattern in Fig. 3.4, and thus conclusions based on the IR spectrum of
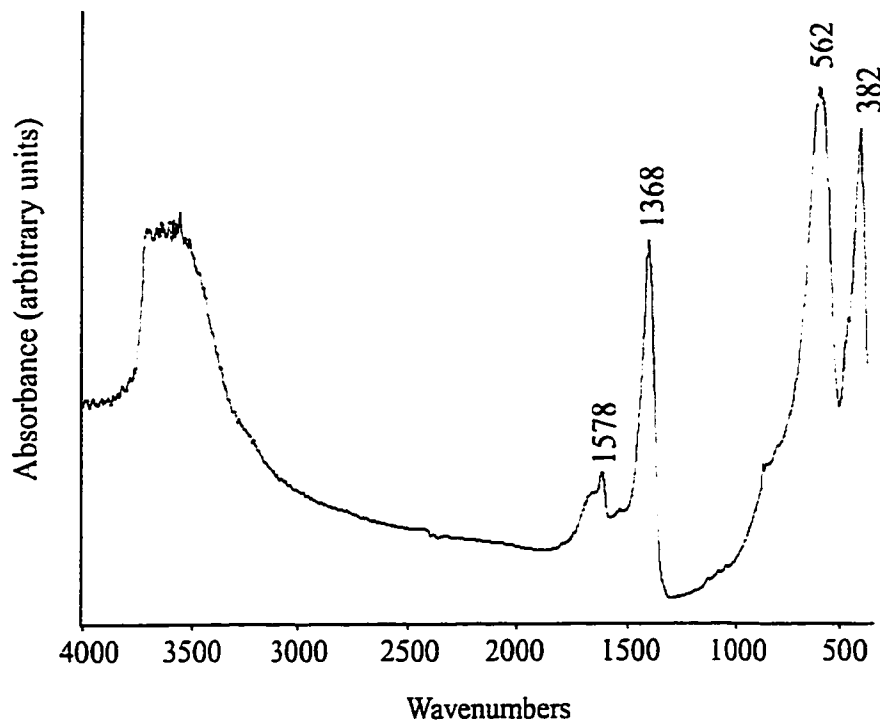
Fig. 3.12: IR spectrum of the "Mg₄Al-TA" product obtained at pH 10.0

the product obtained from the nitrate salts (see Fig. 3.12) should also apply to those

prepared using the chloride salts.

The IR spectrum in Fig. 3.12 was obtained from Mg₄Ga-TA prepared at pH 10.0

using the metal nitrate salts instead of the chloride salts, as described above. A broad

band between 3300-3700 cm⁻¹ is due to stretching modes of hydrogen bonded hydroxyl

groups of the LDH layers and interlayer water[110]. In addition, there are two bands

associated with the metal-oxygen modes of the LDH layers around 562 and 382 cm^{-1}. A broad water deformation band is present at about 1650 cm^{-1}, with a sharper band at 1578 cm^{-1} superimposed on top. The band at 1578 cm^{-1} is known to be one of the two main bands corresponding to terephthalate (the other is at about 1390 cm^{-1} and is always of nearly the same strength as the one at 1578 cm^{-1}). Finally, a very strong band appears at 1368 cm^{-1}, which could correspond to either the v_3 absorption band of the nitrate (1384 cm^{-1} in simple salts) or of the carbonate (1370 cm^{-1}) anions. We assign this band to the nitrate anion and assume that upon intercalation the position of the absorption band shifts by approximately 12 cm^{-1}. This assumption is supported by the observation of a similar shift of 14 cm^{-1} of the v_3 absorption of carbonate in Mg$_3$Al-CO$_3$ samples prepared by direct coprecipitation. A qualitative analysis of the interlayer anions based on the positions and relative intensities of the absorption bands indicates that there is minimal incorporation of terephthalate anions and that nitrate anions are preferentially incorporated under these synthesis conditions. Elemental analysis revealed that the sample contained 1.7% nitrogen and 2.9% carbon by weight, providing additional evidence that a considerable amount of nitrate incorporation occurred, and that only a trace amount (<15%) of terephthalate is present.

Thus, it is apparent that the layer composition exerts an influence on the incorporation of the gallery species. High layer charge density materials (i.e. R=2) are capable of incorporating the bulky terephthalate dianions, whereas the lower layer charge

density materials preferentially intercalate nitrate anions. The results for both Mg_RM^{3+}-TA series precipitated at pH 10.0 are consistent with those previously published by Kooli et al.[47] for the Mg_RAl-TA and Mg_RAl-BA series (BA=$C_7H_5O_2^-$, benzoate anion), where it was found that the carboxylate anion was incorporated at pH 10.0 only if the Mg:Al ratio was less than or equal to 2:1.

One possible explanation for this difference in behavior is that a high layer charge density is necessary for the incorporation of hydrophobic anionic species such as terephthalate or benzoate in order to create a continuous hydrophobic layer between the inorganic sheets. The anions are known to align with the aromatic plane perpendicular to the LDH layers[8,47], allowing the hydrophilic carboxylate groups to interact with the surface hydroxyl groups while the benzene rings occupy the central region of the interlayer space in order to minimize the hydrophobic forces. Lower surface charge density LDHs impose a larger inter-anion separation, which would be expected to be more highly hydrated and therefore result in a product with a higher free energy[8]. The reduction in free energy associated with the intercalation of the smaller nitrate anions would favor the latter over the former as the gallery species.

3.2.3 Effect of coprecipitation pH on the $Mg:M^{3+}$ ratios

Additional syntheses were performed at lower pH values in an attempt to produce terephthalate containing materials with higher $M^{2+}:M^{3+}$ ratios. The POXRD patterns obtained for Mg_RGa-TA samples precipitated at pH 8.6, 7.7 and 6.8 are presented in Figs.

3.5, 3.6 and 3.7. The corresponding patterns for the Mg_RAl-TA samples are presented in Figs. 3.9, 3.10 and 3.11. As shown in Table 3.2 for both the Mg_RGa-TA and Mg_RAl-TA analogues incomplete incorporation of Mg^{2+} is observed below pH 10.0. $Mg(OH)_2$ is fairly soluble at pH 8 and below, thus a large amount of Mg^{2+} remains in solution and is lost during the washing step (i.e. ICP analysis shows up to 1000 times as much Mg^{2+} as Ga^{3+} in the supernatant).

The Mg:Ga ratio of Mg_3Ga-TA precipitated at pH 8.6 was determined to be about 2.5:1 by ICP-AES spectroscopy. As indicated by the POXRD pattern of this product in Fig. 3.5 (middle pattern) an R value of 2.5:1 appears to be very close to the upper limit for the partial incorporation of TA into the interlayer space. In fact two separate phases are readily identified in the powder pattern: the LDH-TA (d_{003} = 14.2 Å, 2θ = 6.22°) and the LDH-Cl (d_{003} = 7.9 Å, 2θ = 10.90°). Both phases give rise to broad d_{003} reflections and therefore appear to be rather poorly crystallized compared to the LDH-Cl that forms at a Mg:Ga ratio greater than 2.5:1 (top pattern) or the LDH-TA that forms below 2.5:1 (lower pattern). The reduced crystallinity in this case is probably due to the intergrowth of the two phases, which hinders the orientation of the crystallites during the sample preparation.

The IR spectra shown in Fig. 3.13 for the region between 400 cm^{-1} to 1800 cm^{-1} correspond to the same samples from which the POXRD patterns appearing in Fig. 3.5 were obtained. A similar mass of LDH material and KBr was used to prepare each pellet, and therefore the relative intensities of the two main terephthalate bands at 1567 cm^{-1} and
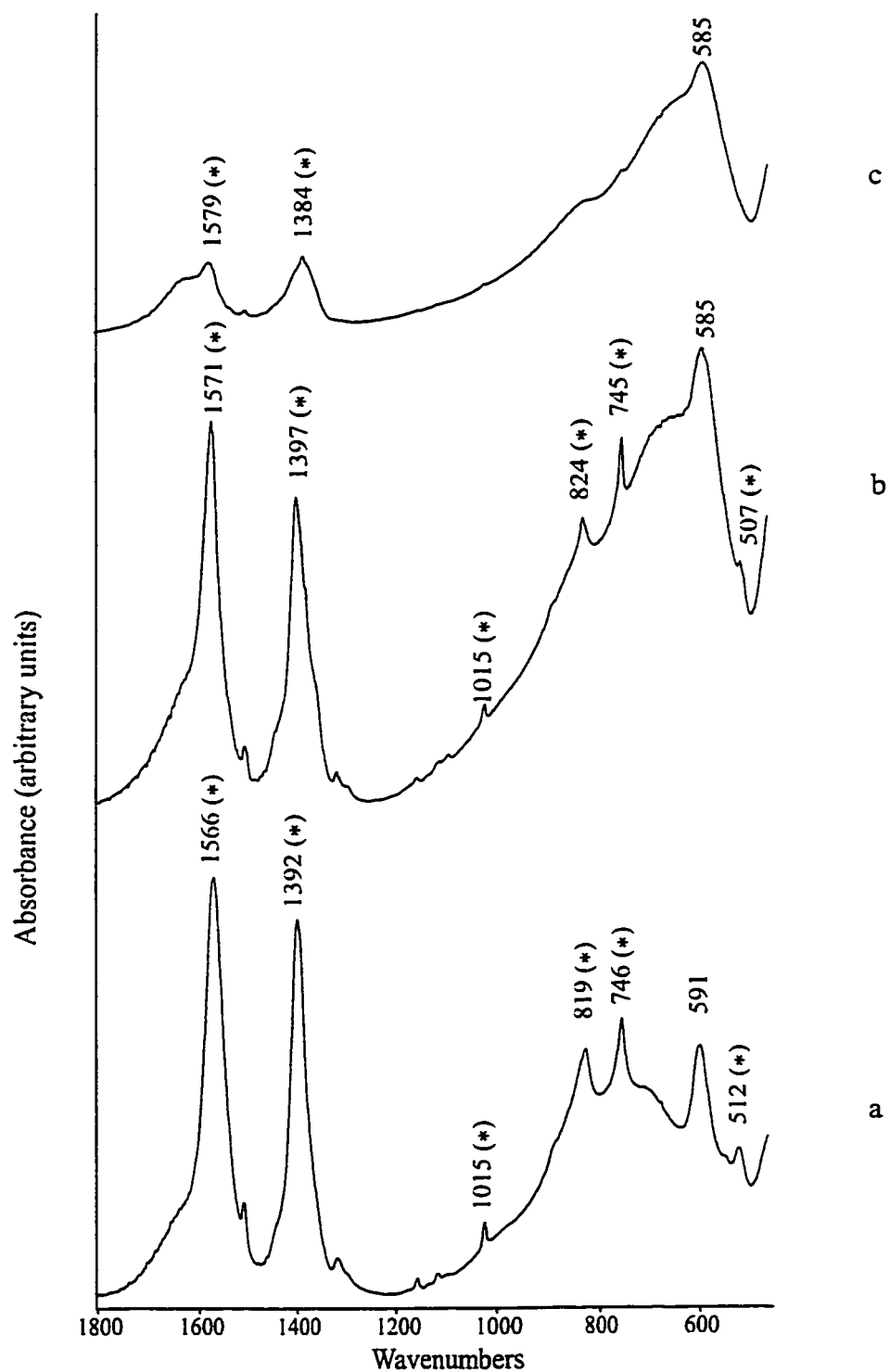
Fig. 3.13: IR spectra of a) Mg_2Ga-TA b) Mg_3Ga-TA and c) Mg_4Ga-TA precipitated at pH 8.6. Asterisks denote peaks attributed to terephthalate anions

1390 cm^{-1} compared to the LDH band at 590 cm^{-1} should provide a reliable estimate of the terephthalate content of each product. Note that the relative intensities of both terephthalate bands increase in the order Mg$_4$Ga-TA < Mg$_3$Ga-TA < Mg$_2$Ga-TA, indicating that these samples are actually a "pure" LDH-chloride, a mixture of LDH-chloride and LDH-terephthalate, and finally a "pure" LDH-terephthalate, respectively. Carbon analysis of the Mg$_4$Ga-TA material revealed that the sample contained only 2.2 weight percent carbon, compared to 11.8 % in Mg$_{2.3}$Ga-TA obtained at pH 10.0 which is known to be a true terephthalate-intercalated LDH.

The behavior of the Mg$_R$Al-TA analogues at pH 8.6 (see Fig. 3.9) is only slightly different than that observed for the Mg$_R$Ga-TA series above. POXRD patterns corresponding to very poorly crystallized LDH-TA samples are evident over all Mg:Al ratios. The product obtained from a mixed salt solution with an initial Mg:Al ratio of 2:1 appears to be composed of a single LDH-TA phase, with no evidence of LDH-Cl or other crystalline phase appearing in the POXRD pattern. The middle pattern corresponds to an initial Mg:Al ratio of 3:1, which at first glance appears to be a single LDH-TA phase. However the reflection around 12.5° 2θ is broader and has shifted to a lower angle, and may in fact contain a contribution from the d$_{003}$ of the LDH-Cl at 11.0° 2θ. In addition, the d$_{009}$ and d$_{0012}$ reflections that were clearly visible in the lower pattern are broadened considerably in the middle pattern, and appear to be coalescing into a single peak. The same characteristics are displayed in the upper pattern, which corresponds to an initial

Mg:Al ratio of 4:1. In fact the d_{003} reflection is much less obvious, and clearly the LDH-Cl d_{003} and d_{006} reflections are becoming sharper as the crystallinity of the product increases. As indicated in Table 3.2, the $M^{2+}:M^{3+}$ ratios determined by ICP-AES are virtually the same in both the Mg/Ga and Mg/Al series for products that were precipitated at pH 8.6 from initial metal salt solutions with the same $M^{2+}:M^{3+}$ ratio.

Rather surprisingly the best-crystallized LDH-TA samples were obtained at a precipitation pH of 7.7 for the Mg_RGa-TA series. As shown in Fig. 3.6, sharp POXRD patterns were obtained at all ratios, however, an additional peak at $2\theta=21.4°$ was also observed for most of the Mg_RGa-TA products; this peak must arise from gallium oxide hydroxide, GaO(OH), which is isomorphous with diaspor α-AlO(OH)[111,112,113]. The formation of a separate pure gallium phase immobilizes some of the gallium and thus the measured Mg:Ga ratios reported in Table 3.2 do not accurately reflect the true composition of the LDH layers. The actual Mg:Ga ratio of the layers was determined indirectly by analyzing the product for weight percent carbon and assuming that all of the carbon could be attributed to charge balancing terephthalate anions in the gallery region. Since the layer charge is due entirely to the presence of gallium within the layers, the weight percent carbon provides an estimate of the moles of gallium in the layers, per gram of product. From ICP-AES analysis the total moles of gallium (i.e. layer plus non-layer) per gram of product is also known, therefore it is possible to arrive at the fraction of gallium that actually exists in the layers. By assuming that all Mg detected by ICP analysis occurred in the layers, the ratio of Mg:Ga in the layers could be calculated; the

results are tabulated in Table 3.3. It is significant to note that the Mg:Ga ratio in the layers was virtually constant at 2:1 regardless of the metal cation ratio in the initial synthesis mixture.

Table 3.3: $Mg^{2+}:M^{3+}$ molar ratios calculated for total M^{3+} content and layer M^{3+} content at pH 7.7

$M^{2+}:M^{3+}$ molar ratio, R, in synthesis mixture	Wt%			$Mg:M^{3+}$ molar ratio	
	$M^{3+(a)}$	Mg^a	C^b	total	layer
Mg:Ga=4	29.5_6	13.7_3	13.0_5	1.3_3	2.0_8
Mg:Ga=3	29.3_0	12.7_3	12.8_5	1.2_5	1.9_6
Mg:Ga=2	36.2_2	12.0_5	10.9_4	0.9_6	2.1_8
Mg:Al=4	13.8_6	17.8_3	16.2_3	1.9_8	1.9_9
Mg:Al=3	9.4_0	14.5_1	-	1.6_3	-
Mg:Al=2	10.4_3	18.2_2	18.1_0	1.4_4	2.1_4

[a] ICP analysis on Thermo Jarrell Ash Atom Scan 16 Spectrometer.
[b] C analysis on CEC Corporation Elemental Analyzer.

The POXRD patterns for the corresponding Mg_RAl-TA products in Fig. 3.10 once again reveal very few differences. Well formed terephthalate-containing LDHs were obtained regardless of the Mg:Al ratio in the initial salt solution, but in no case was there evidence of a separate crystalline pure aluminum phase. The ICP-AES results that are tabulated in Table 3.2 indicate moderately higher $Mg:M^{3+}$ ratios for the Al species compared to the corresponding gallium analogues, but the measured ratio is always lower than the ratio in the initial salt solution. Assuming that an x-ray amorphous pure aluminum phase did in fact precipitate as in the gallium containing samples, the Mg:Al

content of the LDH layers produced at pH 7.7 was determined. This again indicated that the ratio present in the layers is virtually constant at about 2:1.

Fig. 3.7 indicates that the intensity of the GaO(OH) reflections increases as the co-precipitation pH is further decreased to pH 6.8. ICP analysis indicates that the Mg:Ga ratio of the Mg_2Ga-TA product synthesized at pH 6.8 is actually 0.20:1, and thus virtually no Mg^{2+} was incorporated into this product. As can be seen from the POXRD pattern in Fig. 3.7, it is apparently a pure GaO(OH) sample (there is no reflection around $d_{003} = 14.3\text{Å}, 2\theta = 6.17°$). The GaO(OH) formed in these synthesis is a relatively high surface area material, and the BET-N_2 surface areas tend to increase as the $Mg^{2+}:M^{3+}$ ratios decrease and the $21.4°$ 2θ peak becomes more prominent. A maximum surface area of 96 m^2/g was obtained for the "pure" GaO(OH) product synthesized at pH 6.8.

The behavior of the Mg_RAl-TA analogues appears to deviate from that of the Ga containing species. POXRD patterns corresponding to poorly ordered LDH-TA materials (Fig. 3.11) were obtained from salt solutions with initial $Mg^{2+}:Al^{3+}$ ratios of 2:1, 3:1 and 4:1. Furthermore, there is no evidence for the formation of a separate pure aluminum phase analogous to GaO(OH), which was the only phase detected for the Mg_2Ga species precipitated at pH 6.8. Upon closer examination, however, a very similar trend is apparent in the $M^{2+}:M^{3+}$ ratios determined by ICP-AES and tabulated in Table 3.2. For both the aluminum and gallium containing LDHs the $M^{2+}:M^{3+}$ ratio is approximately 1:1 or less. Thus the increased solubility of $Mg(OH)_2$ at pH 6.8 resulted in Mg:Al ratios that

lie outside the theoretical limits for LDH formation. It therefore seems likely that some of the aluminum in the sample was present not in the layers, but instead as an amorphous, and therefore undetectable, separate phase.

3.2.4 Microtextural structure of LDH-TA products

The BET-N_2 surface area of each $Mg^{2+}_R M^{3+}$-TA precursor was measured after pretreatment at 125°C under vacuum, and the results are tabulated in Table 3.1. There does not appear to be a definite trend with respect to either the layer composition or the pH at which the product was obtained. Several comments of a general nature may be made, however, regarding the specific surface areas of the LDH-TA precursors. To begin with, the specific surface area increases considerably for products that appear to contain a significant amount GaO(OH) or a similar aluminum containing phase. Thus great care must be taken when evaluating the microtextural properties of LDH materials in which separate phases may be present, particularly in light of the fact that the contaminant phase may be x-ray amorphous, and therefore difficult to detect.

Secondly, it has previously been reported that LDH-TA precursors are non-porous, slightly flattened bead-like particles of approximately 1000-2000 Å in diameter[8]. Assuming that the density[114,115] of the spheres is 2.10 g/cm^3 and that the spheres pack with 74% efficiency (close packed), the surface area is given by 36000/d, where d is the sphere diameter in Å and the surface area is in m^2/g. Thus, surface areas of 18-36 m^2/g would be expected from pure LDH-TA materials, which is in fair agreement

with most of the values in Table 3.1. The possibility that LDH-TA precursors may possess a small amount of microporous surface area was investigated by determining the pore size distribution (psd) from the argon adsorption isotherm using the model developed by Saito and Foley[96] for cylindrical pore geometry. The cylindrical pore model was assumed to be valid for LDH materials since the pores created by the expansion of the gallery height would be expected to be bounded on two sides by the LDH layers and on the other two sides by interlayer anion species. The resulting channel-like system of pores would be expected to exhibit curvature effects similar to those that affect adsorption in zeolites.

To test the procedure, the pore size distribution (psd) of zeolite NaY was determined. Fig. 3.14 shows the results, which give a maximum at 0.70 nm, in excellent agreement with the actual value of 0.74 nm as determined by x-ray diffraction studies[96]. The experimental error for the maximum in the psd of Na-Y is about 5.4%. Results obtained for the psd of all LDH-TA precursors measured were very similar, and therefore a single representative argon adsorption isotherm and psd plot is shown in Fig. 3.15. The adsorption isotherm is of type I according to the BDDT classification[116]; most noticeably the adsorption of argon at low relative pressure is much less steep than was observed for the zeolite standard (adsorption at low relative pressure is indicative of microporosity). The psd plot for Mg₃Ga-TA shown in Fig. 3.15 appears to be bimodal with a poorly defined maximum, which is probably due to the small volume of argon that was adsorbed by the sample resulting in considerable noise. Based on the relatively flat shape of the
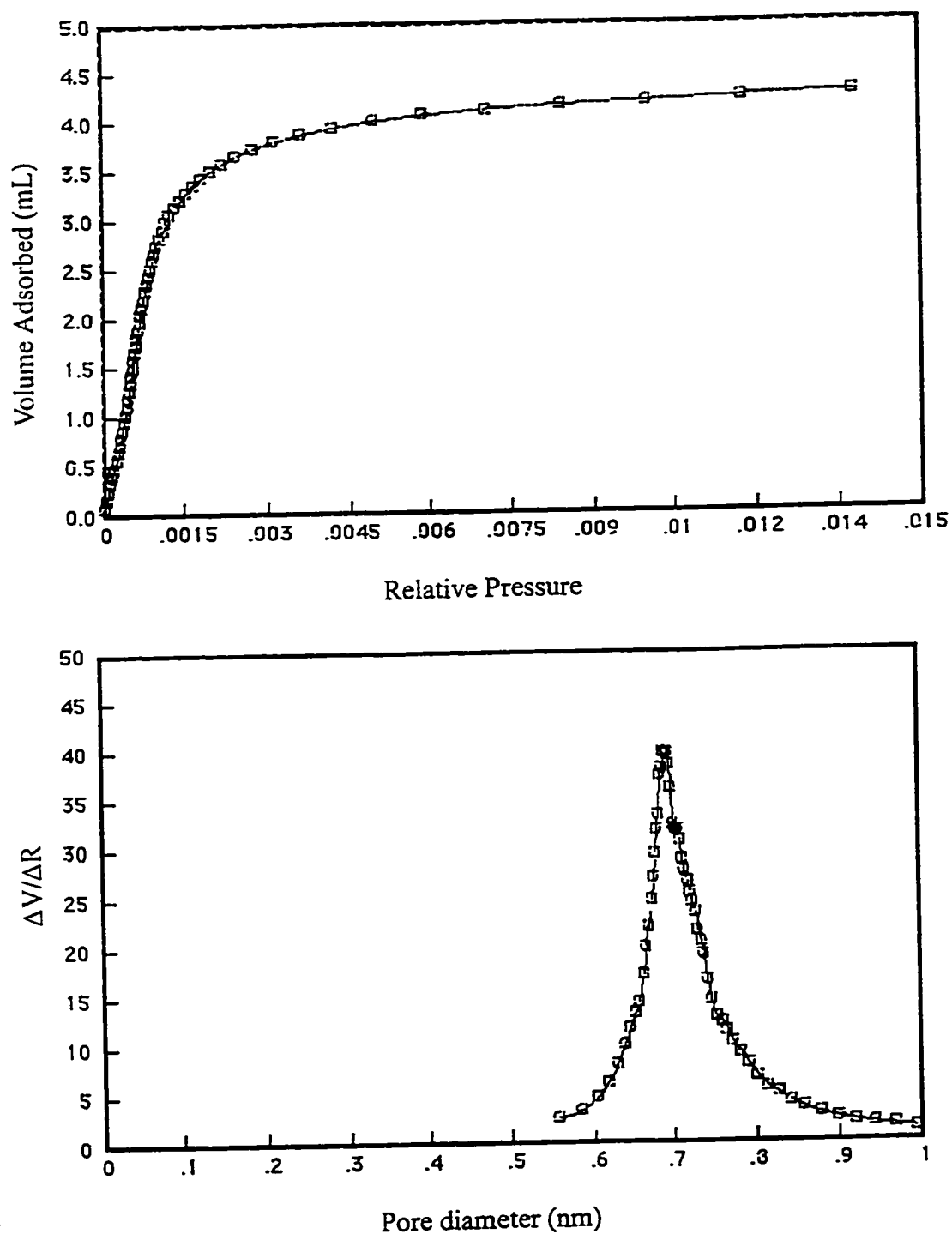
Fig. 3.14: Argon adsorption isotherm (top) and micropore size distribution plot
(bottom) for NaY Zeolite
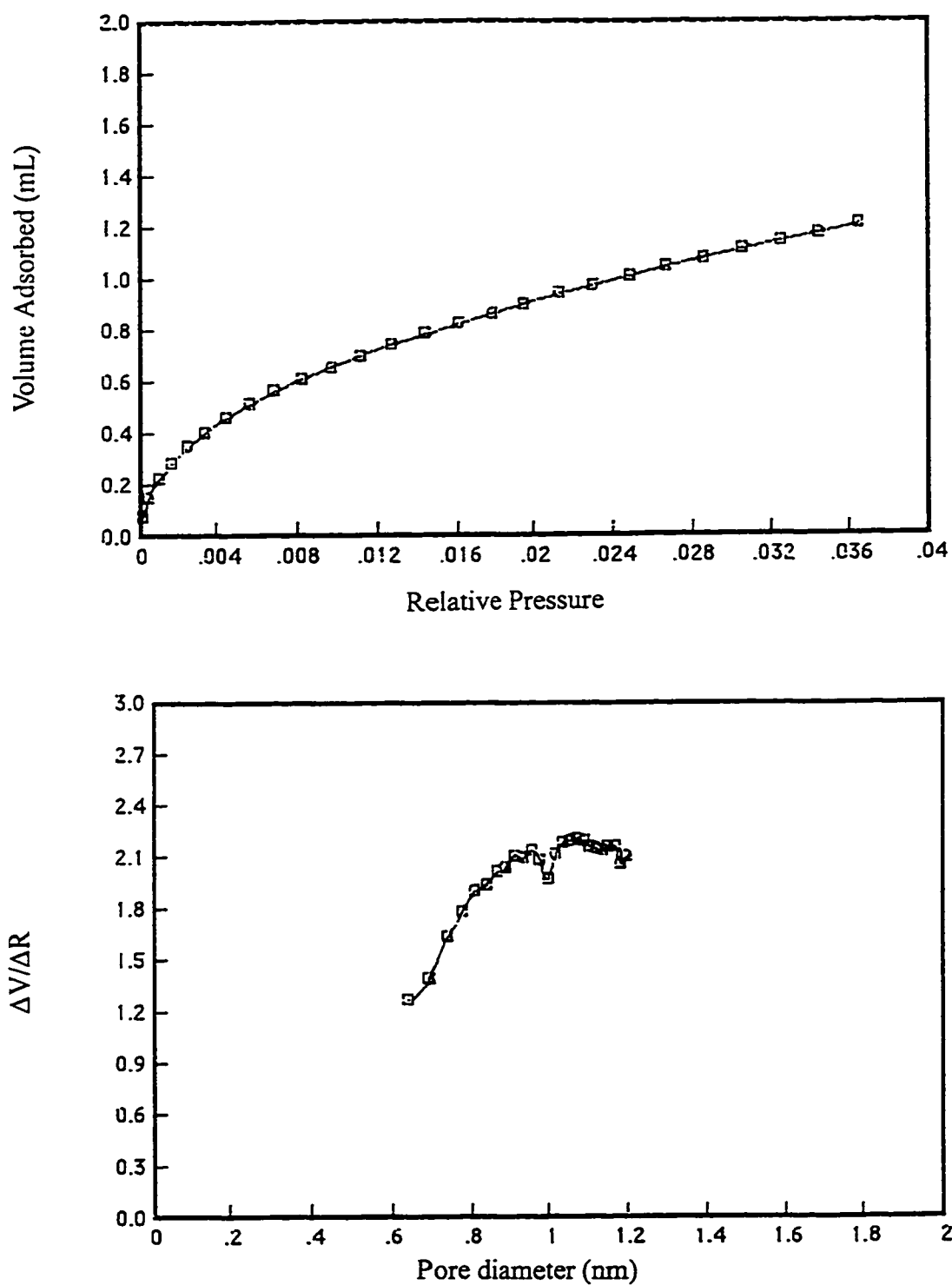
Fig. 3.15: Argon adsorption isotherm (top) and micropore size distribution plot (bottom) for Mg$_2$Ga-TA coprecipitated at pH 8.6

peak and the lack of a clearly identifiable baseline, it appears that the LDH-TA precursors are completely non-porous, as was suggested previously.

3.2.5 POM anion exchange reactions with Mg/M^{3+} precursors

The POXRD patterns of a Mg$_3$Ga-TA precursor prepared at pH 7.7 and the corresponding anion exchanged species, Mg$_3$Ga-PW$_{11}$O$_{39}$$^{7-}$ and Mg$_3$Ga-H$_2$W$_{12}$O$_{40}$$^{6-}$ are presented in Fig. 3.16a, 3.16b and 3.16c, respectively. There is a slight increase in the d$_{003}$ value from 14.2 Å in the terephthalate precursor to 14.6 Å and 14.8 Å for anion exchanged products containing PW$_{11}$ and H$_2$W$_{12}$, respectively. Each POXRD pattern of a POM exchanged LDH contains a broad reflection around 2θ = 8.08° (d = 11Å) that was not present in the precursor. Other workers have suggested that this by-product is a poorly ordered Mg rich salt of the Keggin ion[30,91].

The specific surface area increased only slightly from 39 m^2/g for the precursor to about 45 m^2/g for both of the POM exchanged products. Micropore size distribution experiments failed to reveal an accessible microporous structure in the POM anion exchanged products. It is likely that the interior surface area is blocked due to crowding of inorganic anions between the sheets. Pore blockage is probably attributable to the fact that the Mg:Ga ratio in the layers of the precursor is 2:1, and thus the surface charge density is very high, requiring the POM anions to "stuff" the interlayer region in order to satisfy electroneutrality. Carbon analysis performed on the samples indicate 0.12 weight percent carbon in the case of the H$_2$W$_{12}$ exchanged product, and 0.67 weight
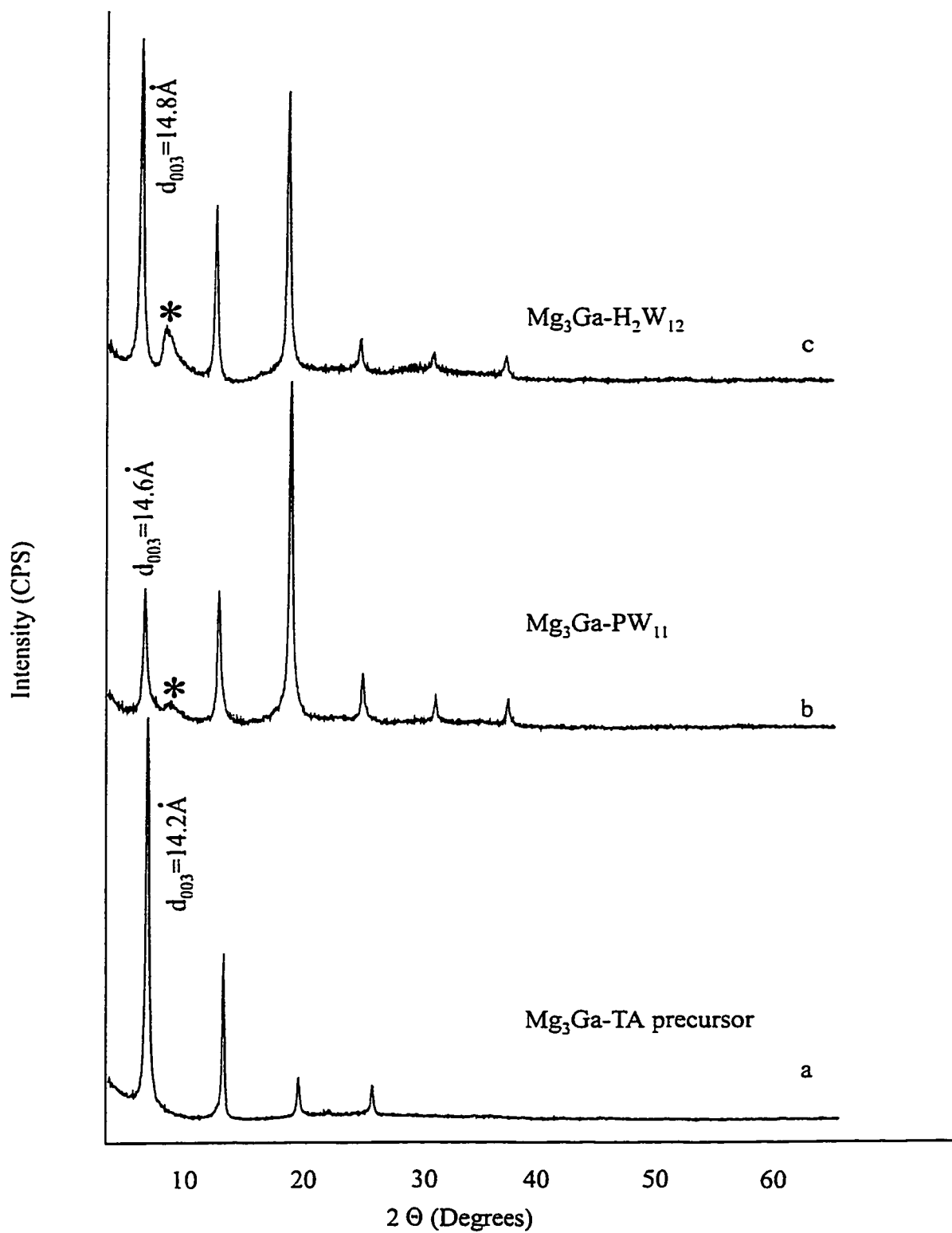
Fig. 3.16: POXRD patterns of a) Mg₃Ga-TA precursor prepared at pH 7.7 b) Mg₃Ga-PW₁₁ and c) Mg₃Ga-H₂W₁₂ (* denotes presence of impurity salt phase).

percent carbon in the case of the PW_{11} exchanged product. It appears that the extent of

exchange is nearly complete for the former (H_2W_{12}), whereas some organic anions must

be retained in the latter (PW_{11}). In addition, the W:Ga ratio for $Mg_3Ga-H_2W_{12}$ was 1.86:1

(theoretical value is 2.0:1) which supports the view that exchange is nearly complete. For

the Mg_3Ga-PW_{11} LDH, the W:Ga ratio was determined to be 0.93:1 (theoretical value is

1.57:1) indicating that there are insufficient POM anions present to counterbalance the

positive charge of the layers, and therefore the interlayer region must also contain residual

terephthalate anions. In both cases, the Mg:Ga ratio as determined by ICP-AES analysis

increased from 1.25:1 in the terephthalate precursor to 1.99:1 for $Mg_3Ga-H_2W_{12}$ and to

1.46:1 for Mg_3Ga-PW_{11}. The increased Mg:Ga ratios can probably be attributed to

dissolution of GaO(OH) at low pH (pH = 5.5) during the anion exchange reaction[109].

3.3 LDH layers containing acidic cations: the Zn_RAl series

The partial success achieved using terephthalate containing Mg/Al and Mg/Ga

LDHs as precursors for the synthesis of POM-intercalated LDH materials suggested

attempting the same method with the Zn/Al analogues. It was anticipated that the greater

stability of the Zn/Al layers in moderately acidic solutions would reduce leaching of M^{2+}

from the layers, and thus larger values of R could be obtained. Since the lateral spacing

of the POM pillars is ultimately determined by the layer charge density, it was hoped that

improved compositional control in the Zn_RAl-TA precursors would result in the creation

of accessible internal surface area in the LDH-POM products.

3.3.1 Synthesis of Zn_RAl-TA

The method used to prepare Zn_RAl-TA precursors was modified only slightly from the one described in Section 2.1.1. Essentially, the nitrate salts $Zn(NO_3)_2$ and $Al(NO_3)_3$ were used instead of the chloride salts, and the coprecipitation reaction was carried out at pH 8.5. These conditions were found to yield highly crystalline samples that exhibit four orders of diffraction from the basal planes and a d_{003} value comparable to that observed in the Mg containing LDHs. Additional characterization was not carried out on the Zn_RAl-TA precursors since the main focus was to compare the compositional and microtextural properties of the corresponding POM pillared products.

3.3.2 POM anion exchange reactions with Zn_RAl-TA precursors

Although it was relatively easy to synthesize Zn_RAl-TA precursors, the subsequent POM exchange did not proceed. The POXRD pattern of the precursor is shown in Fig. 3.17a along with the pattern obtained from a film prepared using the product obtained with 15 minutes of aging time at 70°C in Fig. 3.17b and the product obtained after 18 hours stirring at 70°C in Fig. 3.17c. It is apparent that the layered structure of the Zn_RAl-TA precursor is more stable than that of either the Mg_RAl-TA or Mg_RGa-TA analogues since the powder pattern was virtually unaltered after 18 hour in contact with a mildly acidic aqueous solution (pH 6.0). Unfortunately, despite the fact that the Zn/Al layers appeared stable under the conditions of the exchange reaction, the use of terephthalate-intercalated LDH precursors is precluded since the terephthalate anions were not displaced by the POM anions in solution.
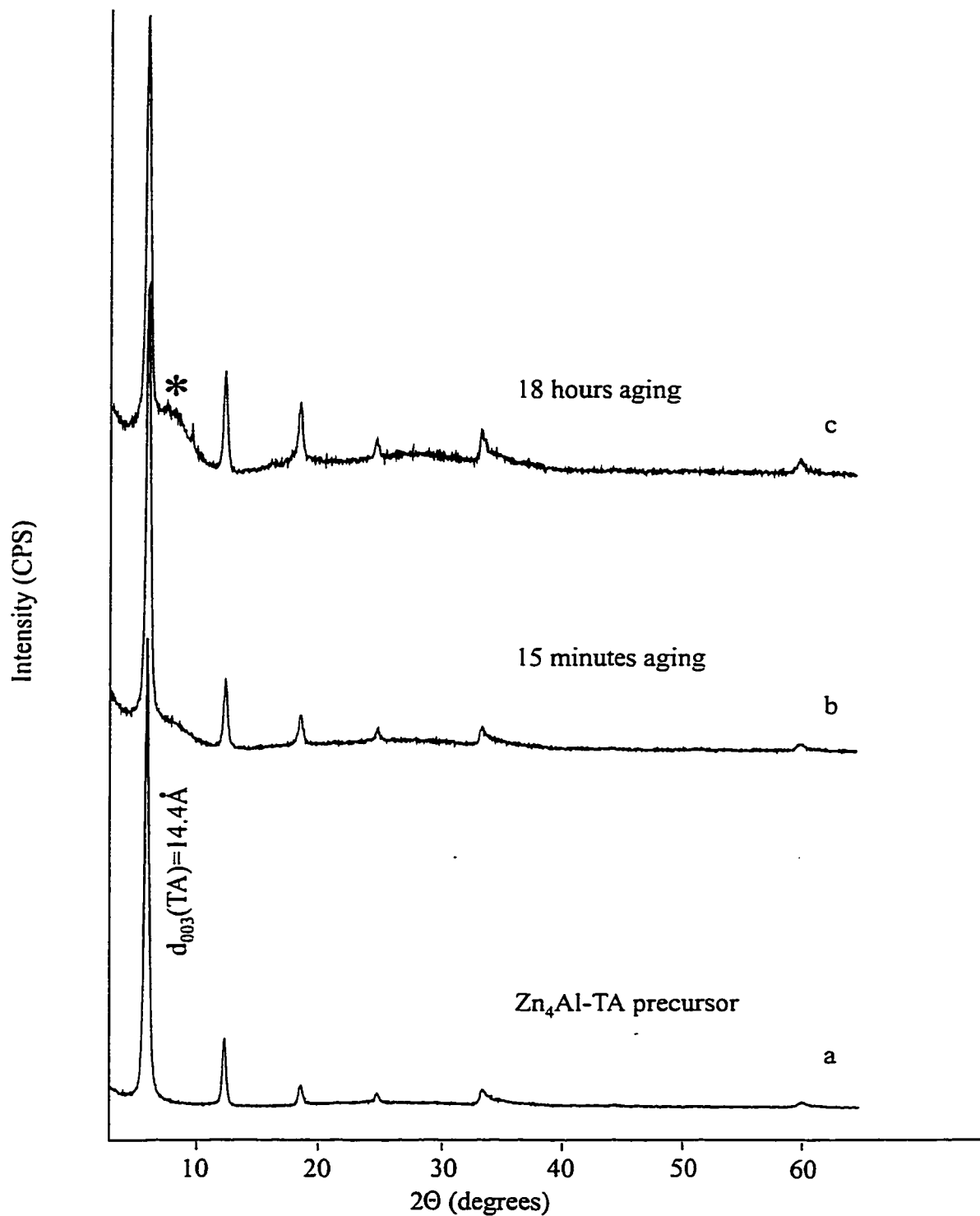
Fig. 3.17: POXRD patterns of a) Zn_4Al-TA precursor and the products obtained b) 15 minutes and c) 18 hours after the complete addition of $(NH_4)_6H_2W_{12}O_{40}$ solution (*denotes presence of impurity salt phase).

3.3.3 Extension to other organic anions: the Zn$_R$Al-BA and Zn$_R$Al-p-HyBA series

In view of the difficulties encountered while attempting to replace the interlayer terephthalate anions with POM anions, LDH precursors intercalated with benzoate or *p*-hydroxybenzoate anions were prepared in the hope that these anions would be more easily displaced during the exchange step. Representative POXRD patterns for Zn$_2$Al-BA and Zn$_2$Al-*p*-HyBA are presented in Fig. 3.18b and 3.18c, respectively. The POXRD pattern for the Zn$_2$Al-TA precursor that was discussed in the previous section has also been included in Fig. 3.18a for comparison. An inspection of Fig. 3.18 reveals that the d$_{003}$ value obtained from the POXRD pattern of the Zn$_2$Al-BA precursor is slightly larger than the value observed for the terephthalate containing LDH. The larger gallery height in the Zn$_2$Al-BA precursor is inconsistent with the actual lengths of the anions (as measured along the C$_2$ axis that passes through C$_1$ and C$_4$ of the aromatic ring). The explanation is that the benzoate anions enter the gallery region of the LDH and form a bilayer, probably in order to create a more hydrophobic region occupied by the aromatic rings while the carboxylate groups interact with the LDH layers.

With the exception that a bilayer arrangement results upon intercalation of benzoate anions, the properties of LDH-BA precursors and LDH-TA precursors are very similar, and displacement by POM anions during the anion exchange step does not occur. The LDH-*p*-HyBA precursors, however, did undergo some exchange. It was found that at pH 4.5 and a reaction temperature of 65 °C the *p*-hydroxybenzoate anions were replaced by the POM anions after one hour of stirring. The initially formed product
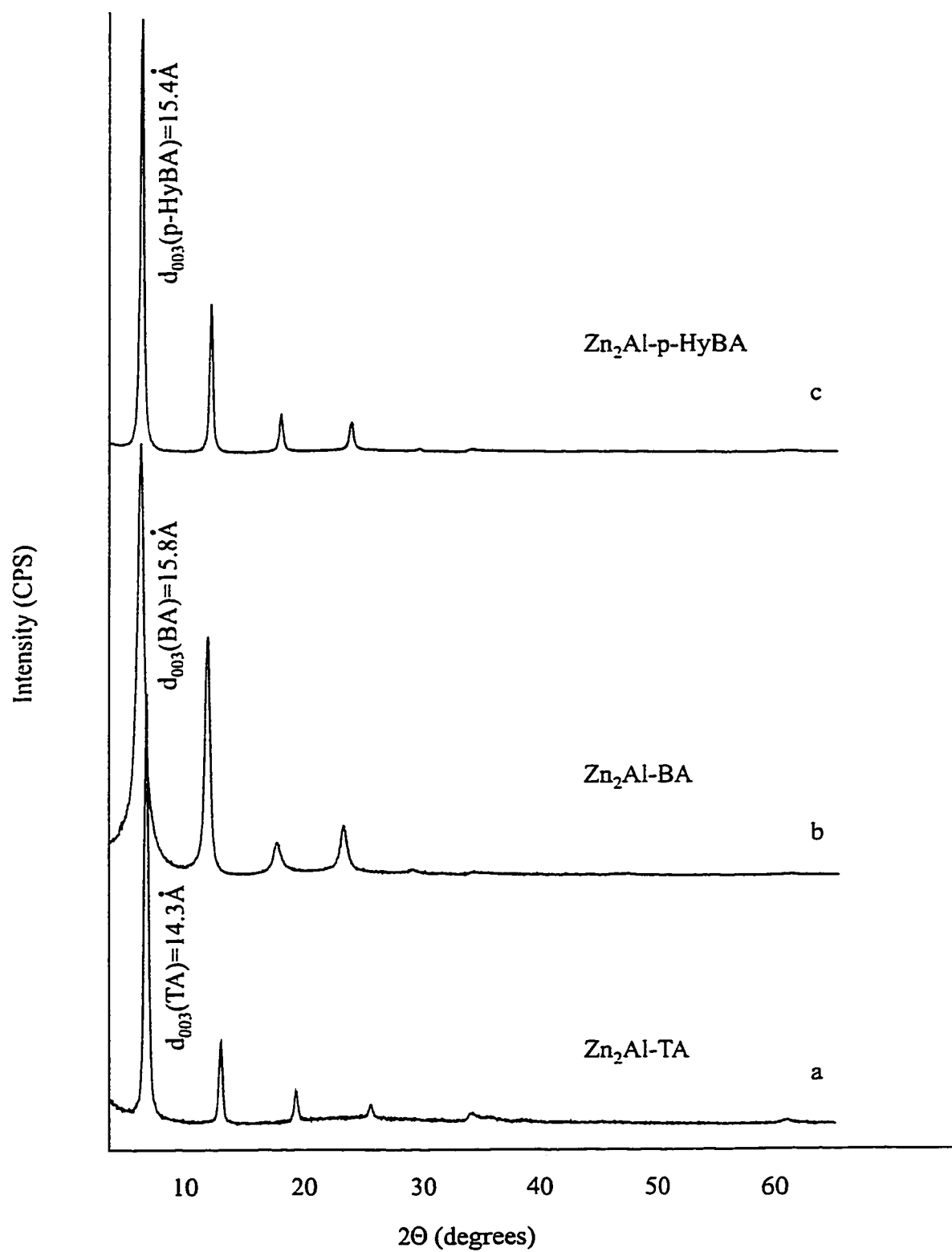
Fig. 3.18: POXRD patterns of a) Zn_2Al-TA b) Zn_2Al-BA and c) Zn_2Al-p-HyBA

appeared to be rather poorly crystallized, and the d_{003} peak was partially obscured by the

broad reflection arising from the impurity salt phase (see Fig. 3.19b). Prolonged aging

times of up to four days resulted in a gradual improvement of the product crystallinity

(Fig. 3.19c-e), however additional peaks arising from unidentified phases not associated

with the LDH structure also began to appear in the POXRD pattern. One possibility is

that the new lines are higher order reflections of the broad peak from the salt phase,

which may also become more crystalline with increased aging time.

3.4 Assessment of the potential of the organic anion precursor route

The utility of the organic anion precursor route has been evaluated for the first

time for the synthesis of Mg_RGa-POM materials. The work carried out during the course

of this project was published and contains the first description of Mg_RGa-TA and

Mg_RGa-POM products[48]. Comparisons were drawn between the Mg/Ga LDHs and the

more widely studied Mg/Al LDHs, leading to the conclusion that nearly identical

behavior was exhibited by both series of materials during the preparation of the LDH-TA

precursors, and subsequently during the POM exchange reactions. Although the initial

ICP-AES results indicated that a series of LDH-TA precursors with a wide range of layer

compositions had been synthesized, further experiments eventually revealed that the

composition of the layers was considerably different than that of the bulk sample. The

invariance of the layer composition was attributed to increased solubility of Mg^{2+}, as well

as the formation of pure gallium phases at low solution pH. Furthermore, under
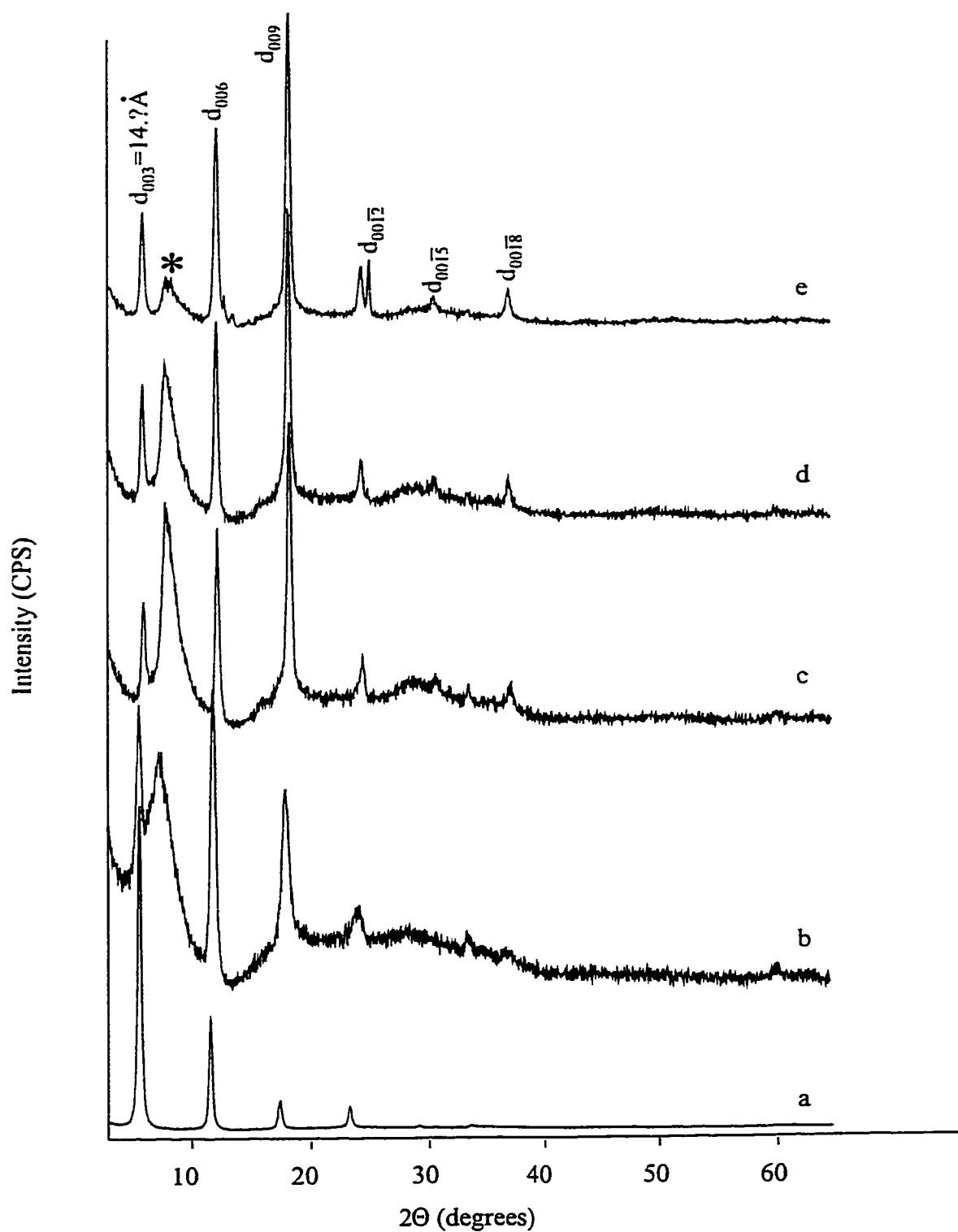
Fig. 3.19: POXRD patterns of a) Zn₄Al-p-HyBA precursor and the products obtained
b) 1 hour c) 18 hours d) 3 days and e) 4 days after addition of $(NH_4)_6H_2W_{12}O_{40}$ solution
(* denotes presence of impurity salt phase).

conditions appropriate for true coprecipitation to occur, there appeared to be an upper value of the $M^{2+}:M^{3+}$ ratio that was capable of incorporating terephthalate anions as the interlayer species. Thus at pH 10 it was possible to obtain LDH materials with a 2:1, 3:1 or 4:1 ratio of $M^{2+}:M^{3+}$ in the layers, but the precursors with larger ratios preferentially incorporated chloride anions.

Anion exchange under ambient pH conditions proceeded smoothly for the $Mg_R Ga$ series, yielding well ordered POM containing LDH phases with a gallery height of approximately 10 Å, in excellent agreement with the value that is expected based on the spherical radius of the Keggin structure. Despite the fact that the exchange appeared to proceed to completion and only minimal contamination by terephthalate anions was observed, the BET-N_2 surface areas only increased from 39 m^2/g to about 45 m^2/g in the LDH-POM. It was inferred from the surface area measurements that attempts to create an accessible microporous structure between the LDH layers had been largely unsuccessful, and therefore the products were unlikely to display shape or size selectivity in catalytic reactions. This method does seem suitable, however, for preparing LDH-POM materials to be used in catalytic application following calcination at high temperature. Thermal decomposition of the LDH structure should increase accessibility to the active sites, which may occur as either basic sites on the mixed oxide support, or as acidic or redox sites on the residue formed by the decomposition of the pillar.

Attempts to apply this method to the Zn/Al LDH materials met with similar difficulties, but in addition the interaction between the LDH layers and the precursor

anions was stronger than in the Mg^{2+} containing analogues, thus anion exchange did not

occur for the terephthalate or benzoate containing precursors. The composition of the

POM pillared product obtained from anion exchange of the Zn_4Al-p-HyBA precursor was

dubious, with multiple high 2θ reflections appearing in the POXRD pattern after

prolonged aging time.

Despite offering the advantages of relative simplicity and in most cases short

preparation times, the disadvantages mentioned above prevented the implementation of

the organic anion precursor route as the synthetic method used in this laboratory for the

preparation of POM-pillared LDH materials. An alternative method was adopted in an

attempt to gain better control over the layer composition and thus be able to manipulate

the microtextural properties of the final products. The LDH-OH/LDH-adipate precursor

route, which was first proposed by Yun and Pinnavaia[30], was optimized for the synthesis

of LDH-POM phases containing different M^{2+}, M^{3+} cations in different ratios. This

method will be the focus of Chapter 4.

Chapter 4

The LDH-OH/LDH-adipate Precursor Route

4.1 Overview

A synthesis method that was first reported[30] for the pillaring of LDH materials

with a 3:1 Mg:Al ratio in the LDH layers has been adopted as a general route for the

synthesis of LDH materials with different layer compositions. The LDH-OH/LDH-

adipate precursor route involves several additional steps compared to the organic anion

precursor method discussed in Chapter 3, and takes approximately three times as long to

complete. Despite these drawbacks, the superior control over the composition and

microporous structure of the LDH-POM products that is achieved by this route (see

subsequent discussion) have made it the synthesis method of choice for the preparation of

the catalyst samples to be used for the work described in Chapter 5.

The first step in the synthesis is to form an LDH-carbonate precursor with the

desired ratio of M^{2+} and M^{3+} cations via the well-known coprecipitation reaction[46]. Since

carbonate anions are readily incorporated into the LDH structure[11], it is generally possible

to work under conditions where true coprecipitation of the layer cations occurs, and thus

the actual M^{2+}:M^{3+} ratio of the layers will be the same as in the initial mixed metal salt

solution. Furthermore, since the goal is to incorporate carbonate anions into the interlayer region there is no need to work under an inert atmosphere at this stage of the synthesis. Working under an ambient atmosphere greatly facilitates the addition of solutions to the reaction mixture and reduces the need for specialized equipment or glassware.

Since carbonate anions are notoriously difficult to remove by ion exchange methods, the initially formed precursor must be thermally decomposed at temperatures between 450°C and 550°C. At these temperatures the LDH structure is reversibly decomposed, and the interlayer carbonate anions and surface hydroxyl groups are evolved as CO_2 and water, respectively, resulting in a mixed metal oxide solid solution. The mixed oxide exhibits a so called "memory effect", and will reconstitute upon stirring in water for a period of five days. By carefully excluding anions, including carbonate anions from atmospheric CO_2 sources, from solution during the reconstitution phase the mixed oxide will incorporate hydroxide anions present in the deionized water as the LDH structure reforms. The resulting intermediate that is obtained after reconstituting a Mg_3Al mixed metal oxide[117,118] is a synthetic form of the naturally occurring mineral meixnerite, $Mg_3Al(OH)_8OH$, which in the general case is denoted as $M^{2+}_RM^{3+}$-OH.

In order to facilitate the incorporation of bulky polyoxometalate anions, however, the LDH-OH is further modified by an anion exchange reaction with adipic acid at elevated temperatures. The interlayer hydroxide anions are replaced by adipate anions, producing an LDH-adipate in which the gallery height between the LDH layers is expanded from about 8.0 to 12.9 Å. The next and final step involves the replacement by

anion exchange of the interlayer adipate anions with the desired POM species, yielding the desired LDH-POM product. The exchange reaction generally proceeds at ambient pH values[30], and no effort is made to control the solution pH by the addition of a dilute mineral acid. Attempts to improve the resulting LDH-POM products by controlling the pH during anion exchange generally result in hydrolysis of the POM anions and partial or total dissolution of the LDH layers[30].

The LDH-OH/LDH-adipate method has been evaluated in Section 4.2 in terms of the control that may be achieved over the layer composition in the final POM-pillared LDH products for the series $Mg_RAl-H_2W_{12}$ (R = 2, 3, 4). The primary motivation for conducting this type of study was to determine to what extent the microporous structure of the pillared material may be varied within a homologous series such as the $Mg_RAl-H_2W_{12}$ (R = 2, 3, 4). Only after satisfactory control over the chemical and physical properties of the Mg/Al series had been obtained could the study be extended to include other LDH materials containing different metal cations. Section 4.3 discusses the Mg/Ga analogues and Section 4.4 discusses the Zn/Al analogues.

4.2 Examination of the precursors formed during the synthesis of Mg$_R$Al-POM

In the hopes of identifying any problematic steps in the overall synthetic procedure, a systematic study was undertaken. Each precursor formed during the synthesis of $Mg_RAl-H_2W_{12}$ (R = 2, 3 and 4) was extensively characterized by chemical and spectroscopic techniques. POXRD patterns appearing in the following sections were

obtained using either oriented films or random powder mounts of the Mg_RAl-CO_3,

Mg_RAl mixed metal oxide solid solution, Mg_RAl-OH and Mg_RAl-adipate precursors for

R = 2, 3 and 4. The chemical composition of each precursor was determined by ICP-AES

and CHN elemental analysis. For convenience these data are summarized in Table 4.1.

The elemental analysis data will be discussed as appropriate in the subsequent sections of

this chapter.

Table 4.1: Chemical composition and weight percent carbon content of Mg_RAl-A^{n-} precursors for POM pillared products

Sample	Layer composition (Mg:Al)[a]	Carbon (weight %)[b]	Hydrogen (weight %)[b]	Nitrogen (weight %)[b]
Mg_4Al-CO_3	4.12:1.00	1.66	3.16	0.91
Mg_3Al-CO_3	3.15:1.00	1.39	6.97	0.10
Mg_2Al-CO_3	2.16:1.00	2.40	3.52	0.05
Calcined Mg_4Al-CO_3	4.05:1.00	0.11	0.25	0.32
Calcined Mg_3Al-CO_3	3.07:1.00	0.26	0.10	0.03
Calcined Mg_2Al-CO_3	2.06:1.00	0.85	0.57	0.0
Mg_4Al-adipate	3.94:1.00	10.21	4.00	0.07
Mg_3Al-adipate	-	14.07	3.66	0.02
Mg_2Al-adipate	1.95:1.00	13.64	4.28	0.0

[a] ICP analysis on Thermo Jarrell Ash Atom Scan 16 spectrometer.

[b] CHN analysis on Control Equipment Corporation (CEC) 440 Elemental Analyzer.

4.2.1 Synthesis of the Mg_RAl-CO_3 precursors (R = 2, 3, 4)

The $LDH-CO_3$ precursors were synthesized under appropriate conditions to ensure

that coprecipitation of the divalent and trivalent metal cations would occur. As was

mentioned previously in Section 1.1.2 the hydroxides of the more basic metal cations (i.e. Mg^{2+}) become soluble below pH 8. Therefore the reaction mixture was maintained at a pH value of 10.0 during the entire course of the reaction. Furthermore, low supersaturation conditions were observed in order to prevent the rate of nucleation of new crystals from becoming appreciably larger than the rate of crystal growth, which would yield a product of lower crystallinity. Since the overall process is topotactic, the morphology of the initially formed LDH-carbonate is preserved in the final product, and thus it is desirable to achieve a highly crystalline product in the early stages of the reaction. Finally, the mixed metal salt solution was added dropwise to the reaction mixture (3 mL/minute) in order to avoid the occurrence of high local concentrations of metal cations. Local increases of the cation concentration would provide opportunities for new LDH crystallites to nucleate, resulting in an overall decrease of the crystallinity of the product.

Following complete addition of the mixed metal nitrate salt solution, the resulting gel-like suspension was aged at 65°C for an additional 48 hours. The gel that was formed immediately after complete addition was amorphous, and required an additional aging period in order for the LDH structure to form. Previous studies have indicated that larger crystals (i.e. more crystalline products) were obtained when the aging was carried out at higher temperatures or if the duration of the aging period was increased. During this time, the pH of the solution remained virtually constant and therefore external control was not required. After cooling the reaction mixture, the clay-like product was collected

by centrifuging the suspension and decanting the liquid. The solid product was then washed several times by repeated cycles of shaking in fresh DDI water followed by centrifuging. The product was oven dried at 90°C, and then was ground to a coarse powder prior to use in the subsequent step of the synthesis.

4.2.2 POXRD study of the Mg_RAl-CO_3 precursors (R = 2, 3, 4)

The POXRD patterns of Mg_2Al-CO_3, Mg_3Al-CO_3 and Mg_4Al-CO_3 are presented in Fig. 4.1a, 4.1b and 4.1c, respectively. The most striking feature is the similarity that exists between all three patterns, which indicates that a well ordered Mg_RAl-CO_3 phase was obtained regardless of the initial $Mg^{2+}:Al^{3+}$ ratio in the synthesis mixture. It is apparent that the d_{003} spacing decreases by approximately 0.29 Å upon changing the $M^{2+}:M^{3+}$ ratio from 4:1 to 2:1. The smaller basal spacing that is observed in the lower R material is due to the increased strength of the hydrogen bonding that exists between the layer hydroxyl groups and the interlayer carbonate anion as the layer charge density increases. As was discussed in the introduction to Chapter 4, the increased electrostatic attraction between the layers and the interlayer carbonate anions in high surface charge density materials reduces the ease of anion exchange. The continuous contraction of the basal spacing, as observed in the series of POXRD patterns that is presented in Fig. 4.1a-c, provides evidence that the actual composition of the LDH layers can be influenced by the choice of the $Mg^{2+}:Al^{3+}$ ratio in the mixed metal salt solution.
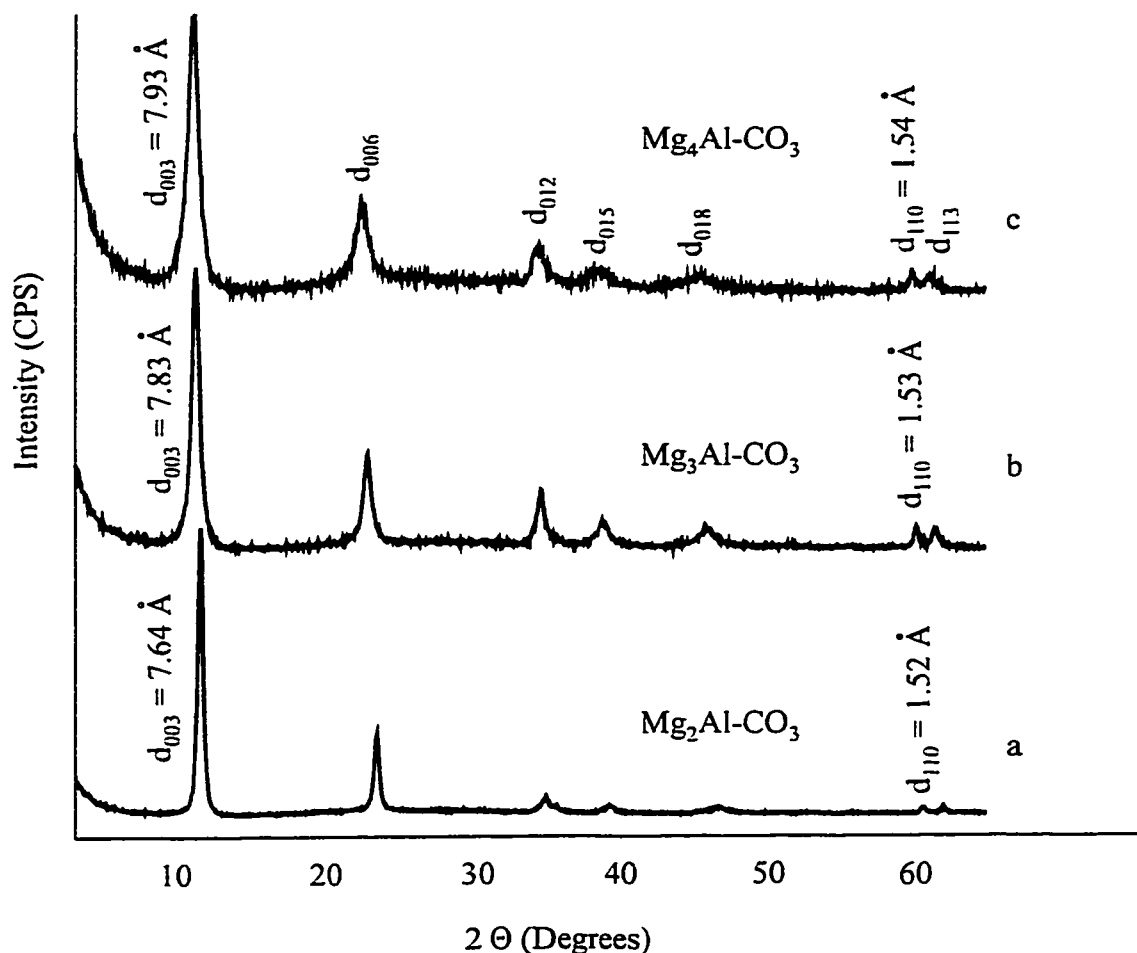
Fig. 4.1: POXRD patterns of a) Mg₂Al-CO₃ b) Mg₃Al-CO₃ and c) Mg₄Al-CO₃

Based on the observed d_{003} reflections in Fig. 4.1a-c, the crystallinity of each sample was evaluated in terms of the D value calculated using the Scherrer equation[105]. It was found that the estimated mean crystallite size determined from this equation decreased from 193 Å for the 2:1 product to 134 Å for the 3:1 and 122 Å for the 4:1. It is possible that the higher total cation concentration of the mixed metal salt solutions prepared with a 4:1 or 3:1 Mg^{2+}:Al^{3+} ratio resulted in higher nucleation rates of new LDH crystallites during coprecipitation, which would result in a less crystalline product.

Different total cation concentrations occurred in the mixed metal salt solutions because in each case the same amount of $Al(NO_3)_3$ was always dissolved in a fixed amount of DDI water, followed by the addition of an appropriate amount of $Mg(NO_3)_2$ to obtain the desired $Mg^{2+}:Al^{3+}$ ratio. Alternatively, it is also possible that greater anion disordering within the interlayer regions of the lower surface charge density materials is responsible for the observed broadening of the diffraction peaks. The latter explanation also illustrates that in many cases there is a preferred structure or composition that the LDH will most readily adopt; generally speaking the preferred composition is the one that is found in the naturally occurring mineral, as in this case the apparent preference is to form Mg_2Al-CO_3 which is analogous to the mineral hydrotalcite. Thus, it may be possible to induce the LDH structure to form over a wide range of compositions (i.e. different $M^{2+}:M^{3+}$ ratios or with interlayer anions other than carbonate) if conditions are carefully controlled. However, even greater care must be taken during the subsequent steps to ensure that the more highly preferred LDH compositions do not have an opportunity to form.

4.2.3 Layer composition of the Mg$_R$Al-CO$_3$ precursors (R = 2, 3, 4)

The Mg:Al ratios determined by ICP-AES and tabulated in Table 4.1 are very close to the expected values, confirming that nearly complete precipitation of both metal cations has occurred. It is possible, however, that a separate x-ray amorphous phase may have been formed in addition to the desired LDH-CO$_3$ product, as was previously

described in Section 3.2.3.   The apparent layer compositions were confirmed by

examining the d_{110} reflections of the three POXRD patterns presented in Fig. 4.1. The

d_{110} reflection is equal to one half the a parameter of the unit cell, which is determined by

the average inter-cation separation within the LDH layers.   It is known that the a

parameter changes almost linearly with the $M^{2+}:M^{3+}$ ratio[11], therefore it is possible to use

the position of the d_{110} reflection to estimate the true layer composition of the LDH-CO$_3$,

free of the possible interference from other phases. The a values were determined to be

3.07, 3.06 and 3.04 Å for the 4:1, 3:1 and 2:1, respectively, corresponding[11] to R values

of 3.8, 3.0 and 2.0. These values deviate by as much as 8% from the values determined

by ICP-AES analysis, but provide convincing evidence that the layer compositions of the

LDH-CO$_3$ precursors are very close to the desired values.

Carbon analysis of the samples was also consistent with these results, with the

LDH-carbonates containing about 1.4-2.4 percent carbon by weight. Based on a charge

balance analysis it was expected that the material with the highest surface charge density

(lowest R) would contain the most carbon, and the material with the lowest surface

charge density would contain the least carbon. Assuming that there are four water

molecules of crystallization associated with the LDH structure, the expected weight

percent carbon values were calculated to be 2.48%, 2.00% and 1.68% for the materials

with R values of 2, 3 and 4, respectively. The values that were obtained experimentally

for the Mg$_2$Al-CO$_3$ and Mg$_4$Al-CO$_3$ precursors are in excellent agreement with the

expected values, whereas the Mg$_3$Al-CO$_3$ precursor appears to be substantially deficient

in carbonate. The deviation from the expected trend is likely due to varying degrees of hydration of the materials, which could increase the total mass and thus decrease the weight percent carbon. As indicated in Table 4.1 the $Mg_3Al\text{-}CO_3$ product contains almost twice as much hydrogen as do the other two layer compositions, likely in the form of zeolitic water, which partially accounts for the low weight percent carbon of the material.

The absence of nitrogen in the $Mg_2Al\text{-}CO_3$ and $Mg_3Al\text{-}CO_3$ samples indicates that that preferential incorporation of carbonate anions occurred, and therefore the nitrate anion of the metal salts was not incorporated. It is interesting to note, however, that the $Mg_4Al\text{-}CO_3$ precursor contains approximately 0.9 weight percent nitrogen, and therefore some nitrate anions were intercalated. While it is thermodynamically more stable to form separate NO_3^- and CO_3^{2-} containing phases compared to a single phase with mixed interlayer anion species, there is no direct evidence in the POXRD pattern to suggest that this has occurred (see Fig. 4.1c). In fact, the broad d_{003} reflection suggests a more highly disordered interlayer region, which is consistent with there being two different anions simultaneously intercalated within the interlayer region of a single LDH phase.

4.2.4 The Mg$_R$Al mixed metal oxide precursors (R = 2, 3, 4)

The preceding discussion has shown that excellent control over the layer composition may be achieved within the series $Mg_RAl\text{-}CO_3$ (R = 2, 3, 4). The precursor materials obtained by coprecipitation of mixed metal salt solutions with $Mg^{2+}:Al^{3+}$ ratios of 2:1, 3:1 and 4:1 appear to be of medium to high crystallinity for this type of material,

and furthermore they are essentially free of contamination by other phases. Having ascertained the flexibility of the first step in the synthesis scheme, the next step involved assessing the effect of layer composition on the thermal decomposition process, which was necessary in order to volatilize and thereby remove the interlayer carbonate anions prior to attempting to form the LDH-OH precursor.

The mixed oxide solid solutions were obtained by thermally decomposing the Mg_RAl-CO_3 precursor in a quartz tube furnace at 550°C under flowing nitrogen. After calcination the residue retained approximately 50% of the mass of the original precursor; the remainder was evolved as CO_2 and water. The POXRD patterns of the mixed oxide solid solutions with Mg:Al ratios of 2:1, 3:1 and 4:1 are presented in Fig. 4.2a, 4.2b and 4.2c, respectively. In each case, the POXRD patterns resemble a diffuse MgO diffraction pattern, with three broad reflections that correspond to three of the most intense lines that are visible below $2\theta = 60°$ in the MgO pattern. The diffraction peaks for MgO are tabulated in Table 4.2 for comparison with the POXRD patterns that appear in Fig. 4.2. Since all lines can be indexed to the MgO powder pattern, there is no evidence that a spinel ($MgAl_2O_4$) phase was formed under these decomposition conditions.

Table 4.2: Diffraction lines, intensities and indexing for MgO[119]

d (Å)	Intensity (%)	h k l
2.43	33	1 1 1
2.10	17	2 0 0
1.49	100	2 2 0
1.27	17	3 1 1
1.21	17	2 2 2
1.05	8	4 0 0

Intensity (CPS)

$d_{111} = 2.50\ \text{Å}$

$d_{200} = 2.11\ \text{Å}$

$d_{220} = 1.48\ \text{Å}$

Mg:Al = 4:1   c

Mg:Al = 3.1   b

Mg:Al = 2:1   a

10   20   30   40   50   60

2 Θ (Degrees)
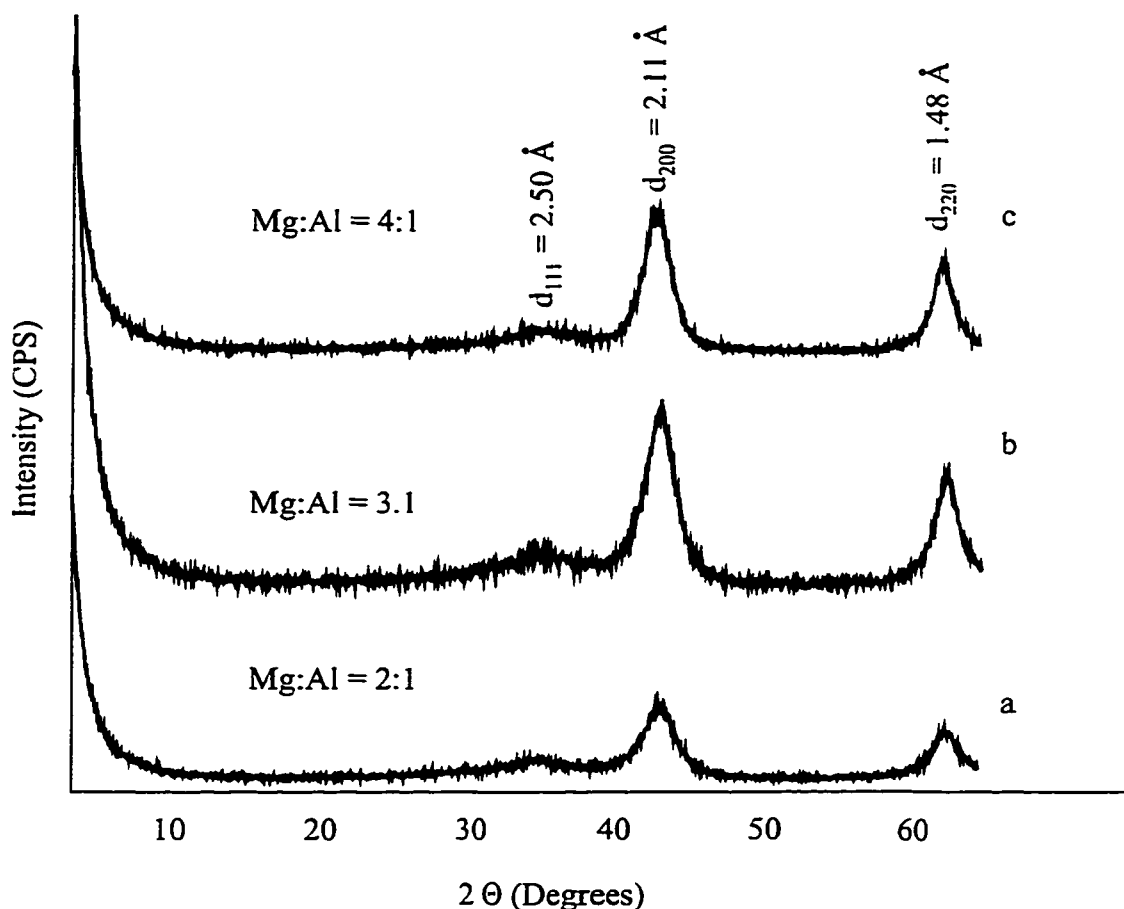
Fig. 4.2: POXRD patterns of Mg/Al mixed metal oxides with a) R=2 b) R=3 c) R=4

The effect of thermal decomposition on the coordination of Al^{3+} cations in the LDH layers of the Mg_RAl-CO_3 precursors was probed by ^{27}Al MAS-NMR spectroscopy. The spectra corresponding to Mg_3Al-CO_3, Mg_3Al mixed oxide and Mg_3Al-H_2W_{12} appear in Fig. 4.3a, 4.3b and 4.3c, respectively. In each case, the δ values are reported with respect to $Al(H_2O)_6^{3+}$. The presence of a single resonance around 13.5 ppm in Fig. 4.3a indicates that aluminum exists only in an octahedrally coordinated environment in the sample, which is consistent with all aluminum being incorporated into the brucite-like
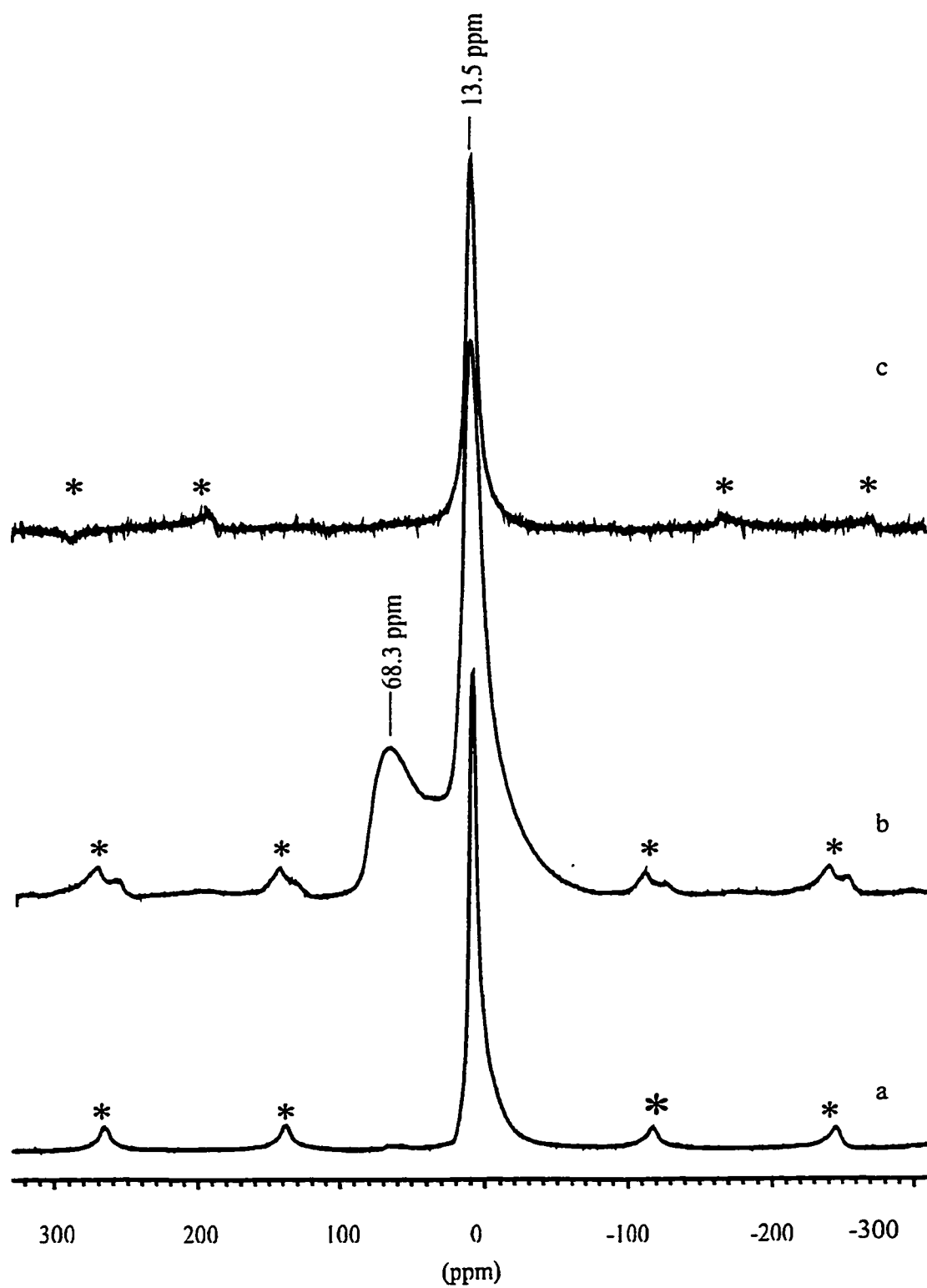
Fig. 4.3: ^{27}Al MAS-NMR spectra of a) Mg_3Al-CO_3 b)Mg_3Al mixed metal oxide solid solution and c) Mg_3Al-H_2W_{12} (note: * denotes spinning sidebands).

structure of the LDH layers. After calcination at 550°C, however, some of the aluminum has become tetrahedrally coordinated, as indicated by a second resonance that appears around 68.3 ppm. Although the amount of tetrahedral aluminum cannot be quantified by this method, other reports have estimated that approximately 20% of the aluminum cations exist in a tetrahedral environment following calcination[37]. The change in coordination of aluminum from octahedral to tetrahedral is not associated with the formation of a spinel phase, but instead is the result of aluminum cations migrating into the interlayer region as the carbonate anions are evolved as CO_2. Following the rehydration and POM anion exchange steps, all aluminum reverts to an octahedral environment, as shown in Fig. 4.3c, demonstrating the reversibility of the thermal decomposition step. Note that the signal to noise ratio is lower in Fig. 4.3c compared to Fig. 4.3a, which is due to the dilution of Al^{3+} that occurs upon the incorporation of the high molecular weight, bulky POM anions into the gallery region of the LDH.

The elemental analysis data that were obtained for each mixed oxide sample was tabulated in Table 4.1. Simply heating the samples to 550°C is not expected to affect the $Mg^{2+}:Al^{3+}$ ratio of the calcined samples, and ICP analysis confirms that the ratios are unchanged compared to the LDH-carbonates. The degree of decarboxylation, however, is known to depend upon the aluminum content in the layers[44], and carbon analysis reveals that the Mg_2Al mixed oxide is composed of 0.85% carbon by weight, which corresponds to approximately 20-30% of the original carbonate anions being retained. As the Mg^{2+} content of the layers increases, the amount of residual carbonate decreases to a minimum

of approximately 0.11 weight percent. The residual carbonate anions are believed to be coordinated to the Mg^{2+} cations[44], which thermogravimetric differential thermal analysis (TG-DTA) studies have shown are not evolved until the sample is heated to 900°C. Heating the LDH structure to temperatures approaching 900°C, however, results in migration of the Al^{3+} cations into the MgO matrix, irreversibly forming a spinel phase ($MgAl_2O_4$) and consequently lowering the Al^{3+} content in the mixed oxide solid solution.

The formation of a mixed metal oxide solid solution by thermal decomposition of the Mg_RAl-CO_3 precursor presents a potential limitation to the use of the current method as a general route for the synthesis of LDH-POM materials with different layer compositions. Within the homologous series Mg_RAl-CO_3 it is not possible to remove 100% of the carbonate anions from the low R materials. Extensive studies dealing with the decarboxylation behavior of other $M^{2+}_RM^{3+}$ materials have not yet appeared, and therefore it is not possible to determine whether or not similar limitations will be encountered when working with other layer compositions. Despite the incomplete removal of carbonate anions during this step, however, it will be shown that subsequent stages of the synthesis method may still be performed, ultimately yielding well ordered LDH-POM materials.

4.2.5 The Mg_RAl-OH precursors (R = 2, 3, 4)

The POXRD patterns shown in Fig. 4.4 correspond to the LDH-OH precursors that were formed after stirring an aqueous 1 % (w/w) suspension of the mixed oxide in
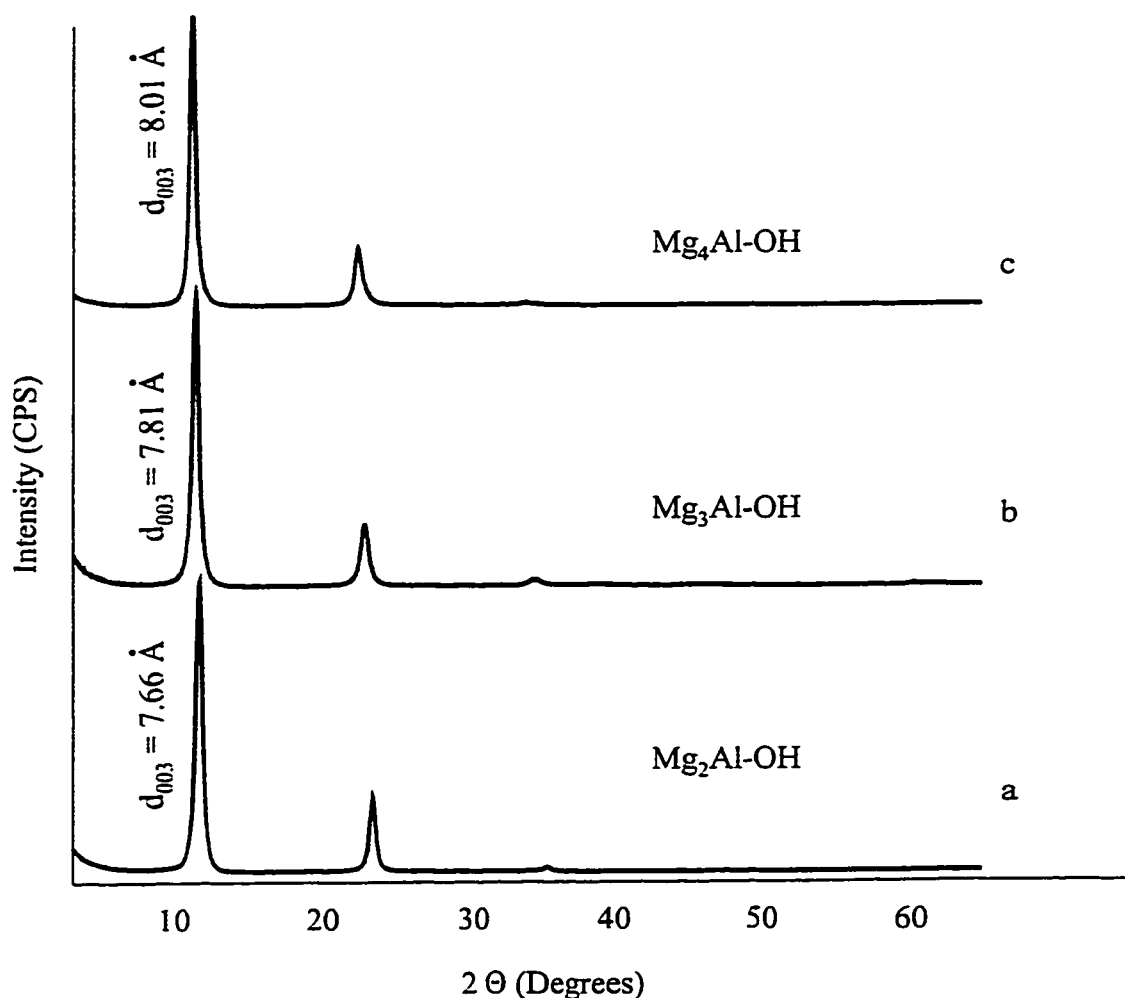
Fig. 4.4: POXRD patterns of a) Mg_2Al-OH b) Mg_3Al-OH and c) Mg_4Al-OH

DDI water under nitrogen for five days. As was previously observed for the Mg_RAl-CO_3 precursors, the d_{003} values were found to change significantly from 7.66 Å for the 2:1 to 7.81 Å for the 3:1 and 8.00 Å for the 4:1 precursors. The magnitude of the change in the d_{003} position with changing layer composition is larger in the LDH-OH precursors than for any other interlayer anion species (i.e. Cl^-, NO_3^-, CO_3^{2-} etc.). It is also interesting to

note that the intensity of the d_{003} peak in each pattern is approximately an order of magnitude greater than the d_{003} peak intensities in the corresponding LDH-CO_3 precursors. One possible explanation is that the interlayer hydroxide anions have properties that are very similar to those of the interlayer water molecules, thus permitting the two interlayer species to form a loosely associated, hydrogen bonded network within the gallery region. The highly delocalized nature of the negative charge within the ordered network could allow the interaction with the layer hydroxyl groups to be optimized; if true, this would result in optimal reproducibility in the layer stacking.

It is apparent that for all three layer compositions the mixed oxide solid solution readily rehydrated to reform the initial LDH structure and that a highly crystalline phase was obtained in each case. The presence of residual carbonate anions in the Mg_2Al mixed oxide solid solution did not interfere with the formation of the Mg_2Al-OH phase, suggesting that the limitation that was identified in the previous section may not pose a serious problem within the context of the overall method.

4.2.6 The Mg_RAl-adipate precursors (R = 2, 3, 4)

The final precursor, the LDH-adipate, showed the most variation from one layer composition to the next, as can be seen in the powder patterns shown in Fig. 4.5. In each case a large excess of adipic acid was used to convert the LDH-hydroxide to the LDH-adipate (218%, 215% and 394%, respectively, for the 2:1, 3:1 and 4:1 samples). The POXRD pattern of Mg_2Al-adipate (Fig. 4.5a) suggests an LDH material in which the
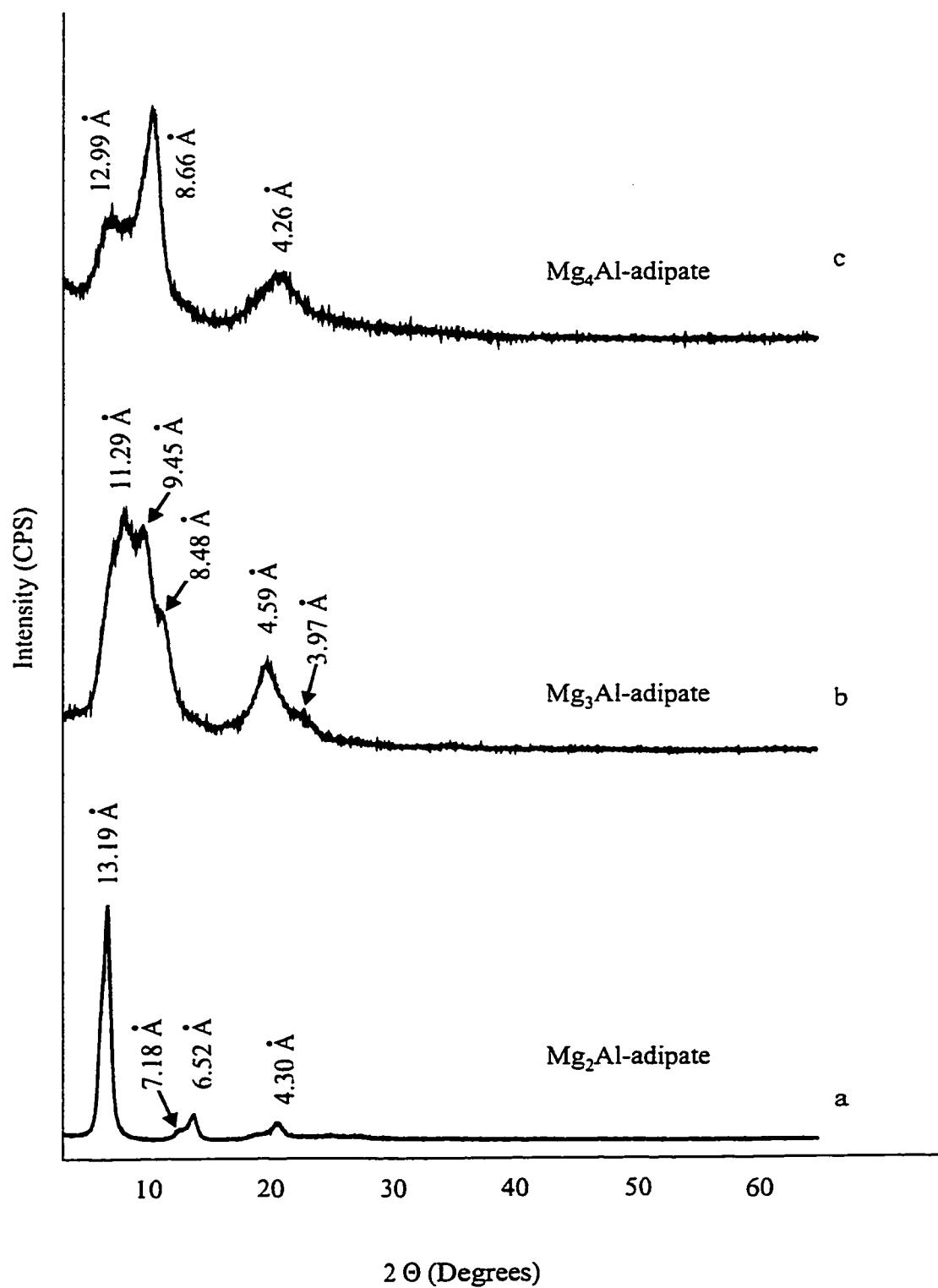
Fig. 4.5: POXRD patterns of a) Mg₂Al-adipate b) Mg₃Al-adipate and c) Mg₄Al-adipate

intercalated adipate anions are preferentially orientated with their long axes perpendicular

to the inorganic layers. The d_{003} spacing of this material is 13.19 Å, which agrees very

well with the value that would be expected for this orientation based on the calculated

length of the adipate anion[8].

Elemental analysis of the Mg_2Al-adipate precursor (Table 4.1) confirmed that the

$Mg^{2+}:Al^{3+}$ ratio was retained at least until the penultimate step of the overall synthetic

method, and that the weight percent carbon content of the sample is 13.64%. The amount

of carbon (as adipate) necessary to exactly balance the layer charge is 12.56 weight

percent and thus an excess of adipate anions are present in the LDH material. It is likely

that some of the excess adipate anions are adsorbed on the surface of the LDH

crystallites. However, the presence of singly deprotonated adipate anions is also possible,

which would necessitate the incorporation of additional anions above the amount

expected based on the presence of doubly deprotonated species only in the gallery region.

A similar amount of adipic acid (215% excess) was added to the Mg_3Al-OH

slurry, however, an LDH-adipate characterized by a substantially different POXRD

pattern (Fig. 4.5b) was obtained. In this case there appears to be very little ordering of

adipate anions in the interlayer region, and multiple orientations may be present. There is

also a much larger weight percent carbon than was expected (14.07% compared to

10.42% expected). The lower surface charge density of the Mg_3Al-OH precursor may

have resulted in some adipate anions adopting an orientation in which the carbon chain

is inclined at an angle with respect to the LDH layers, which could contract the LDH

basal spacing to a value close to 9.45 Å. Other phases are apparently present as well, and

may be characterized by basal spacings of about 11.3 Å and 8.5 Å (this small shoulder at

8.5 Å may indicate a separate phase with a second order diffraction close to 4.0 Å).

These additional reflections are tentatively assigned to LDH-adipate phases in which the

adipate anions are oriented either perpendicular to (11.3 Å) or parallel to (8.5 Å) the LDH

layers. The former orientation is routinely observed, while the latter orientation has

previously been suggested for terephthalate anions present in the gallery space of low

surface charge density LDH materials[47].

Finally, it was found that a significantly larger excess of adipic acid had to be

added to the Mg_4Al-OH slurry in order to obtain an LDH-adipate that would undergo

POM anion exchange. A 394% excess of adipic acid reacted with the Mg_4Al-OH

precursor yielded the POXRD pattern that is shown in Fig. 4.5c. This POXRD pattern

qualitatively resembles that in Fig. 4.5b, at least in terms of the line breadth. Although it

is rather difficult to draw definite conclusions regarding the nature of the Mg_4Al-adipate

phase, the Mg^{2+}:Al^{3+} ratio determined by ICP-AES spectroscopy was 3.94:1, indicating

nearly complete retention of the initial ratio. In addition, the amount of excess carbon

present in the Mg_4Al-OH precursor was very similar to the excess determined for the

Mg_2Al-adipate, and was substantially lower than the Mg_3Al-adipate.

The behavior of the Mg_4Al-adipate precursor was quite interesting, and therefore

it was probed in greater detail than for the other two layer compositions. Fig. 4.6 presents

the POXRD patterns obtained by reacting the Mg_4Al-OH precursor with various amounts of adipic acid. When a stoichiometric amount of adipic acid was used (Fig. 4.6a), two distinct LDH phases are present. These correspond to a pure LDH-adipate in which the adipate anions are orientated parallel to the inorganic layers (based on the d_{003} spacing of 8.61 Å) and unreacted LDH-OH (d_{003} = 8.13Å). It is not possible to determine the relative amount of each phase, however it is possible to conclude that a deficiency of adipate anions was present during this reaction. The most likely explanation is that a substantial number of adipate anions were not fully deprotonated and therefore were incapable of balancing two layer charges.

Increasing the amount of adipic acid such that a 50% excess was used resulted in the POXRD pattern shown in Fig. 4.6b. The d_{003} peak has shifted to 8.88Å, and only a shoulder remains at 8.13Å, indicating that the LDH-adipate in which the anions are oriented parallel to the LDH layers now dominates over the unreacted LDH-OH phase. It was found that these adipate anions were more difficult to exchange with POM than the anions with a perpendicular orientation relative to the layers, and thus even larger excesses of adipic acid were examined. Using between 100 to 177% excess (i.e. 2 – 3 fold excess) of adipic acid based on the fully deprotonated form resulted in the appearance of a broad shoulder at 2θ values below that of the d_{003} peak (Fig. 4.6c-e). The gradual shift to larger d values (i.e. lower 2θ) was also accompanied by a broadening of the d_{003} (adipate oriented parallel) reflection, signaling decreased order of the adipate
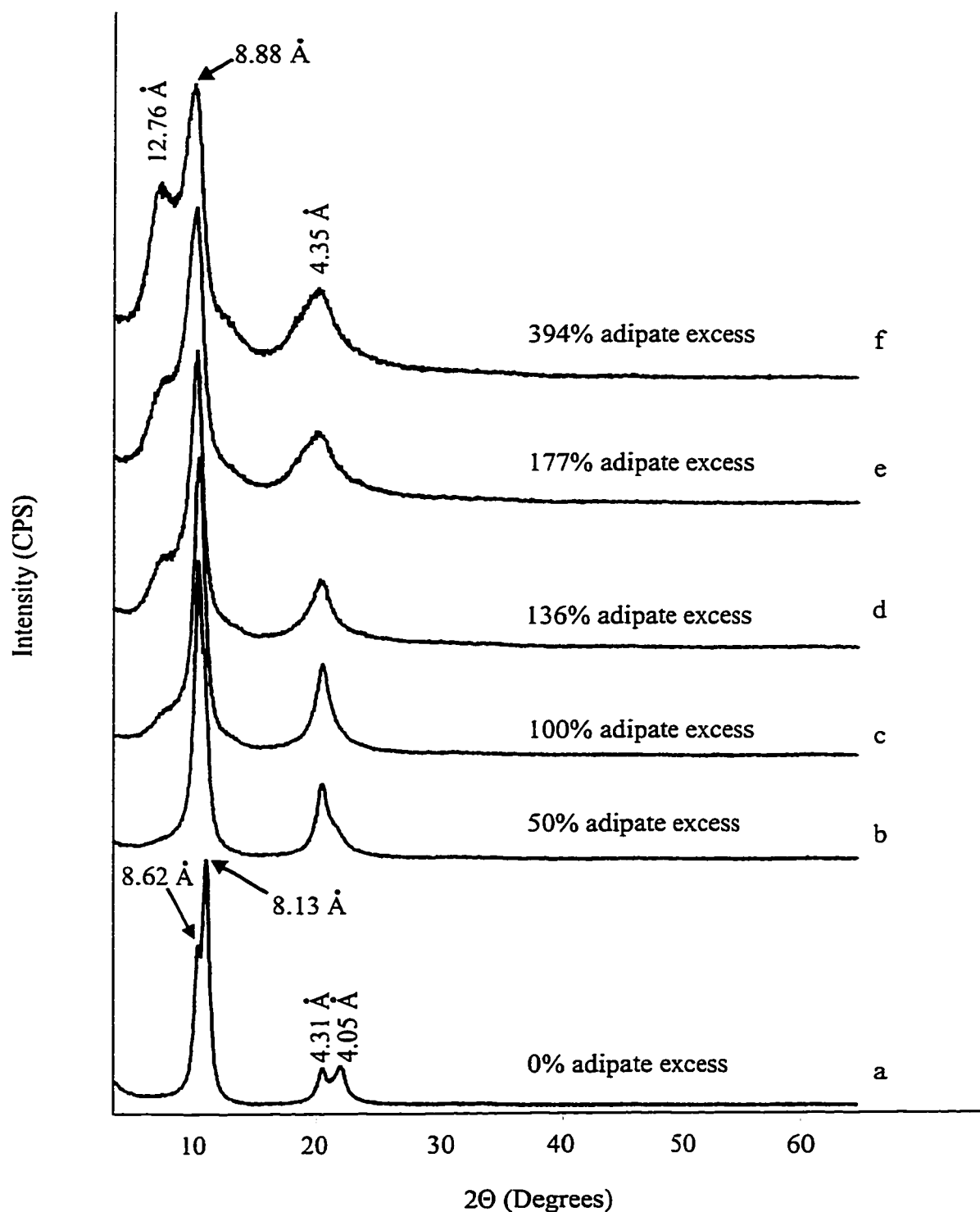
Fig. 4.6: POXRD patterns of Mg₄Al-adipate prepared using a) 0% b) 50% c) 100% d) 136% e) 177% and f) 394% excess of adipate anions

anions in the gallery space. Upon using a 394% excess of adipic acid, the POXRD pattern shown in Fig. 4.6f was obtained, which was discussed previously within the context of the other layer compositions.

4.2.7 Control over layer composition in the Mg_RAl-H_2W_{12} series (R = 2, 3, 4)

The final step of the synthesis route involved the replacement of the interlayer adipate species with metatungstate anions (H_2W_{12}) by anion exchange under ambient pH conditions. The reaction was carried out at near reflux temperature (94°C) and was complete in less than 5 minutes, as indicated by the POXRD patterns of the final products, presented in Fig. 4.7a-c. In each case the basal spacing is 14.8-14.9 Å, corresponding to a gallery height of approximately 10.0 Å which is in excellent agreement with the spherical diameter of the Keggin ion. The ubiquitous impurity phase is also present, as indicated by the broad reflection that is observed around 11 Å and has been denoted by an asterisk in each pattern.

As discussed in the Introduction section, control over the M^{2+}:M^{3+} ratio at all stages of the synthesis is important since the layer charge density affects the lateral spacing between the pillars in the final product. The discussion presented in the preceding sections indicates that the Mg:Al ratios did in fact remain very close to the desired value in each of the precursors that were formed. The ICP results presented in Table 4.3 reveal that the Mg:Al ratios in the final Mg_RAl-H_2W_{12} products are slightly lower than the desired values, and thus some dissolution of magnesium from the layers
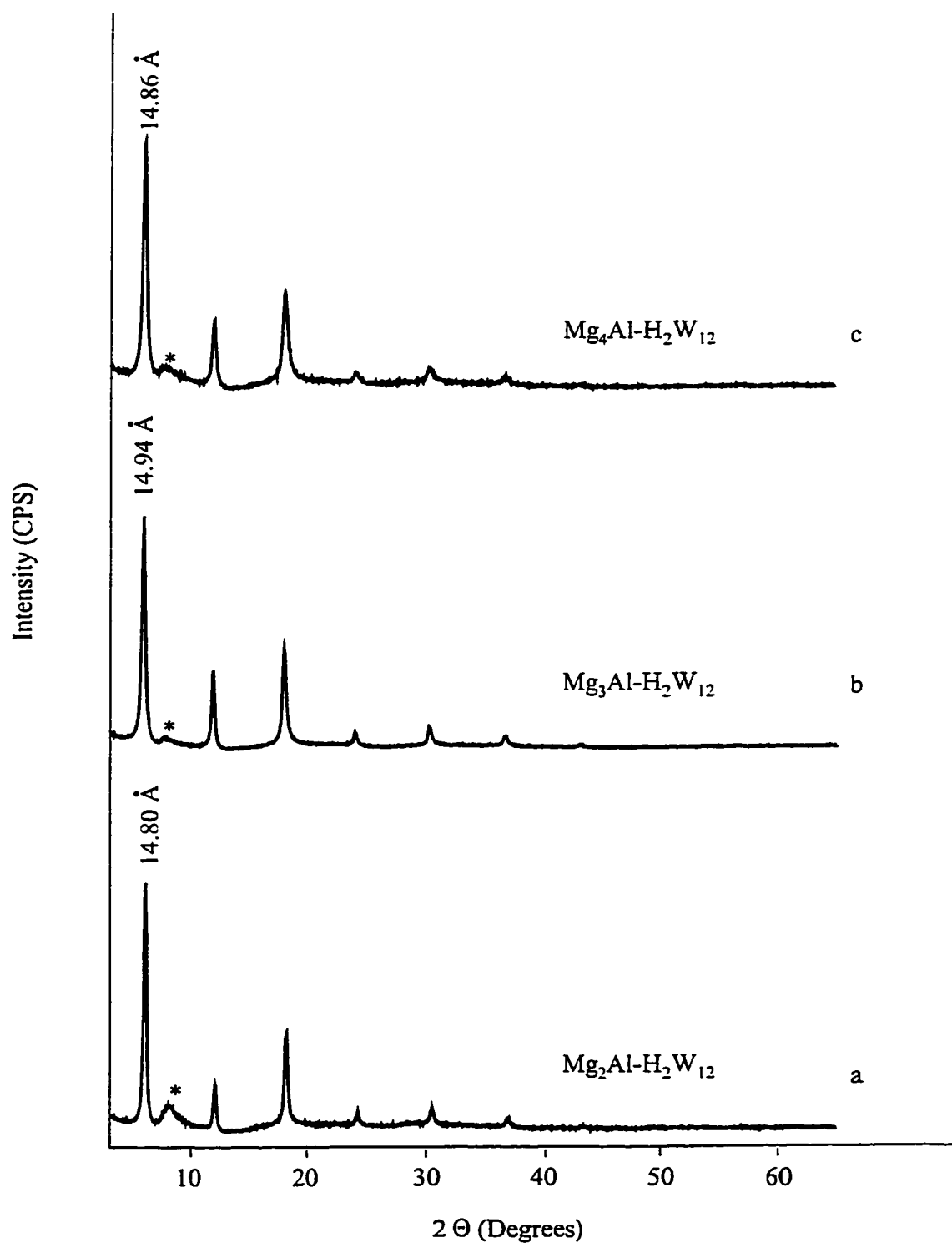
Fig. 4.7: POXRD patterns of a) Mg_2Al-H_2W_{12} b) Mg_3Al-H_2W_{12} and c) Mg_4Al-H_2W_{12} (note: * denotes presence of impurity phase).

has occurred in the final step. It is significant to note, however, that dissolution is minimal, and thus a series of POM-pillared LDH materials was produced with a relatively wide range of Mg:Al ratios. These results are in contrast to earlier work in which we synthesized POM pillared LDH materials using organic anion pillared precursors according to the method described by Drezdzon[8]. As discussed in Chapter 3, the Mg:Al ratio of the inorganic layers was 2:1 in all cases, regardless of the ratio that was present in the initial metal salt solutions[48].

Table 4.3: Chemical composition, BET surface areas and micropore volumes of Mg$_R$Al-H$_2$W$_{12}$ products

Sample	d_{003} Å	Composition[a] (Mg:Al:W)	S_{BET} (m^2/g)	S_{BET} (Å^2/e$^+$)	Micropore volume (mLg^{-1})
Mg$_3$Al-CO$_3$	7.88	3.08:1:00	94	4.2	–
Mg$_2$Al-H$_2$W$_{12}$	14.80	1.75:1.00:1.87	114	11.5	0.026
Mg$_3$Al-H$_2$W$_{12}$	14.94	2.31:1.00:1.97	140	15.6	0.039
Mg$_4$Al-H$_2$W$_{12}$	14.86	3.51:1.00:2.36	110	15.1	0.029

[a] ICP analysis on Thermo Jarrell Ash Atom Scan 16 spectrometer.

The W:Al ratio also appears in the same column of Table 4.3 as the Mg:Al ratios. As previously mentioned, the W:Al ratio is close to the expected value of 2:1 in each case and thus POM anion exchange is nearly complete for each Mg:Al ratio. It is interesting to note that the W:Al ratio increases from 1.87:1.00 in the case of the Mg$_2$Al-H$_2$W$_{12}$ material to 1.97:1.00 for the Mg$_3$Al-H$_2$W$_{12}$ and 2.36:1.00 for the Mg$_4$AlH$_2$W$_{12}$. One possibility is that these differences simply reflect different levels of contamination by the impurity phase, which is of unknown composition. However, because the W:Al ratio

decreases as the Mg:Al ratio decreases, another possibility is that the bulky Keggin ion pillars become increasingly crowded in the interlayers of LDHs with higher surface charge densities, resulting in the intercalation of fewer of them than is necessary to fully balance the surface charge. It is possible that other anions present in solution are small enough to fit between the pillars and balance the residual positive layer charge. In the case of Mg_3Al-H_2W_{12}, however, the Keggin ions appear to be able to fit between the inorganic layers and exactly balance the positive charges. Finally, the Mg_4Al-H_2W_{12} material, in which the surface charge density is the lowest, exhibits a W:Al ratio of 2.36:1.00, indicating that there are more Keggin ions present than are necessary to balance the layer charge. This situation may arise if some of the metatungstate anions become partially protonated within the gallery space of the LDH, or if counter cations (i.e. Na^+) are present within the interlayer region and partially balance the anion charge. The presence of NH_4^+ is unlikely, due to the absence of its vibrational bands in the IR spectrum (not shown).

It is also important to recognize that the specific surface area of each Mg_RAl-H_2W_{12} product is between $110 - 140 \ m^2g^{-1}$. This value represents a significant increase over the value measured for the corresponding carbonate (typically about $95 \ m^2g^{-1}$), and suggests that significant microporous surface area is produced in the POM pillared products. The increase in surface area that is achieved by pillaring tends to be understated when expressed in terms of m^2 per gram due to the high molecular weight of the POM anions compared to carbonate, thus it is more informative to compare the

accessible surface area (in $Å^2$) per unit layer charge $(e^+)^{30}$. The accessible surface area of the pillared materials is between two and four times greater than for the carbonate containing precursor, as summarized in the fifth column of Table 4.3.

4.2.8 Pore size variation within the Mg_RAl-H_2W_{12} series (R = 2, 3, 4)

An examination of the micropore volume and size distribution was undertaken in order to determine whether the variation achieved in the layer composition induced any differences in the microporous structure of the final products. The micropore volume determined for each of the Mg_RAl-H_2W_{12} materials is tabulated in Table 4.3. A representative Argon adsorption isotherm appears in Fig. 4.8, and the pore size distribution plots are presented in Fig. 4.9a-c. The presence of very small micropores is indicated by the very steep argon adsorption isotherm at low relative pressure, which quickly reaches a plateau. The shape of the argon adsorption isotherm is very different at low relative pressure compared to the one shown in Fig. 3.15 which was obtained using a non-microporous Mg_2Al-TA LDH material.

The micropore distribution plots shown in Fig. 4.9 a-c are all bimodal, which is possibly due to the presence of two types of micropores, namely interlayer pores and intercrystalline pores[25]. Although it is difficult to accurately measure the distribution of pores with diameters of ca. 5 Å, we believe that Fig. 4.9 demonstrates a shift to smaller pore diameters with a very narrow distribution of sizes as the layer composition is varied from Mg:Al=4:1 to Mg:Al=2:1. This is particularly true for the 2:1 sample, where the
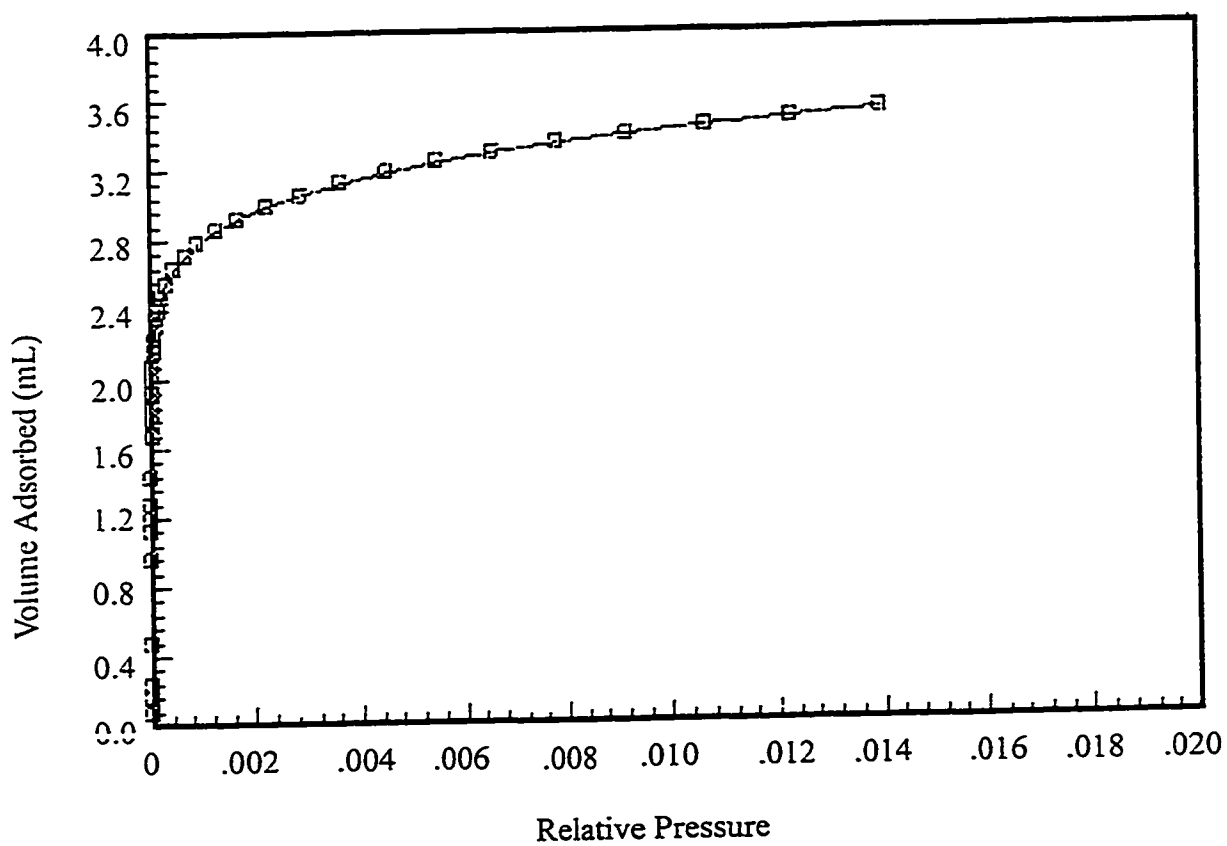
Fig. 4.8: Representative argon adsorption isotherm (obtained using $Mg_3Al\text{-}H_2W_{12}$)
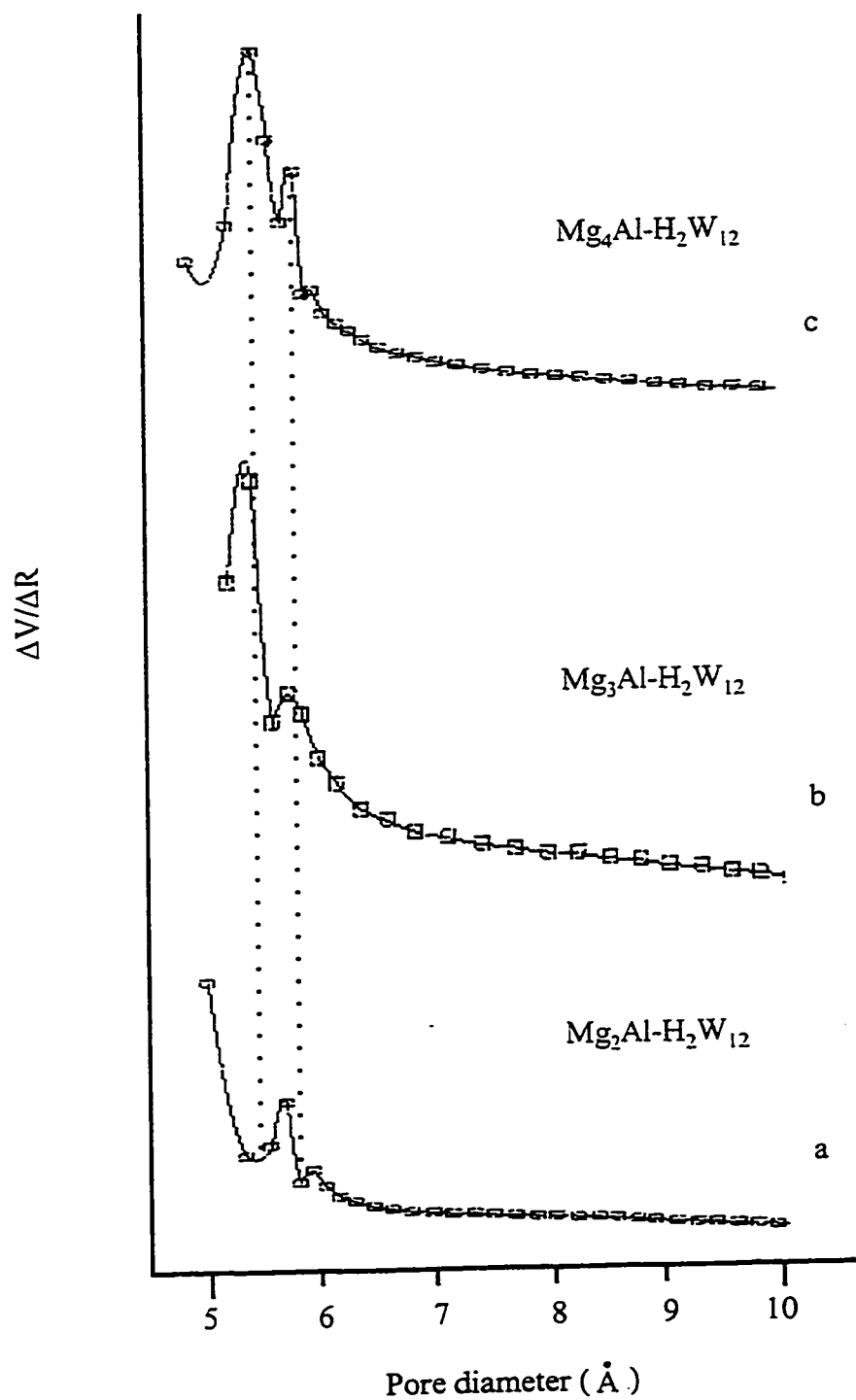
Fig. 4.9: Micropore size-distribution plots for a) $Mg_2Al-H_2W_{12}$ **b)** $Mg_3Al-H_2W_{12}$ **and c)** $Mg_4Al-H_2W_{12}$

more intense peak appears to be below the lower limit (c.a. 5 Å) of this method. If this is the case, then it is likely that the peak representing the smaller diameter pores corresponds to interlayer pores, where the dimensions are influenced by the inter-pillar spacing rather than the gallery height. There is no evidence of pores with a diameter of approximately 10 Å, which corresponds to the gallery height in POM-pillared LDHs containing the spherical Keggin ions.

Micropore volumes were determined from the argon adsorption isotherm assuming that the plateau of the adsorption isotherm represents the volume of argon (at standard temperature and pressure) that is required in order to fill completely the micropores of the sample. The largest micropore volume was found for $Mg_3Al-H_2W_{12}$, which also had the largest BET surface area (140 m^2g^{-1}). Although the surface area of $Mg_2Al-H_2W_{12}$ (114 m^2g^{-1}) was 4% larger than that of $Mg_4Al-H_2W_{12}$ (110 m^2g^{-1}), it had a micropore volume that was 10% smaller (0.026 mLg^{-1} c.f. 0.029 mLg^{-1}), which supports the view that smaller pores were formed in the material that had the higher surface charge density. In addition, comparing the specific surface area that was calculated on an $Å^2/e^+$ basis shows that the micropore volume of each material follows the same trend as the accessible surface area per unit charge.

4.3 The Mg₃Ga series

The work described in Section 4.3 is a continuation of our study of the physical, chemical and catalytic properties of polyoxometalate-pillared layered double hydroxide

materials containing gallium in the LDH layers. Previous results have indicated that the same synthesis conditions that are used to produce aluminum containing LDH materials may also be applied to the gallium containing analogues with good results[48,102]. In the following sections the potential of the synthesis method which proceeds through LDH-CO_3, mixed oxide, LDH-OH and LDH-adipate precursors is evaluated as a possible method for the synthesis of POM pillared LDH materials containing Ga^{3+} as the trivalent metal cation in the LDH layers.

4.3.1 POXRD study of the Mg₃Ga precursor series and POM pillared products

It was found that the Mg/Ga containing precursors underwent transformations very similar to the Mg/Al containing analogues, which were the subject of Section 4.2. The POXRD patterns obtained from Mg_3Ga-CO_3, Mg_3Ga-OH and Mg_3Ga-adipate are presented in Fig. 4.10a, 4.10b and 4.10c, respectively. The POXRD pattern of the initially formed Mg_3Ga-CO_3 precursor is virtually identical to that obtained for the Mg_3Al-CO_3 analogue (Fig. 4.1b). A diffraction pattern was not obtained for the Mg_3Ga mixed oxide, however it is assumed that the LDH structure decomposed reversibly with loss of carbonate anions as CO_2 since the Mg_3Ga-OH precursor was obtained (see Fig. 4.10b) after rehydrating the thermal decomposition product. Subsequent reaction of the Mg_3Ga-OH precursor with adipic acid yielded the Mg_3Ga-adipate precursor that produced the POXRD pattern shown in Fig. 4.10c. The exact appearance of the POXRD pattern was highly dependent on the amount of adipate used, but generally appeared to be
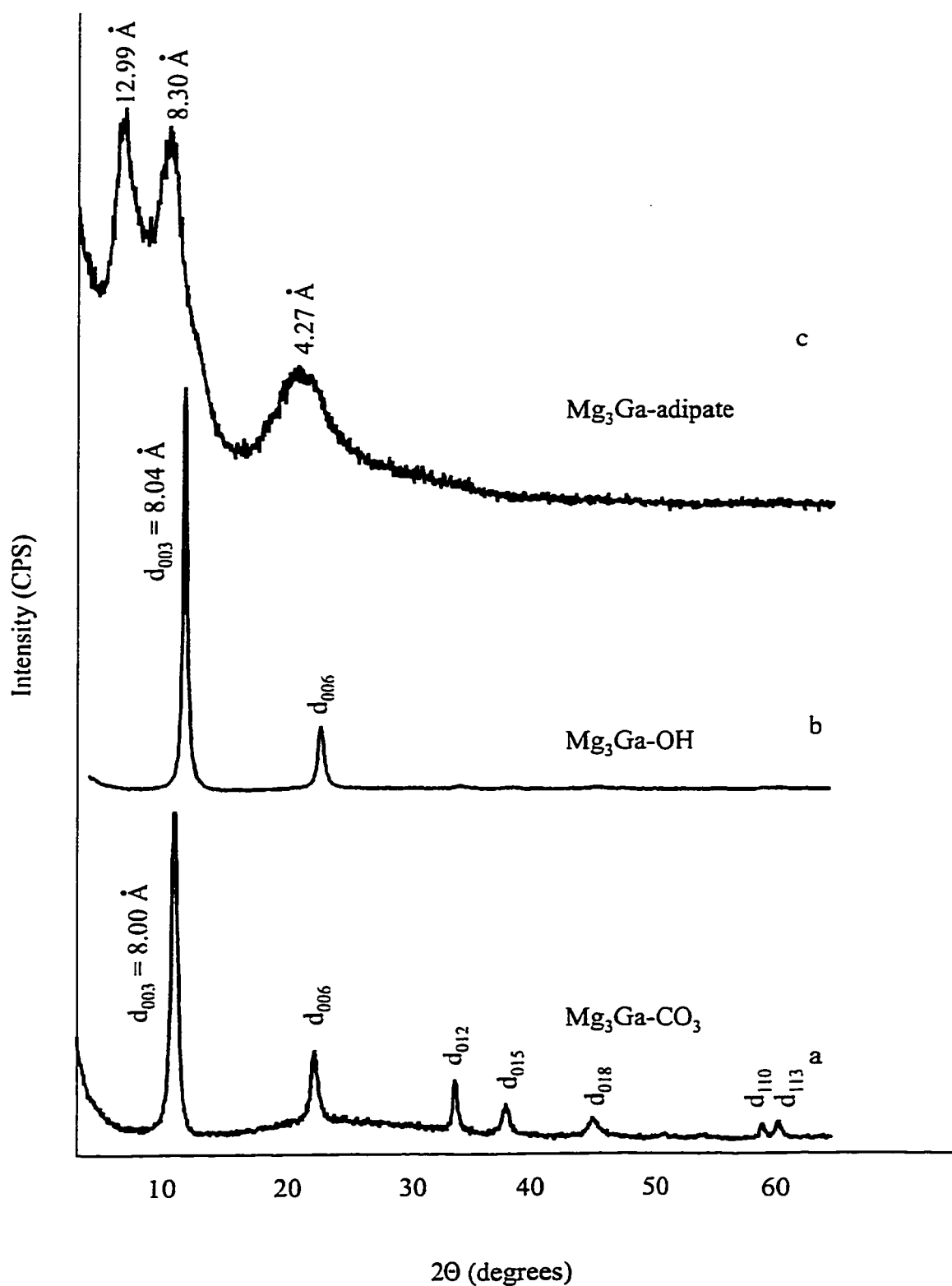
Fig 4.10: POXRD patterns of a) Mg$_3$Ga-CO$_3$ b) Mg$_3$Ga-OH and c) Mg$_3$Ga-adipate

qualitatively similar to the patterns produced by the Mg_4Al-adipate and Mg_3Al-adipate precursors discussed in Section 4.2.6. It is assumed that the description of the interlayer provided for the Mg/Al species also applies to the Mg/Ga analogues as well, based on the similar appearance of the POXRD patterns. The POXRD patterns of the final Mg_3Ga-H_2W_{12} and Mg_3Ga-PW_{11} products appear in Fig. 4.11a and 4.11b, respectively. These patterns are nearly identical to one another, which is expected since in each case the spherical diameter of the POM pillar is the same at approximately 9.8 Å. Six orders of diffraction from the basal spacing are observed, and the sharpness of the d_{003} reflection indicate that both products are exceptionally well ordered LDH materials, comparable to the Mg_3Al-H_2W_{12} product discussed in Section 4.2.7.

4.3.2 Physico-chemical properties of the Mg₃Ga-POM products

The aging period following POM anion exchange had an impact on the specific surface area of the various LDH-POM materials. To investigate the effect of aging, the product of a Mg_3Ga-H_2W_{12} synthesis was divided into two parts, where the first half was stirred for 5 minutes at 95°C following exchange, and the second half was stirred at the same temperature for an additional 3 hours. Comparison of the IR spectra (not shown) of the Mg_3Ga-H_2W_{12} sample aged for 5 minutes and of the sample aged for 3 hours indicate that the adipate anions are completely exchanged after only 5 minutes aging time. The POXRD patterns of each product (Fig. 4.12) appeared to be virtually identical as well. The only difference between the two samples was that the product that was stirred for 3
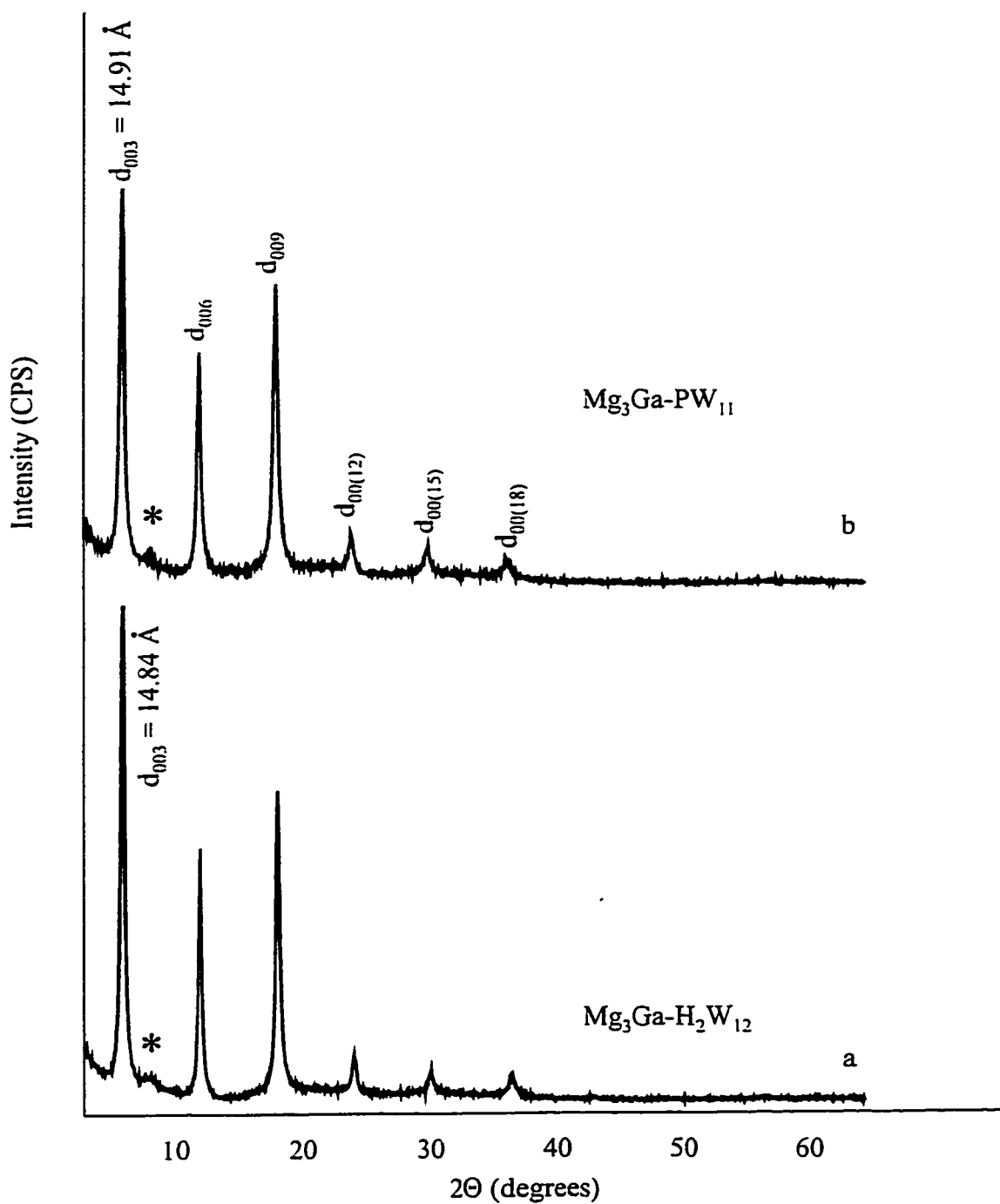
Fig 4.11: POXRD patterns of a) Mg₃Ga-H₂W₁₂ and c) Mg₃Ga-PW₁₁ (note: * denotes the presence of impurity phase).
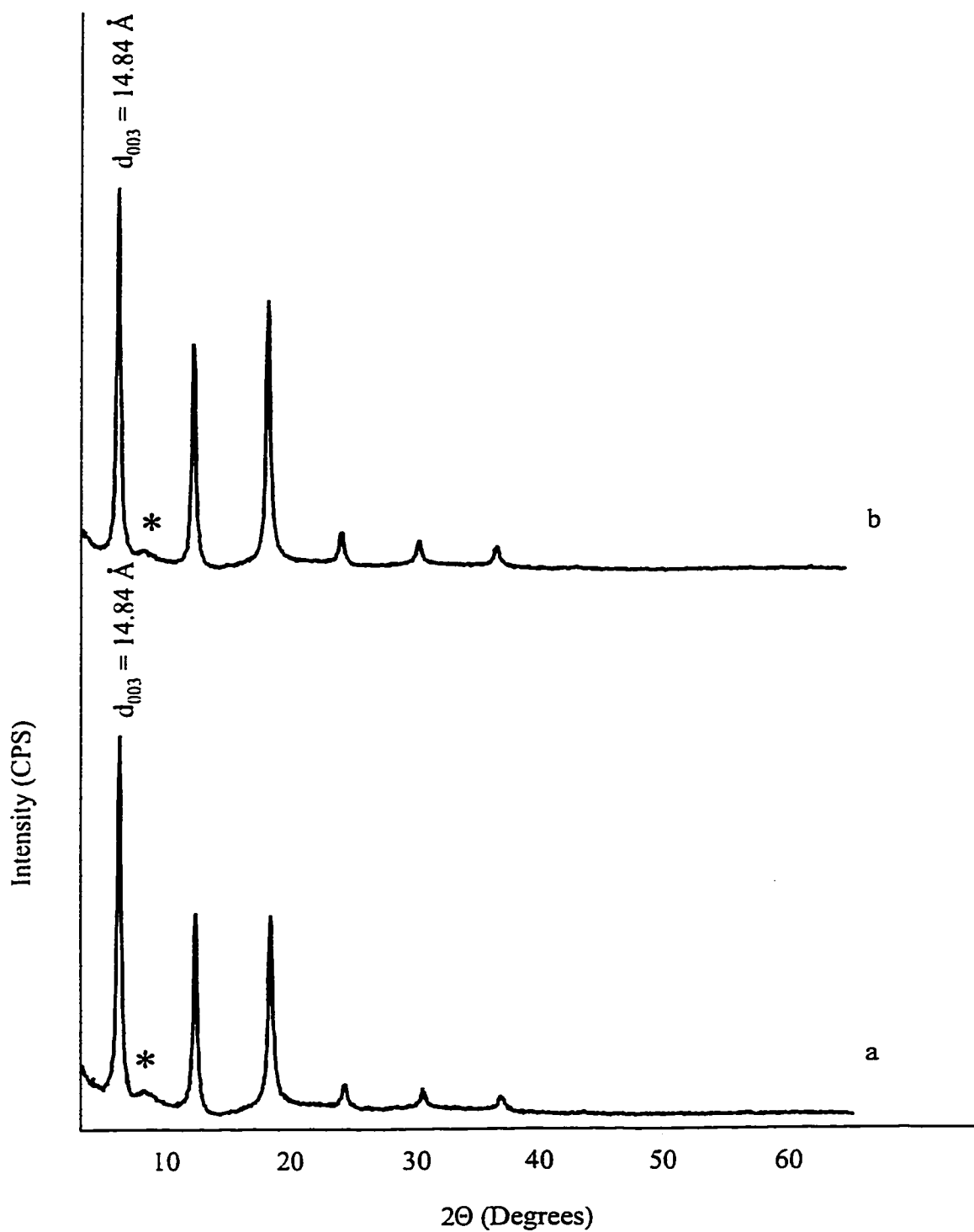
Fig. 4.12: POXRD patterns of Mg_3Ga-H_2W_{12} after a) 8 minutes aging time and
b) 3.5 hours aging time (note: * denotes presence of impurity phase).

hours displayed a BET surface area of 118 m^2g^{-1} compared to only 95 m^2g^{-1} for the

product that was stirred for 5 minutes. Since an extended aging period resulted in a more

highly microporous product, a two hour aging time was used in all subsequent syntheses.

Table 4.4: d_{003} values, chemical composition and BET surface areas for the Mg_3Ga-CO_3 precursor and POM-pillared products

Sample	d_{003} (Å)	Wt% Carbon[a]	M^{II}:M^{III}:W^b	BET surface area (m^2g^{-1})
Mg_3Ga-CO_3	8.0	1.41	-	40
Mg_3Ga-PW_{11}	14.9	0.1	1.6 : 1.0 : 1.0	77
Mg_3Ga-H_2W_{12}	14.7	0.2	1.7 : 1.0 : 1.9	118

[a] Carbon analysis on Control Equipment Corporation (CEC) 440 Elemental Analyzer.
[b] ICP analysis on Thermo Jarrell Ash Atom Scan 16 spectrometer.

4.3.3 ^{71}Ga MAS-NMR study of the changes to the LDH layer structure during synthesis of Mg_3Ga-H_2W_{12}

The transformations that the LDH layers underwent during the course of the

synthesis were also examined by solid state NMR techniques. The ^{71}Ga MAS-NMR

spectra of Mg_3Ga-CO_3, Mg_3Ga mixed metal oxide solid solution and Mg_3Ga-H_2W_{12} are

presented in Fig. 4.13a, 4.13b and 4.13c, respectively. These spectra are complicated by

the presence of strong spinning side bands (denoted by *) and by line broadening due to

rapid quadrupolar relaxation (^{71}Ga is a spin 3/2 nucleus). In addition the distortion of the

Ga^{3+} octahedra in the LDH layers, as described in Section 1.1.2, increases the effect of the

quadrupolar interaction. This causes the signal to vanish into the noise and thus further

complicates the analysis.
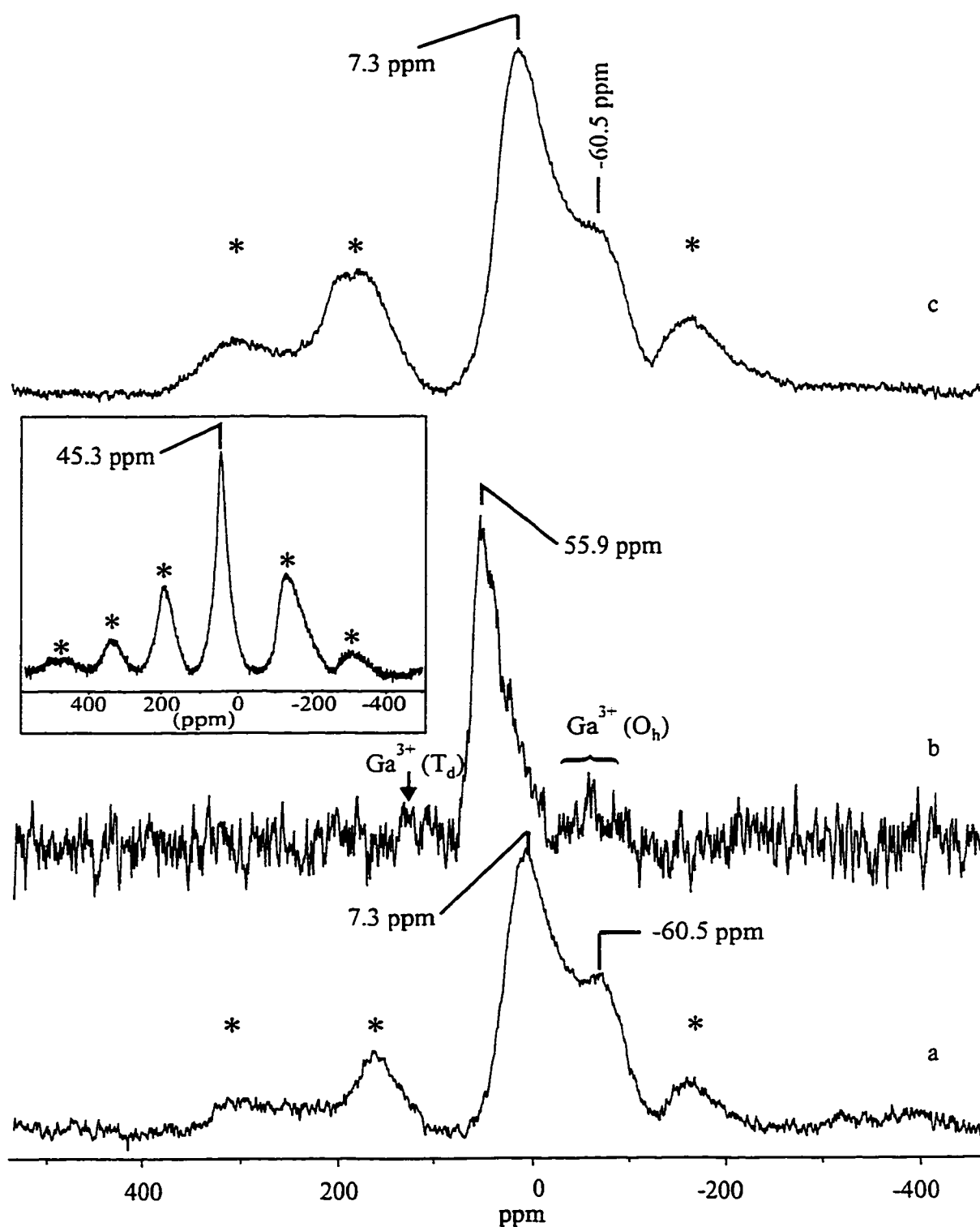
Fig. 4.13: ^{71}Ga MAS-NMR spectra of a) Mg$_3$Ga-CO$_3$ b) Mg$_3$Ga mixed oxide solid
   solution and c) Mg$_3$Ga-H$_2$W$_{12}$; inset is the spectrum of α-GaO(OH).
   (note: * denotes spinning side bands).

Despite the experimental difficulties of observing spin 3/2 nuclei the spectrum obtained from the Mg_3Ga-CO_3 material was found to contain two distinct resonances, one at $\delta = 7.3$ ppm and the other at $\delta = -60.5$ ppm, each with respect to $Ga(H_2O)_6^{3+}$. The resonance at $\delta = 7.3$ ppm is tentatively assigned to gallium in a relatively symmetric octahedral environment, probably within the LDH layers near the edge of the sheets, or alternatively in areas where the local Mg^{2+}:Ga^{3+} ratio is exceptionally large (i.e. >3:1). In each case, the absence of other close lying Ga^{3+} octahedra may prevent the LDH layers from becoming corrugated in an attempt to minimize the repulsion between the positively charged Ga^{3+} octahedra, thus resulting in less distorted octahedral coordination.

The second resonance, centered near $\delta = -60.5$ ppm, is believed to be a real peak and not merely a spinning sideband associated with the 7.3 ppm peak since other spectra that were obtained at different spinning speeds (8 kHz and 11 kHz) also displayed a signal in the same position. The higher field peak is attributed to gallium in highly distorted octahedral environments within the LDH layers, of the type that have previously been described in Section 1.1.2. The assignment of a resonance occurring at such a large negative chemical shift is not without precedent; octahedral gallium in a Ga-alunite phase has previously assigned to a resonance at -95 ppm[109].

Heating Mg_3Ga-CO_3 at 550°C under flowing N_2 for five hours resulted in the partial or total collapse of the LDH structure, as indicated by the NMR spectrum in Fig. 4.13b in which a single resonance at $\delta = 55.9$ ppm is visible. The resonance at $\delta = 55.9$

ppm has previously been observed and was attributed to gallium in a tetrahedral environment[102], which is consistent with the formation of a Mg(Ga)O mixed metal oxide solid solution. However this assignment seems rather dubious. Although tetrahedrally coordinated gallium is undoubtedly present in the calcined Mg_3Ga-CO_3 sample, one would expect the associated resonance to occur around $\delta = 125$ ppm, as indicated in Fig. 4.13b.

An alternative assignment for the resonance at $\delta = 55.9$ ppm is that it is due to the presence of a separate gallium rich phase, probably α-GaO(OH), which was formed either during the initial coprecipitation of the Mg_3Ga-CO_3 phase or during the subsequent calcination step. The main argument for making this assignment comes from a comparison between the ^{71}Ga MAS-NMR spectrum in Fig. 4.13b and the ^{71}Ga MAS-NMR spectrum (see inset, Fig. 4.13) obtained from the sample that produced the POXRD pattern shown in Fig. 3.7 (bottom pattern). The only crystalline phase that is apparent in the POXRD pattern of the Mg_2Ga-TA material formed at a coprecipitation pH value of 6.8 (actual Mg:Ga ratio was 0.20:1.00) was α-GaO(OH). The ^{71}Ga MAS-NMR spectrum of the $Mg_{0.2}Ga$ sample contained a single resonance at $\delta = 45.3$ ppm, which is quite close to the line at $\delta = 55.9$ ppm indicated on Fig. 4.13b. The resonance at $\delta = 55.9$ ppm does not appear to be present in the carbonate or POM-pillared materials (bottom and top spectra, respectively), although possibly it is present (weakly) and hidden by the broad signal at $\delta = 7.3$ ppm. If indeed it is absent, then that indicates that α-GaO(OH) is

formed during calcination and then subsequently redissolved and incorporated back into the brucite-like sheets of the LDH structure as the mixed metal oxide solid solution is rehydrated to form the LDH-OH precursor. It is suggested that the signals due to gallium within the mixed oxide in both tetrahedral and octahedral environments have been broadened sufficiently that they have disappeared into the noise, except for the very weak resonance around $\delta = -60$ ppm that is barely discernable above the level of the noise and possibly a shoulder on the high field side of the main $\delta = 55.9$ ppm peak.

Finally, the NMR spectrum obtained from the $Mg_3Ga-H_2W_{12}$ final product is presented in Fig. 4.13c, and appears to be virtually identical to the spectrum obtained from the original Mg_3Ga-CO_3. The fact that the ^{71}Ga MAS-NMR spectrum obtained from the $Mg_3Ga-H_2W_{12}$ final product appears to be identical to the original Mg_3Ga-CO_3 precursor supports the POXRD evidence that the LDH structure reforms after the mixed oxide intermediate is rehydrated. Thus the only obvious change that occurs in the structure of the LDH material during the overall synthesis reaction is the replacement of carbonate anions by POM anions in the interlayer region.

4.4 The Zn_RAl series

In order to evaluate the usefulness of the current method as a truly general route for the synthesis of LDH-POM materials with both acidic and basic LDH layers, an examination of the acidic Zn_RAl-POM series was also conducted. Although other suitable methods previously existed for the synthesis of Zn_RAl-POM materials[9,19,49, 92], it

was interesting to attempt to use a method that was very successful at producing basic

LDH-POM materials since there was a lack of a generally applicable synthesis. The

development of a general synthesis would allow the study of pillared LDHs with different

layer types without the uncertainty that is introduced by using different synthesis

methods. In addition, a single reaction system could be used to prepare a wide variety of

LDH materials, which would increase the attractiveness of pillared LDH materials in

industrial applications where production costs are a concern.

4.4.1 Modifications to the synthesis conditions

Zn_RAl LDH materials are considered to be more acidic than the Mg^{2+} containing

analogues. In fact it has been reported that the layer structure remains intact even after

stirring in boiling water at pH 3.6 for two hours[20]. In general, Zn_RAl LDHs are

coprecipitated from mixed metal salt solutions at pH 7 - 9, thus in the initial step of this

synthesis, the Zn_3Al-CO_3 precursor was coprecipitated at pH 7.7, which is very close to

the middle of this range. Fresh DDI water was used to prepare all solutions, however, no

effort was made to isolate the synthesis mixture from the ambient atmosphere.

The second major modification to the general synthesis involved calcining the

Zn_3Al-CO_3 precursor at a lower temperature, specifically 450°C instead of 550°C.

Previous studies[120] have indicated that the Zn_3Al-CO_3 materials are thermally

decomposed to the mixed oxide solid solution at 450°C, and therefore it was decided not

to risk inducing any additional transformations by using an unnecessarily high calcination

temperature. Each of the remaining steps of the synthesis were performed in exactly the same way as for the Mg_RM^{3+} series described previously (Sections 4.2.6 and 4.2.7).

4.4.2 ^{27}Al MAS-NMR study of the layer structure during synthesis of $Zn_3Al-H_2W_{12}$

The ^{27}Al MAS-NMR spectra of Zn_3Al-CO_3, Zn_3Al mixed metal oxide solid solution and $Zn_3Al-H_2W_{12}$ are presented in Fig. 4.14a, 4.14b and 4.14c, respectively. Comparison of Fig. 4.14a with Fig 4.3a for the corresponding Mg_3Al-CO_3 precursor reveals that the ^{27}Al MAS-NMR spectra of both precursors are virtually identical, each being characterized by a single resonance in a position that indicates the presence of octahedrally coordinated aluminum. The resonance in Fig. 4.14a, however, is less symmetric than in the Mg_3Al-CO_3 spectrum, indicating the presence of octahedrally coordinated aluminum in a slightly different environment. The shoulder may be related to the presence of additional peaks observed in the POXRD pattern (see Section 4.4.3).

Thermal decomposition of the Zn_3Al-CO_3 precursor at 450°C yielded a slightly yellowish residue from which the NMR spectrum presented in Fig. 4.14b was obtained. This spectrum differs markedly from the one that was obtained from the Mg_3Al-CO_3 decomposition product (Fig. 4.3b) due to the presence of a third resonance at 48.6 ppm. In the literature a peak at this position has been attributed to pentacoordinate aluminum, which forms only upon decomposition of Zn_RAl LDH phases that have divalent anions (i.e. CO_3^{2-} or SO_4^{2-}) in the interlayer[120]. It was suggested that the unique bridging that the divalent anions are capable of allow the formation of the pentacoordinate aluminum
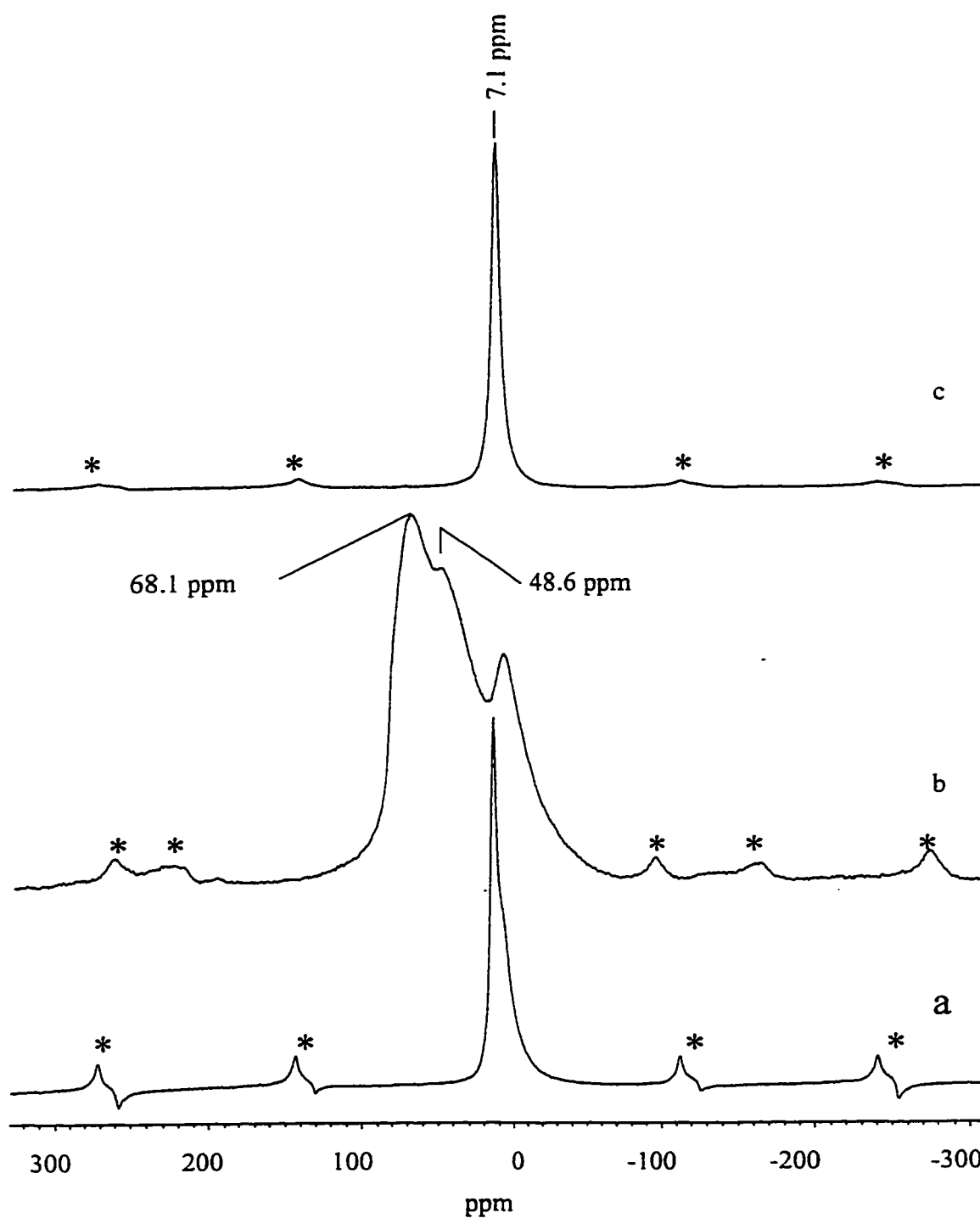
Fig. 4.14: ^{27}Al MAS-NMR spectra of a) Zn_3Al-CO_3 b) Zn_3Al mixed oxide solid solution and c) $Zn_3Al-H_2W_{12}$ (note: * denotes spinning side bands).

species as the LDH structure decomposes. The non-observance of pentacoordinate aluminum in the calcined Mg_RAl-CO_3 samples, however, is rather puzzling and there is currently no explanation available.

The formation of pentacoordinate aluminum in addition to tetrahedrally coordinated aluminum after calcination of the Zn_3Al-CO_3 precursors, however, did not affect the reversibility of the decomposition step. As shown in Fig. 4.14c all aluminum reverts to octahedral coordination, as indicated by the single resonance at 7.1 ppm, following rehydration and POM anion exchange. Thus the conditions described in Section 4.4.1 for the synthesis of $Zn_3Al-H_2W_{12}$ by the LDH-OH/LDH-adipate method appear to be suitable, and have resulted in the formation of pillared acidic LDH phases using a method that was developed initially for the basic LDH materials.

4.4.3 Comparative POXRD study of the Zn_3Al precursors vs. the corresponding Mg_3Al and Mg_3Ga precursors

The POXRD patterns for the series of Zn_3Al precursors are presented in Fig. 4.15a-d. Several broad reflections that are not associated with the LDH structure appear in the POXRD pattern of the Zn_3Al-CO_3 precursor (Fig. 4.15a) around 7.01Å, 4.57 Å, 3.34 Å and 2.47 Å, which may indicate the co-formation of an additional phase. Despite repeated attempts to form a pure Zn_3Al-CO_3 phase under optimized synthesis conditions, the additional reflections were always observed.

The POXRD pattern of the mixed metal oxide formed by the thermal decomposition of the Zn_3Al-CO_3 precursor appears in Fig. 4.15b. As expected, the
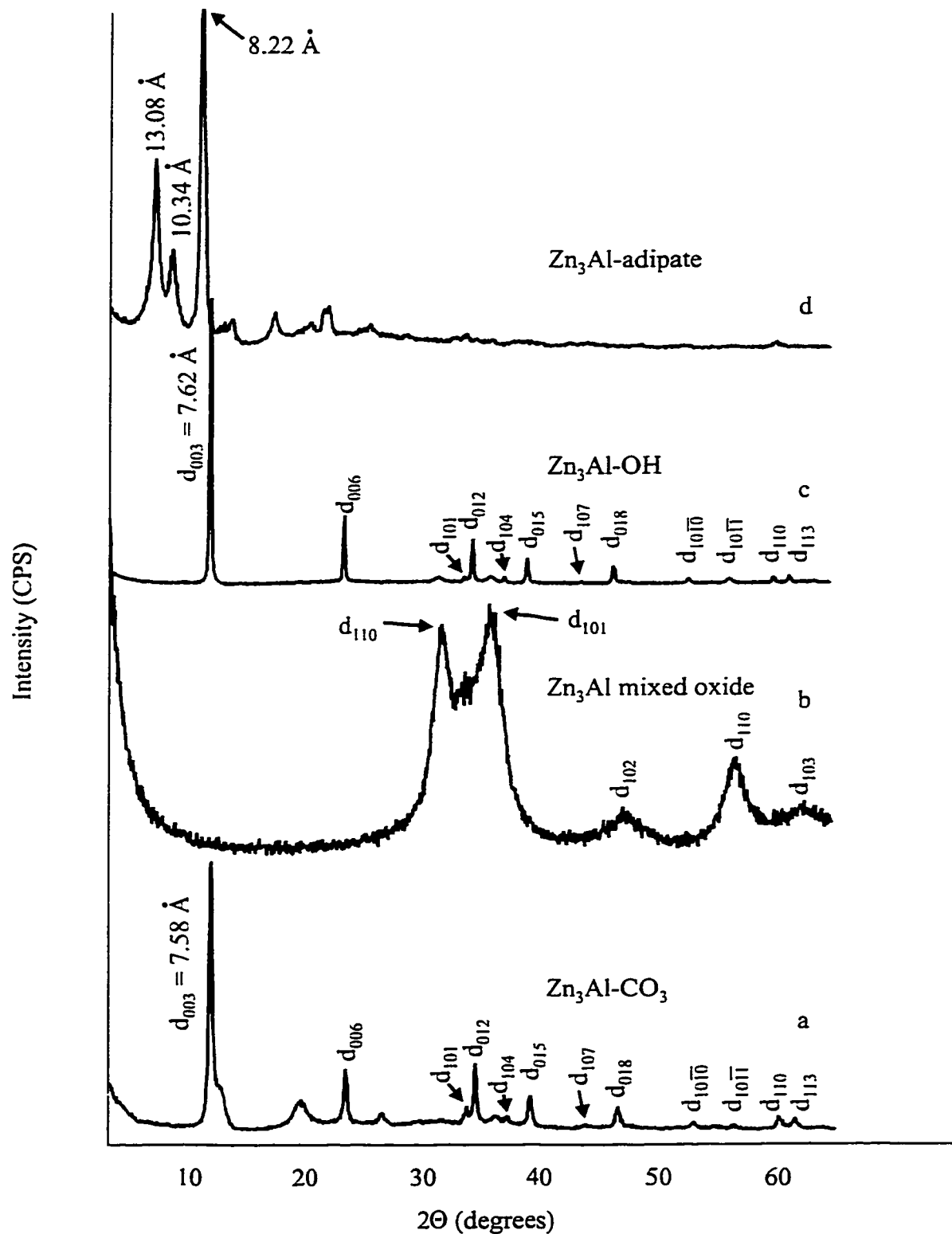
Fig. 4.15: POXRD patterns of a) Zn_3Al-CO_3 b) Zn_3Al mixed metal oxide
solid solution c) Zn_3Al-OH and d) Zn_3Al-adipate.

characteristic $d_{00\ell}$ reflections are no longer present, indicating that the LDH structure has been decomposed. Furthermore, the pattern resembles that of ZnO and the reflections in Fig. 4.15b have been indexed to the ZnO pattern[121], supporting the MAS-NMR evidence that the carbonate precursor is totally decomposed after calcination at 450°C. According to a previous study[120], the lattice *a* parameters were found to be larger than the calculated values of ZnO, indicating the dissolution of aluminum into the ZnO lattice, and that the solubility was greatest for the carbonate containing LDH.

The Zn₃Al-OH precursor that was formed by rehydration of the mixed oxide upon stirring in DDI water resulted in the POXRD pattern shown in Fig. 4.15c, which appears to be virtually identical to the one in Fig. 4.15a except that the diffraction peaks from the apparent impurity phase are missing. Unfortunately, rehydrated Zn/Al mixed oxides do not retain their initial $Zn^{2+}:Al^{3+}$ ratio; it has previously been reported that the final ratio is close to 2:1 in the rehydrated product, regardless of the initial ratio in the LDH-CO_3 precursor[122]. This observation suggests a severe limitation to the usefulness of the current method for the synthesis of Zn_RAl-POM materials; however, in cases where control over the layer composition is not critical this method may still be a viable option.

The POXRD pattern shown in Fig. 4.15d was obtained from a Zn₃Al-adipate precursor. Three distinct peaks appear at low 2θ values, which correspond approximately to the values observed for both the Mg₃Al-adipate and Mg₃Ga-adipate precursors, however the lines in the Zn₃Al-adipate pattern are much sharper. The origins of these

three peaks is likely very similar to that described previously for the basic LDH layer cases, however a higher degree of anion ordering in the interlayer region of the Zn_3Al-adipate precursor is likely.

4.4.4 Zn_RAl-POM products

Anion exchange, in which the interlayer adipate anions were replaced by POM anions, proceeded smoothly in the final step of the synthesis to yield well ordered POM-pillared products. This result represents a significant improvement over the organic anion precursor route, which was the subject of Chapter 3. Unlike the Zn_3Al-adipate precursors, the Zn_3Al-TA and Zn_3Al-BA precursors described in that chapter were totally inert toward POM anion exchange, and even though the Zn_3Al-p-hydroxybenzoate underwent exchange after extremely long reaction times, the resulting product contained extra phases in addition to the desired POM-pillared LDH phase.

The POXRD pattern of Zn_3Al-H_2W_{12} appears in Fig. 4.16a, while the pattern for Zn_3Al-PW_{11} appears in Fig. 4.16b. In each pattern $d_{003} = 14.7$ Å, which is nearly 0.2 Å smaller than the value observed for the Mg^{2+} containing analogues. Furthermore, the d_{003} reflections are considerably sharper than the corresponding reflections for the Mg^{2+} species, typically displaying FWHM values of 0.16 °2θ compared to 0.40 °2θ for each of the Mg_3Ga-POM and Mg_3Al-POM analogues. Comparing the D values obtained from the Scherrer equation, the Zn_3Al-POM materials have a mean crystallite size of approximately 500Å, compared to only 200Å for the Mg^{2+} containing analogues.
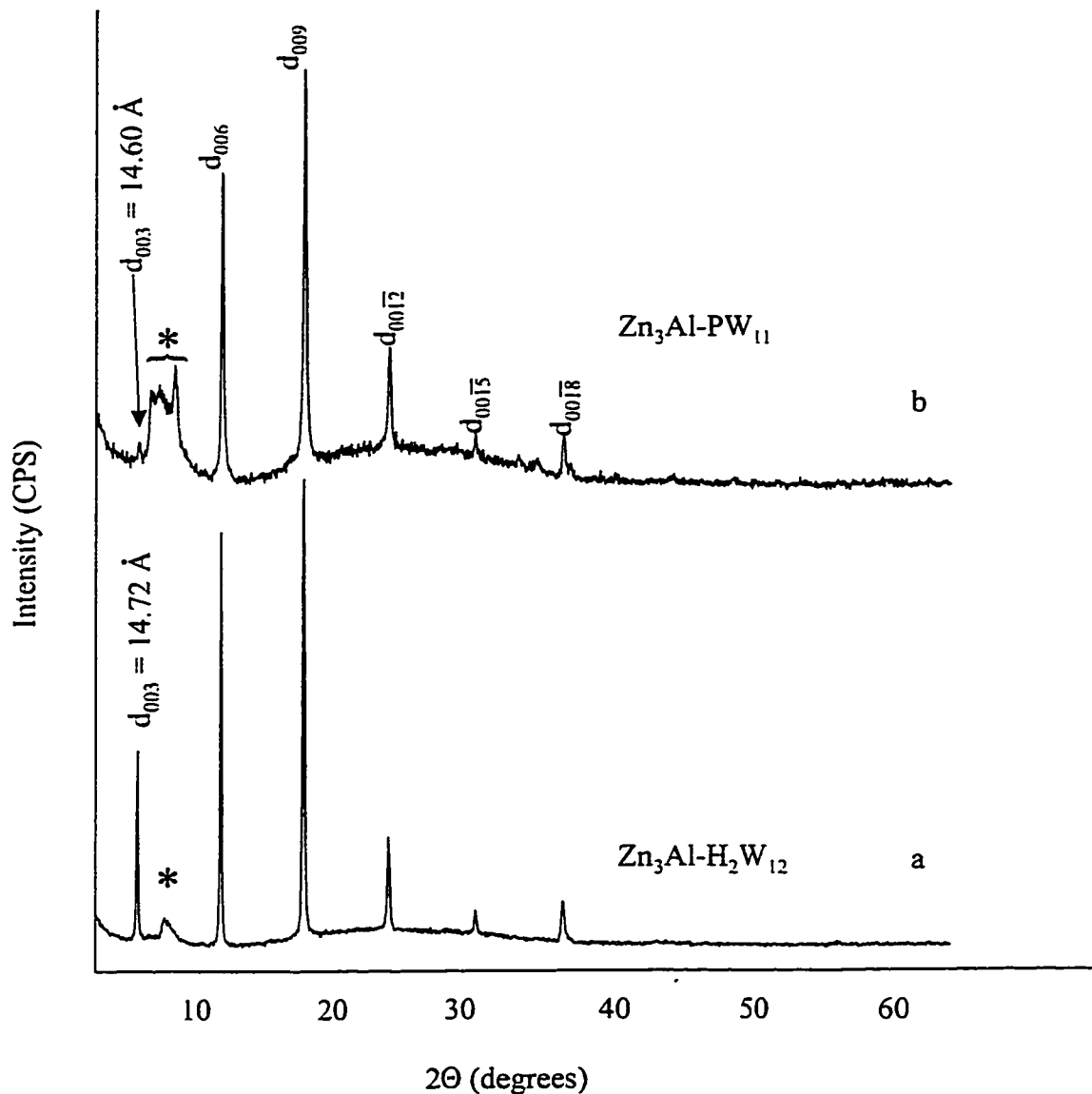
Fig. 4.16: POXRD patterns of a) $Zn_3Al\text{-}H_2W_{12}$ and b) $Zn_3Al\text{-}PW_{11}$
(note: * denotes the presence of impurity phase).

Further evidence for the intercalation of the Keggin ions is provided by IR

spectroscopy. The IR absorption spectra of $Zn_3Al\text{-}PW_{11}$, $Zn_3Al\text{-}H_2W_{12}$ and $Zn_3Al\text{-}H_2W_{12}$

washed with 0.1 M NaOH are presented in Fig. 4.17a, 4.17b and 4.17c, respectively. In

each case, strong bands arising from metal-oxygen stretching modes within the LDH
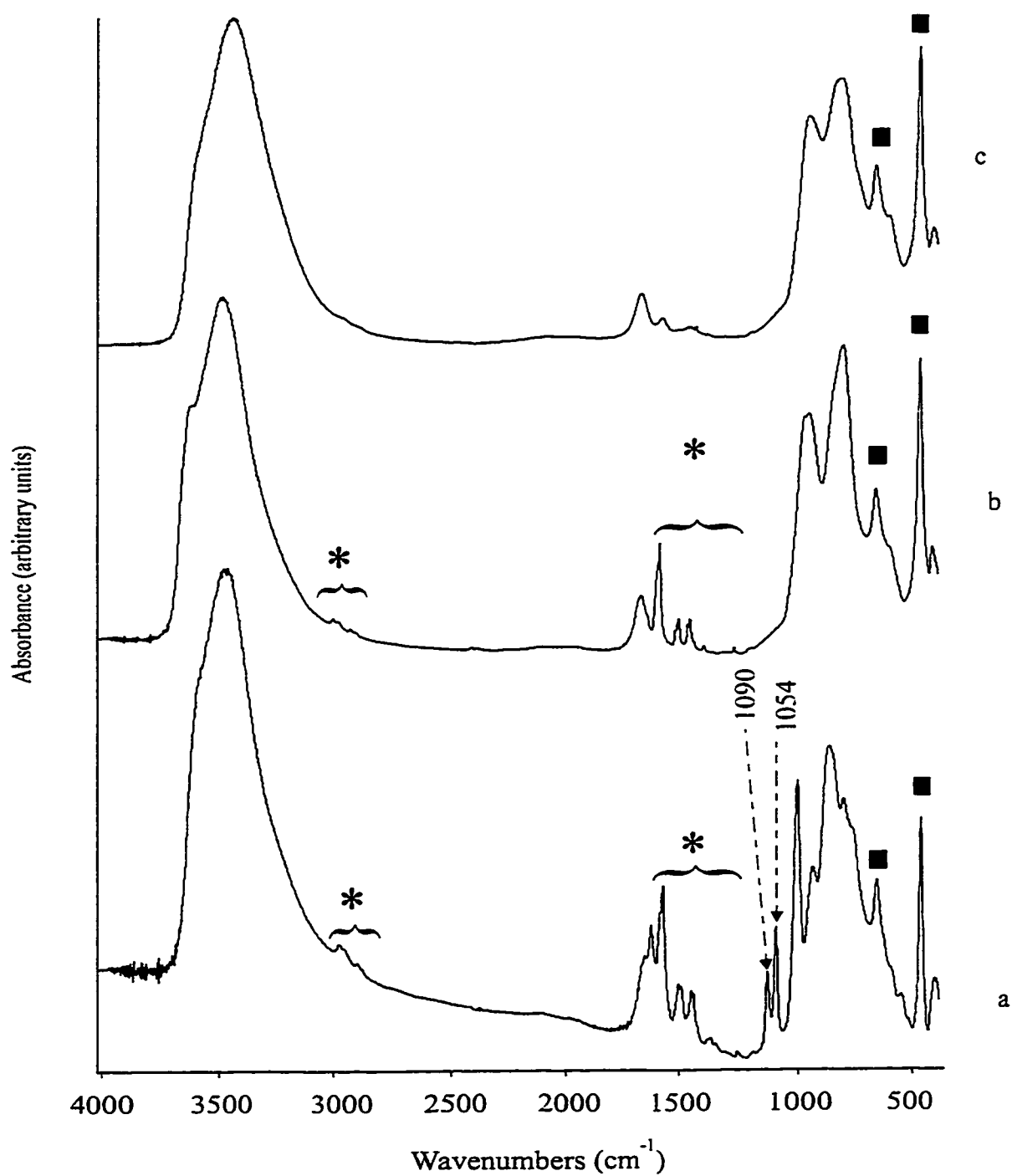
Fig. 4.17: IR spectra of a) Zn_3Al-PW_{11} b) Zn_3Al-H_2W_{12} and c) Zn_3Al-H_2W_{12} washed with 0.1 M NaOH (■ denotes bands due to LDH M-O modes * denotes bands due to residual adipate anions).

layers (denoted by ■) appear at about 624 cm^{-1} and 427 cm^{-1}. Superimposed on top of the

LDH spectrum between 450 cm^{-1} and 1100 cm^{-1} are the characteristic bands of the POM

anion pillars, which occupy the gallery region between the LDH layers. In Fig. 4.17a the

absorption band that normally appears around 1080 cm^{-1} in the IR spectrum of the intact

$PW_{12}O_{40}^{3-}$ Keggin unit ($v(P-O_a)$) has been split into two separate bands at 1090 cm^{-1} and

1054 cm^{-1}. Splitting of the $v(P-O_a)$ band occurs when the Keggin unit undergoes a partial

decomposition[73] and loses a single WO_6 octahedron to form the lacunary (or defect)

Keggin species $PW_{11}O_{39}^{7-}$; thus it appears that $PW_{11}O_{39}^{7-}$ is the actual pillaring species.

The spectrum appearing in Fig. 4.17b is consistent with the IR spectrum of an intact

$H_2W_{12}O_{40}^{6-}$ structure (i.e. the bands 932 cm^{-1} (sh), 899 cm^{-1} (s), 764 cm^{-1} (vs), 422 cm^{-1}

(m), as observed for the authentic α-$(NH_4)_6H_2W_{12}O_{40}$ salt), and thus metatungstate anions

possessing the full Keggin structure are the actual pillaring species in Zn_3Al-H_2W_{12}.

In each case the reaction apparently proceeded to completion within 10 minutes,

as judged by the appearance of the POXRD patterns, however elemental analysis

indicated that each POM-pillared product still contained 2.1 − 2.2% carbon by weight

(see Table 4.5). This amount actually represents a significant amount of adipate since the

mass of each POM pillar is very large (ca. 2900 g/mol) which increases the sample molar

mass dramatically. The IR spectra of both the Zn_3Al-PW_{11} and Zn_3Al-H_2W_{12} materials

(Fig. 4.17a and 4.17b) display bands (*) that are characteristic of residual adipate anions,

suggesting that the POM anion exchange reaction did not proceed to completion despite

the fact that a large POM excess was used. Unlike the Zn_RAl-POM products, the intensity of absorption bands attributed to residual adipate anions was very low in the IR absorption spectra obtained from Mg_RAl-POM and Mg_RGa-POM materials. Elemental analysis to determine the amount of carbon present in each LDH-POM was performed, and it was concluded that the Mg^{2+} containing LDH-POM materials contained less than 0.2 weight percent carbon (see Tables 4.3 and 4.4). It is apparent that the interlayer adipate anions were completely replaced by POM anions in the final step of the synthesis for the Mg_RAl-POM and Mg_RGa-POM products even though very large excesses of adipate anions were initially used, whereas residual adipate anions were retained in the Zn_3Al-POM analogues that were prepared under the same conditions.

The fact that the Zn_RAl-POM products contain residual adipate anions even after undergoing an exchange reaction with a large excess of POM and repeated washing suggests a limitation that was not apparent for the Mg_RM^{3+}-POM analogues. There is, however, no evidence of a separate phase containing adipate anions in either of the Zn_3Al-POM POXRD patterns shown in Fig. 4.16. The W:Al ratios determined by ICP analysis and tabulated in Table 4.5 are very close to the expected values of 1.4:1.0 and 2.0:1.0 for the PW_{11} and H_2W_{12} pillared products, respectively, which suggests that the residual adipate anions are not acting as charge balancing species in the interlayer region of the Zn_3Al products. It is therefore possible that a neutral salt of the adipate anions has deposited on the surface of the LDH crystallites. Regardless of the nature of the residual adipate anions, their presence did not seriously affect the BET surface area of the POM-

pillared products (see Table 4.5), which were determined to be very similar to the values

observed for the Mg_RM^{3+}-POM products in which adipate anions were not retained.

Table 4.5: d_{003} values, chemical composition and BET surface areas for the Zn_3Al-CO_3 precursor and POM-pillared products

Sample	d_{003} (Å)	Wt% Carbon[a]	$M^{II}:M^{III}:W$[b]	BET surface area (m^2g^{-1})
Zn_3Al-CO_3	7.58	-	3.0:1.0:0	66
Zn_3Al-PW_{11}	14.6	2.1	1.7 : 1.0 : 1.4	104
Zn_3Al-H_2W_{12}	14.7	2.2	1.7 : 1.0 : 1.9	92
Zn_3Al-H_2W_{12} (NaOH washed)	14.7	0.37	-	30

[a] Carbon analysis on Control Equipment Corporation (CEC) 440 Elemental Analyzer.
[b] ICP analysis on Thermo Jarrell Ash Atom Scan 16 spectrometer

Attempts to remove the residual adipate anions by washing the product with 0.1

M NaOH were successful in producing well ordered Zn_3Al-POM phases containing only

0.37 wt% carbon, down from 2.1-2.2%. The IR spectrum of this material appears in Fig.

4.17c, and illustrates the near complete removal of adipate anions subsequent to the POM

anion exchange reaction. Surprisingly, the remainder of the absorption spectrum is

virtually unaffected after the product was washed with the dilute base solution, except for

a slight reduction in the intensity of the POM bands compared with the bands arising

from the LDH layers. Unfortunately, the surface area of this product was reduced to

approximately 30 m^2g^{-1} compared to 92 m^2g^{-1} for the product that was washed only with

deionized water. Since the basic nature of the washing solution is unlikely to affect the

LDH layers (and the POXRD patterns confirm this), it is suggested that POM pillars

situated near the edges of the sheets decomposed upon exposure to the base solution,

allowing the layers to collapse around the edges and block the entrances to the micropores. Due to the unacceptable loss of surface area and the uncertainty that the LDH layers and POM pillars would be unaffected by washing with dilute base solution, it was decided to utilize the Zn_3Al-POM products *as synthesized* for the catalytic studies discussed in Chapter 5.

4.5 Assessment of the LDH-OH/LDH-adipate route as a general synthesis method

The results presented in Chapter 4 represent the first serious attempt to synthesize a wide variety of LDH materials encompassing both basic and acidic layer types using a common method. It has been shown for the Mg_RAl-H_2W_{12} series (R = 2, 3, 4) that the final POM-pillared products may be obtained with actual R values between 1.75 and 3.5. These values are admittedly lower than the desired values that were present in the initial mixed metal salt solution, yet they still represent by far the widest range of layer compositions reported to date. In addition, the first evidence for variations in the microporous structure of LDH-POM materials has been detected within this series of products, which suggests the possibility of producing size or shape selective catalysts.

The method was successfully extended to the Mg_RGa-POM series with good results, yielding highly regular, microporous materials with $Mg^{2+}:Ga^{3+}$ ratios slightly lower than 2:1. It was determined by ICP-AES analysis, however, that the pillared products were rich in gallium (compared to the amount of tungsten present) and thus it is likely that an x-ray amorphous, gallium rich phase was co-produced along with the

desired LDH phase. Further optimization of the synthesis conditions to better suit the

Mg/Ga system might improve the situation, however for the purpose of the catalytic study

presented in Chapter 5 the Mg_RGa-POM samples described in Section 4.3 were used.

The application of this method to produce very well ordered Zn_3Al-POM products

was successful, however, it was found that the ratio of Zn:Al in the layers was lower than

the desired value of 3:1 in each case. The main limitation to successful implementation

of this method for the synthesis of Zn_RAl-POM products appears to be the preference of

the Zn_RAl mixed oxide to rehydrate the LDH structure with a Zn:Al ratio of close to 2:1,

regardless of the ratio that was initially present in the LDH-CO_3 precursor. It is uncertain

at this point whether or not it is possible to affect the Zn:Al ratio in the Zn_RAl-OH

precursor by optimizing synthesis conditions to suit this particular system. An additional

limitation of the LDH-OH/LDH-adipate precursor method is that the Zn_3Al-POM

products appeared to contain residual amounts of adipate anions, in addition to the

amount of Keggin ions that were needed to balance the surface charge created by the

presence of Al^{3+} in the LDH layers. The observation that residual adipate anions were

present as well was rationalized after it was found that the adipate anions could be easily

removed by simply washing in dilute base solution, suggesting that they were adsorbed

on the crystallite surface and not present in the gallery region. Despite the lack of control

over the Zn:Al ratio and the presence of residual amounts of adipate anions in the final

product that was achieved under the experimental conditions used in this study, the

current method proved to be superior to the organic anion precursor method of Chapter 3.

The latter method failed to yield POM-pillared Zn/Al phases when the precursor anion was terephthalate or benzoate, and additional phases were detected after long reaction time when the *p*-hydroxybenzoate anion was exchanged with POM.

The true measure of success of the LDH-OH/LDH-adipate precursor method was that it was used to synthesize a wide variety of POM-pillared LDH materials with vastly different compositions, and all products exhibited high specific surface areas and an accessible microporous structure. Although it was not possible to achieve rigorous control over the layer composition in each of the pillared products, it was decided that the Mg$_3$Al-POM, Mg$_3$Ga-POM and Zn$_3$Al-POM (POM = H$_2$W$_{12}$ and PW$_{11}$) products described in Chapter 4 would be used in the study of the catalytic conversion of 2-propanol in Chapter 5. The series of catalysts prepared during this work were all exposed to similar conditions during synthesis, and it was hoped that differences observed in the activity would be primarily due to the presence of the different metal cations in the layers or POM anions in the gallery.

Chapter 5

Preliminary Catalytic Work

5.1 Choice of the decomposition of 2-propanol as the model reaction system

The catalytic decomposition of 2-propanol over metal oxides[97], mixed-metal oxides[123,124,125,126,127,128,129], calcined LDHs[31,130,41], and calcined pillared-LDHs[131] has been studied extensively, and the reaction is well established as a probe for determining the relative acidity and basicity of catalyst surfaces. Similar studies involving the dehydration/dehydrogenation of 2-propanol[132] or ethanol[133] over polyoxometalate anions have also appeared. It is apparent, however, that a comparatively small amount of literature dealing with the activity of pillared-LDHs and calcined pillared-LDHs currently exists. Therefore it was decided to conduct a systematic study of the catalytic decomposition of 2-propanol over the catalysts that were prepared as described in Chapter 4, and to compare the results of this study to the existing literature dealing with the metal oxide and mixed-metal oxide catalyst systems.

Several factors influenced our decision to use the catalytic decomposition of 2-propanol as a probe reaction for examining the relative acidity and basicity of the pillared LDH-POM samples, specifically:

- previous studies have examined the activity of metal oxides for this reaction at temperatures in the range 125-180°C, which is within the limit of thermal stability for the pillared LDH-POM catalysts

- reactant (2-propanol) and expected product (propene and acetone) molecules are all small enough to access micropores with diameters as small as 5 Å, which have been observed for some of the pillared LDH-POM catalysts

- the activity of LDH-POM and calcined LDH-POM catalysts for this reaction remains virtually unexplored, despite the fact that a systematic study could shed a great deal of light on the acid/base character of these materials.

The major disadvantage associated with using the decomposition of 2-propanol as the probe reaction is that the potential size or shape selectivity effects of the catalyst samples cannot be probed. As a result, the focus of this initial investigation of the catalytic properties of LDH-POM materials has been to study the changes in activity that occur upon thermal decomposition of the LDH and POM structure. The study has therefore been divided into two parts: the activity of intact LDH-POM materials activated at 200°C, and the activity of thermally decomposed LDH-POM materials activated at 550°C. The activity of each LDH-POM catalyst was then related to the types of active sites (acidic or basic) that are present after treatment at each temperature.

5.2 Effect of activation conditions on LDH-POM structure

The current section will provide a description of the nature of the active sites that are believed to be present in the LDH-POM samples following activation at 200°C and 550°C. In addition, the effect of thermal treatment on the physical properties will also be discussed. Cumulative sample weight loss and BET surface area data, obtained after heating the LDH-POM or LDH-CO₃ samples at various temperatures, are tabulated in Table 5.1. Data have been included for materials thermally treated at 125°C since this temperature is the typical pretreatment temperature used for reporting the surface areas of the materials in Chapters 3 and 4. Heating LDH-CO₃ or LDH-POM materials to 125°C will result only in the partial loss of interlayer and inter-crystalline water, and will not affect the structure of the gallery anions or the LDH layers. Removal of interlayer water opens up the porous structure prior to measuring surface areas or pore size distributions.

Table 5.1: Physical data for catalysts used

Sample	Weight loss after heating (%)			SA (m^2g^{-1})		
	125°C	200 °C	550 °C	125°C	200°C	550°C
$Mg_3Al-H_2W_{12}$	8.5	10.3	17.6	90	32	25
Mg_3Al-PW_{11}	7.8	9.6	18.9	108	97	29
$Mg_3Ga-H_2W_{12}$	9.9	10.2	16.0	118	32	21
Mg_3Ga-PW_{11}	9.4	7.4	17.6	77	32	11
$Zn_3Al-H_2W_{12}$	6.3	12.1	16.2	84	19	10
Zn_3Al-PW_{11}	6.6	13.1	19.9	104	17	14
Mg_3Al-CO_3	17.7	–	45.7	94	–	253
Mg_3Ga-CO_3	15.6	–	41.4	40	–	254
Zn_3Al-CO_3	8.0	12.7	29.8	66	75	76

The physical data summarized in Table 5.1 indicates that all LDH materials lost less than 10% of their initial weight upon heating to 125°C, the noticeable exceptions being Mg_3Al-CO_3 and Mg_3Ga-CO_3. The two magnesium containing carbonates lost 17.7% and 15.6% weight, indicating either a higher initial degree of hydration or, alternatively, lower energy of activation values for desorption of zeolitic water compared to the Zn_3Al-CO_3 material. The presence of heavy POM anions in the remaining (i.e. LDH-POM) samples precludes a direct comparison with the carbonate containing materials. However, it is apparent that a similar trend exists within the group of LDH-POM products, in which the Mg^{2+} containing species lose a greater amount of water than do the Zn^{2+} analogues. No correlation could be discerned between the extent of sample weight loss and the measured BET surface areas that were obtained following pretreatment at 125°C.

5.2.1 Nature of the LDH-POM structure after activation at 200°C

Layered double hydroxides that have been heated below the temperature that is required to partially dehydroxylate the layers (i.e. < 450-550°C) do not display significant basicity and are probably catalytically inactive[37]. Low temperature activation of LDH-POM materials (i.e. heating to 200°C) in the first part of this study will result in the loss of interlayer water molecules, however the overall morphology of the LDH-POM material will be retained. The most noticeable change in the LDH-POM structure will be a distinct cratering of the crystallite surface, which has been previously observed by TEM,

and is believed to be caused by escaping jets of steam that are produced as the interlayer water is evolved[37]. Defects in the layered structure that are introduced by steam venting may, however, result in increased mesoporosity of the materials and therefore provide better access to the interlayer POM anions by the reactant molecules.

Under low temperature activation conditions the observed activity of the hybrid material is primarily attributed to the presence of the pillaring species and not to the LDH layers themselves. In the current series of LDH-POM materials, the POM pillars are either $H_2W_{12}O_{40}^{6-}$ or $PW_{11}O_{39}^{7-}$; the activity is correlated to the strength of the negative charge on the terminal oxygen atoms, which presumably is inversely related to the acidic strength of either residual or generated protons[134,135,136]. Protons may be generated by the dissociation of water by the metallic elements of the anion to produce Brønsted acid sites[137,138]. It is uncertain, however, whether the POM anion pillars within the gallery space or the partially hydrolyzed Mg^{2+}/Al^{3+} salt of the POM anions on the LDH crystallite surface function as the catalytically active species. Due to the poorly understood nature of these sites the discussion of the catalytic activity of LDH-POM materials activated at low temperatures will make reference only to the presence of 'acid sites', without attempting to describe the true nature of these sites.

As indicated by the data in Table 5.1, heating the LDH-POM materials to 200°C resulted in an additional weight loss of a much smaller magnitude than was observed after heating to 125°C. The additional loss is attributed to removal of most of the interlayer water that remained after heating to 125°C. After low temperature treatment (200°C), the

overall crystal morphology is retained, however the gallery region collapses as the LDH

structure begins to decompose. Substantial decreases in BET surface area were observed

for all materials except the $Mg_3Al\text{-}PW_{11}$, which was $97m^2g^{-1}$ after treatment at 200°C.

The remarkable thermal stability of the layered structure for this material was confirmed

by POXRD, which showed that there was virtually no change in the basal spacing after

thermal treatment. The lowering of the surface areas of the remaining LDH-POM

materials (see Table 5.1) indicates that the microporosity of these samples is destroyed

after heating to 200°C, and thus the internal surface area becomes inaccessible. The

observed surface areas therefore correspond to the external surface area of non-porous

LDH-POM crystallites. Although the surface area was not measured for the Mg

containing LDH-carbonates, the Zn analogue displayed a surface area increase from 66 to

$75 \; m^2g^{-1}$. Increased BET surface areas are routinely observed for LDH carbonates as the

LDH structure is thermally decomposed to the mixed oxide, in agreement with the results

obtained here.

5.2.2 Nature of the LDH-POM structure after activation at 550°C

Activation of the LDH-POM catalysts at 550°C (high temperature activation)

results in the partial dehydroxylation of the LDH layers to form a mixed oxide solid

solution. In addition, the Keggin structure of the POM anions decomposes completely,

leaving a residue that is dispersed throughout the $M^{2+}(M^{3+})O$ mixed oxide crystallites.

Thus, the nature of the active sites in a catalyst that has been subjected to high

temperature activation is considerably more complex than that described above in Section

5.2.1. In fact, relatively little is known about the nature of the acidic and basic surface

sites that are formed during LDH calcination, and even less has been reported concerning

the decomposed Keggin unit. In the remainder of this section an attempt is made to

summarize the current understanding of the nature of the active sites that are likely to be

present in the materials formed by the thermal decomposition of LDH-POM phases.

As was previously discussed in Section 4.2.4 the XRD powder pattern of the

mixed-metal oxide solid solution that is formed by the thermal decomposition of an

(aluminum containing) LDH-carbonate precursor resembles that of a diffuse MgO

powder pattern. ^{27}Al-MAS-NMR indicates that Al^{3+} is present in both tetrahedral and

octahedral environments, but the XRD powder pattern shows no indication of a separate

crystalline, aluminum-containing phase. It is therefore likely that aluminum cations are

distributed more or less randomly throughout the MgO crystals, however there is

evidence that the aluminum migrates toward the surface of the crystallites, and thus the

surface Mg:Al ratio is lower at the surface than in the bulk[31,32]. The presence of Al^{3+} in

the MgO matrix produces defects, and the O^{2-} ions adjacent to the defects may provide

strong basic sites. Thus the basic character of calcined LDH materials may be attributed

to the presence of residual surface hydroxyl groups (Brønsted basicity, Type (a) weak

base sites, see Fig. 5.1) plus a range of M^+-O^- acid-base pairs (in the Lewis sense). The

latter type of sites includes O^{2-} surface basic sites (Type (c) strong basicity) and O^-

located near hydroxyl groups (Type (b) medium basicity)[11] (see Fig. 5.1). As was the case

with the acidic sites described in Section 5.2.1, the discussion of the catalytic results in

the following sections will concentrate mainly on the presence of 'basic sites' without a

rigorous analysis of the types of sites that are present.

Basicity

Type (a)   Type (b)   Type (c)
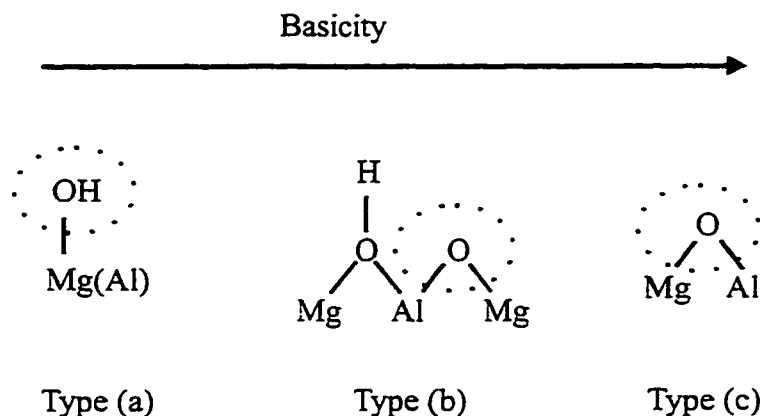
Fig. 5.1: Schematic representation of surface basic sites present on calcined
layered double hydroxides.

In addition to possessing surface basic sites with a range of base strengths,

calcined LDH-POM materials are also expected to display a pronounced acidic character

due to the presence of decomposition products of the interlayer Keggin ions or partially

hydrolyzed Mg^{2+}/Al^{3+}-POM salts. A previous study of $Mg/Al-V_{10}O_{28}$ demonstrated that

the interlayer space of an LDH provides a reactive environment for polyoxometalate

anions, causing the anions to lose their structural integrity even upon gentle thermal

treatment[53]. Thus in the current series of catalysts there are several possibilities,

including: decomposition of the Keggin structure to WO_3 crystallites supported on the

mixed metal oxide, grafting of Keggin ion addenda atoms into the LDH framework prior

to decomposition to form the mixed oxide, or even formation of one or more separate

$Mg_m(W_yO_z)_n$ type species.

The physical data summarized in Table 5.1 indicate that heating the LDH-POM

materials to 550°C results in a cumulative weight loss of between 16-19%. Interestingly,

the weight loss of the LDH-PW$_{11}$ pillared samples appear to be systematically higher than

for the LDH-H$_2$W$_{12}$ samples, which may be due to the loss of the central PO_4^{3-} group as

P_2O_5. In general, the surface areas of the LDH-POM materials are characteristic of non-

porous materials, and with the exception of Mg$_3$Ga-PW$_{11}$ the magnesium containing

LDH-POMs are all approximately 10 m^{2}g^{-1} larger in surface area than the corresponding

Zn^{2+} containing analogues.

The trend that was observed for the LDH-carbonates heated to 125°C is also

apparent at 550°C. Each of the Mg containing LDH-CO$_3$ materials lost approximately

42-46% weight, compared to only 30% for the Zn$_3$Al-CO$_3$. The much greater weight loss

may account at least partially for the substantially larger BET surface areas (253 m^{2}g^{-1})

compared to the Zn analogue which had a BET surface area of only 76 m^{2}g^{-1}.

5.3 Reactivity of 2-propanol over solid acids and solid bases

Studies involving the decomposition of 2-propanol over mixed-metal oxides

have indicated that the rate of dehydration (r_p) is a measure of catalyst acidity, whereas

the ratio of the dehydrogenation rate (r_a) to the dehydration rate (i.e. r_a/r_p) is a measure of

the basicity[123-129]. Mechanistically this implies that the dehydration of 2-propanol is catalyzed by an acid site, while the dehydrogenation is catalyzed by both acid and basic sites through a concerted mechanism. Both reactions are known to be zero order with respect to 2-propanol composition at low conversion[130], which implies that the surface is completely covered by adsorbed 2-propanol molecules under the reaction conditions and the reaction rates are independent of the gas phase concentration of 2-propanol. The above statements are supported by previous studies which have shown that under similar conditions the decomposition of 2-propanol shows virtually 100% selectivity to propene over strong acid catalysts (i.e. alumina) and close to 100% selectivity to acetone over strong base catalysts (i.e. MgO). Thus throughout the remainder of this chapter, the rate of formation of propene (r_p) will be taken as an index of the acidity of a catalyst and the ratio of the dehydrogenation rate to the dehydration rate (r_a/r_p) will be taken as an index of the basicity. The complete reaction network for the decomposition of 2-propanol[41] is shown in Fig. 5.2.
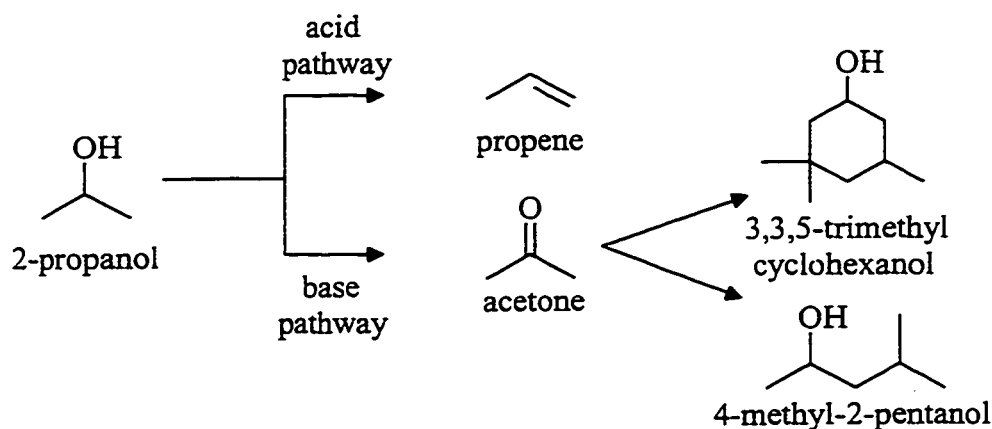
Fig. 5.2: Reaction scheme for the catalytic decomposition of 2-propanol.

As shown in Fig. 5.2, acetone produced by the dehydrogenation of 2-propanol may appear as a primary product, which may further react through an aldol-type condensation to form 3,3,5-trimethylcyclohexanol (TMCHOL) as the stable product. The only other product that may be produced is 4-methyl-2-pentanol (4M2POL). However, both TMCHOL and 4M2POL are generally produced to a negligible extent under the conditions used in the current study, possibly because the formation of TMCHOL and 4M2POL requires stronger basic sites than the dehydrogenation of 2-propanol to acetone[41]. It has been proposed that the incorporation of Al^{3+} into the MgO matrix prevents the formation of strong base sites on the catalyst surface[31], possibly accounting for the apparent stability of acetone under the current reaction conditions.
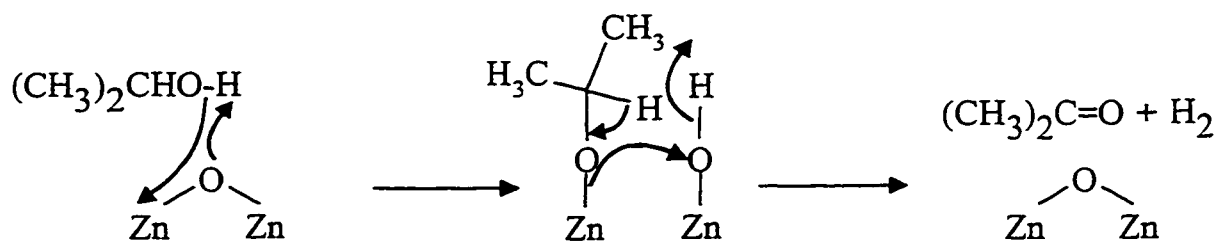
Fig. 5.3: Possible mechanism for the dehydrogenation of 2-propanol to acetone over basic metal oxide active sites.

The dehydrogenation of 2-propanol to acetone is proposed to occur via a concerted mechanism involving both acid and base sites[139]. Fig. 5.3 illustrates one possible mode of adsorption (using ZnO as the surface) that may lead to the dehydrogenation of 2-propanol. The dehydrogenation of 2-propanol to acetone may then occur via a mechanism[139] involving β-hydride elimination to form the adsorbed acetone

species, in which the two energetic steps are i) the removal of the second hydrogen atom from the carbonyl carbon of the adsorbed alkoxide and ii) desorption of acetone. Removal of the second hydrogen from the adsorbed alkoxide species is believed to be the rate-limiting step[139].

5.4 Summary of the activation and reaction conditions examined

Two independent catalytic studies were carried out during the course of this project using the catalysts that were prepared as described in Chapter 4. The objective was to compare the activity that is displayed by intact LDH layers pillared by POM anions possessing the Keggin structure to the activity that results after the LDH layers and POM pillars have been thermally decomposed. In each study, the typical procedure was to activate the sample by pretreatment at either 200°C or 550°C under flowing helium for a period of 2 hours or 4 hours, respectively. The reactor temperature was then lowered to the chosen initial reaction temperature and allowed to stabilize prior to starting the reactant flow. The reactant (2-propanol) was kept in a bubbler maintained at 22.0°C in a circulating water bath. Helium was passed through the bubbler at a constant rate of 22 mL/minute, resulting in a 2-propanol feed rate of 2.58 mmol/h.

As was discussed in Section 5.1.1 the reaction of 2-propanol to form propene and acetone are both known to be zero order under the conditions used in these studies, and therefore the observed rate of reaction is equal to the rate constant for that reaction. Thus a plot of the natural logarithm of the rate of reaction versus the reciprocal of the reaction

temperature yields a linear Arrhenius plot, from which the energy of activation and preexponential factors may be obtained. The Arrhenius plots are linear for all samples which indicates a lack of transport effects on the kinetic data at low total conversions. For some catalysts, however, the rates observed at high temperature (high conversion) were lower than expected, indicating that transport effects could in some cases affect the E_a and A values that were obtained. Therefore the lower conversion data were used in subsequent discussions.

In addition to linear Arrhenius plots, the reproducibility of the conversion data was found to be excellent, supporting the claim that the system was free of transport effects at conversions up to at least 30-40%. The data in Fig. 5.4 display the mole percent propene produced over a 150 mg sample of $Mg_3Al-H_2W_{12}$ that was activated at 550°C under helium for 4 hours. Data was collected first at 300°C (open symbols) for a period of 9.5 hours. After an initial rapid deactivation that occurred within the first 30 minutes, the rate of conversion to propene remained essentially constant. The reactor temperature was then lowered progressively to 275, 250 and 200°C, with at least 2 hours reaction at each temperature (all represented by open symbols) prior to changing the temperature again. After reaction at 200°C the reactor temperature was again increased to 275 and 300°C (closed symbols) and it was found that after prolonged reaction times and temperature cycling the catalyst showed essentially the same conversion at each temperature. This test demonstrates the reproducibility of results despite differences in the reaction history and thermal treatment of the sample.
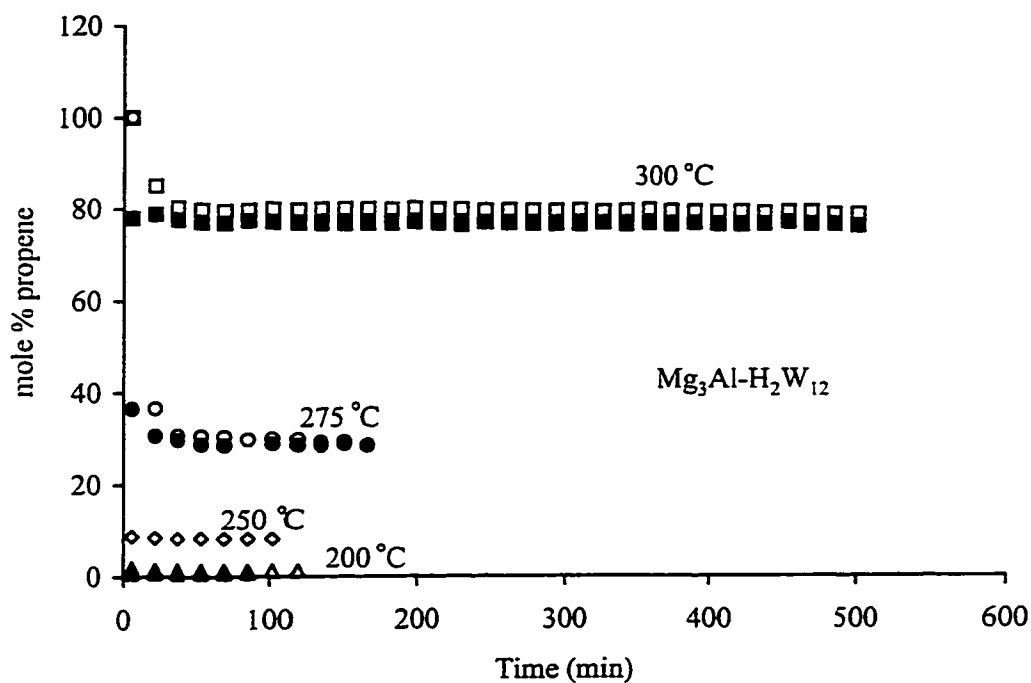
Fig. 5.4: Conversion of 2-propanol over $Mg_3Al-H_2W_{12}$ at various temperatures. Closed symbols represent repeat runs - see text.
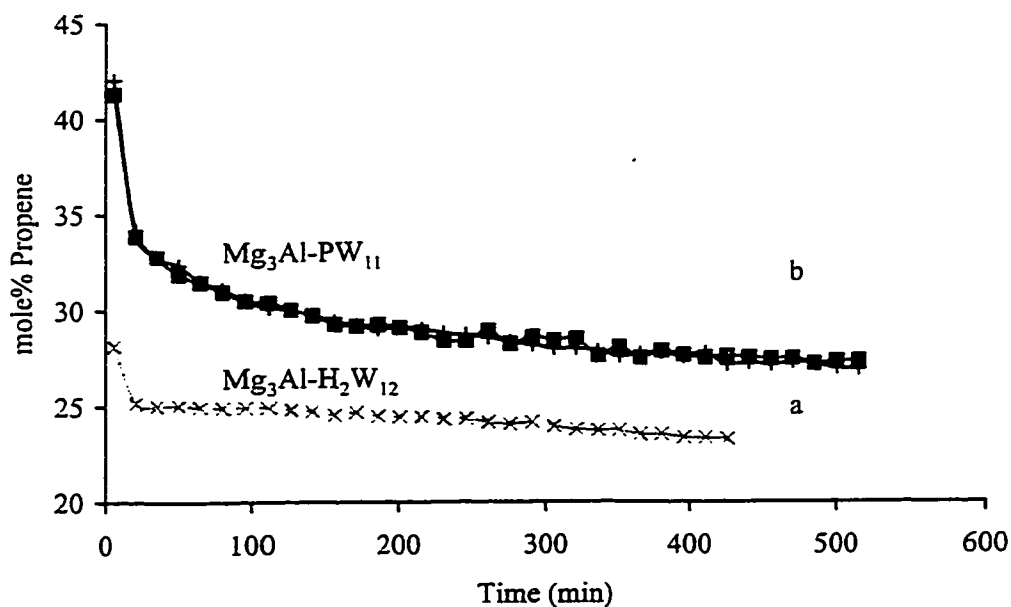
Fig. 5.5: Duplicate runs over fresh samples of a) $Mg_3Al-H_2W_{12}$ and b) Mg_3Al-PW_{11} reaction was at 200 °C after activation at 200 °C

The plots shown in Fig. 5.5 display the conversion of 2-propanol in terms of the

mole percent propene over $Mg_3Al-H_2W_{12}$ and $Mg_3Al- PW_{11}$. For each type of catalyst

two sets of data are shown, each set obtained using a fresh 151.0 mg sample of catalyst.

Thus, the conversion data are virtually unaffected by using a second catalyst sample,

which may have a different particle size composition or a slightly different pretreatment

history compared to the first sample. More importantly, the differences observed when

studying different catalyst compositions are reproducible, indicating that the rate data

obtained are reliable and may be used with confidence to calculate the Arrhenius

parameters.

5.5 Catalytic conversion of 2-propanol over LDH-POM activated at 200°C

The amount of catalyst used was 150 mg (± 2 mg) in each case, thus the total

conversion data listed in Table 5.2 allows a direct comparison of catalyst activity per unit

mass of catalyst. A comparison of the values for the total conversion of 2-propanol over

the various catalysts reveals that the Mg^{2+}-containing LDH-POM catalysts appear to have

higher activity than the Zn^{2+}-containing analogues. Each of the POM-pillared LDHs

display 100% selectivity to the formation of propene, indicating that the active sites are

exclusively acidic in nature, or that the base sites that are present are too weak to catalyze

the dehydrogenation of 2-propanol.

No reaction occurred over the Mg^{2+}-containing LDH-CO_3 materials, which

strongly suggests that after activation at 200°C the LDH layers do not contribute to the

observed activity of the pillared LDH-POM materials. Furthermore, although 5% conversion was achieved over the Zn_3Al-CO_3 material, the selectivity was 100% toward acetone, and thus it appears that basic sites are present on the Zn_3Al-CO_3 after low temperature activation. The presence of base sites on the Zn_3Al-CO_3 material but not on the Mg_3M^{3+}-CO_3 analogues is consistent with the onset of thermal decomposition of the LDH structure in zinc containing materials at lower temperatures[120] than are observed for the Mg^{2+}-containing analogues, as was discussed in Section 4.4.1.

Table 5.2: Conversion, selectivity and deactivation data for 2-propanol decomposition at 200°C (catalysts activated at 200°C under helium)

Sample	Total conversion (% after 2 h)	r_p (mmol h^{-1} m^{-2})	Selectivity to propene (%)	Selectivity to acetone (%)	Deactivation (% after 2 h)
Mg_3Al-H_2W_{12}	25	0.14	100	0	12
Mg_3Al-PW_{11}	26	0.046	100	0	25
Mg_3Ga-H_2W_{12}	32	0.18	100	0	10
Mg_3Ga-PW_{11}	18	0.066	100	0	22
Zn_3Al-H_2W_{12}	15	0.14	100	0	22
Zn_3Al-PW_{11}	5	0.056	100	0	31
Mg_3Al-CO_3	0	0	-	-	-
Mg_3Ga-CO_3	0	0	-	-	-
Zn_3Al-CO_3	4	0	0	100	0

A comparison of the rate of formation of propene (r_p) over each LDH-POM catalyst reveals a slightly different trend (see Table 5.2). The rate data are normalized on a unit surface area basis, and it can be seen that regardless of the layer type the r_p values of H_2W_{12} pillared materials are approximately three times greater than the r_p value of a catalyst that is pillared with PW_{11}. In order to illustrate this trend, the rates of formation

of propene (per m^2 of catalyst surface area) vs. reaction temperature have been plotted in Fig. 5.6 for each of the LDH-POM catalyst samples after activation at 200°C. Two groups of curves may be discerned: an upper group corresponding to the presence of H_2W_{12} pillars and a lower group to the presence of PW_{11} pillars. This observation supports the statement in Section 5.2.1 that the Keggin structure remains intact after activation at 200°C, and thus the difference in activity may be attributed to the differences in the structural and chemical properties of the two Keggin ions.

The r_p values are based on data that were obtained after 2 hours on stream, which may tend to exaggerate the difference between the rates observed for the two pillar types. All catalysts were observed to deactivate over the course of the reaction; the degree of deactivation varied with catalyst composition, and the values appear in the final column of Table 5.2. The general observation is that deactivation occurs to a greater extent in the PW_{11}-pillared catalysts compared to the H_2W_{12}-pillared analogues. Furthermore, the PW_{11}-pillared materials deactivate in two stages: i) an initial rapid deactivation during the first 20 – 40 minutes of reaction, followed by ii) a more gradual but continuous deactivation during the remainder of the reaction (see Fig. 5.5). In contrast, the H_2W_{12}-pillared LDH materials typically displayed only the rapid initial deactivation, but to a smaller extent, after which the reaction rate remained virtually unchanged.

In Fig. 5.7 the Arrhenius plot for the dehydration of 2-propanol to propene over each LDH-POM catalyst was obtained by plotting the natural logarithm of the reaction
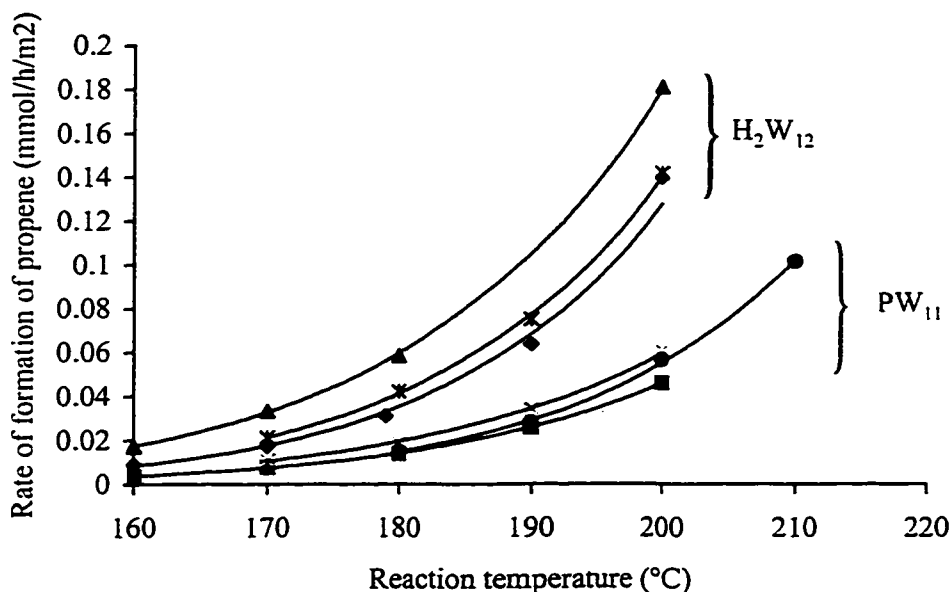
Fig. 5.6: Rate of formation of propene vs. reaction temperature for ▲Mg₃Ga-H₂W₁₂ ✖ Zn₃Al-H₂W₁₂ ◆ Mg₃Al-H₂W₁₂ ✕ Mg₃Ga-PW₁₁ ● Zn₃Al-PW₁₁ ■ Mg₃Al-PW₁₁ (Activation temperature was 200 °C).
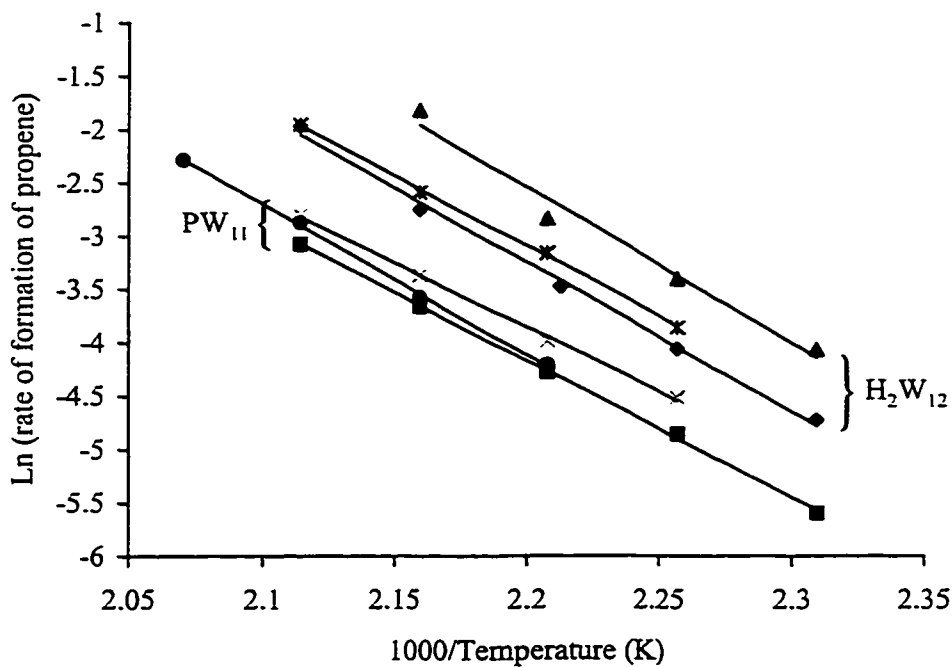
Fig. 5.7: Arrhenius plots for the decomposition of 2-propanol to propene for ▲Mg₃Ga-H₂W₁₂ ✖ Zn₃Al-H₂W₁₂ ◆ Mg₃Al-H₂W₁₂ ✕ Mg₃Ga-PW₁₁ ● Zn₃Al-PW₁₁ ■ Mg₃Al-PW₁₁ (Activation temperature was 200 °C).

rate versus the reciprocal of the reaction temperature. Strictly speaking the natural logarithm of the rate constant should be plotted versus the reciprocal of the reaction temperature. However, the dehydration of 2-propanol is known to be zero order at low conversion, and thus the plots appearing in Figs. 5.7, 5.9 and 5.11 are valid. The Arrhenius parameters obtained from Fig. 5.7 have been tabulated in Table 5.3.

Table 5.3: Arrhenius parameters for 2-propanol decomposition over catalysts activated at 200°C under helium

Sample	Reaction to propene		Reaction to acetone	
	$\ln A^a$	E_a (kJ/mol)^b	$\ln A^a$	E_a (kJ/mol)
$Mg_3Al\text{-}H_2W_{12}$	26	110 ± 2	-	-
$Mg_3Al\text{-}PW_{11}$	25	107 ± 3	-	-
$Mg_3Ga\text{-}H_2W_{12}$	24	100 ± 2	-	-
$Mg_3Ga\text{-}PW_{11}$	24	104 ± 3	-	-
$Zn_3Al\text{-}H_2W_{12}$	26	111 ± 5	-	-
$Zn_3Al\text{-}PW_{11}$	27	118 ± 2	-	-
$Mg_3Al\text{-}CO_3$	-	-	-	-
$Mg_3Ga\text{-}CO_3$	-	-	-	-
$Zn_3Al\text{-}CO_3$	31	136 ± 2	-	-

^{a} A expressed in mmol h^{-1} m^{-2}
^{b} errors were estimated based on the uncertainty of the slope of the Arrhenius plots

The most striking feature of Fig. 5.7 is the similarity of the slope of the Arrhenius plots, regardless of the layer or pillar composition. The energy of activation calculated for the dehydration of 2-propanol to propene over each LDH-POM was obtained from the slope of the corresponding line in Fig. 5.7, and is presented in Table 5.3. Based on the similarity of the E_a values (within experimental error) it is apparent that the strengths of the acid sites are essentially identical for both the H_2W_{12} and PW_{11} pillars. The

difference in activity, therefore, must be related primarily to the number of active sites, or

more likely the number of *accessible* active sites present in each LDH-POM catalyst.

Possible reasons for the presence of fewer accessible active sites in the PW_{11} pillared

products include:

i)   deactivation of more active sites on the PW_{11}-pillared LDH catalysts

        compared to the H_2W_{12}-pillared LDH catalysts during the first two hours

        of reaction

ii)   higher anion charge compared to H_2W_{12}, therefore fewer PW_{11} pillars are

        required to balance the layer charge

iii)   the lacunary Keggin structure of PW_{11} anion contains one less WO_6

        octahedron than the intact Keggin structure of the H_2W_{12} anion

iv)   the vacancy created by the missing WO_6 octahedron may not be totally

        localized, i.e. active sites associated with the entire W_3O_{13} triad may be

        rendered inactive, and

v)   the $LDH-PW_{11}$ layered structure may be more thermally stable than the

        LDH- H_2W_{12} structure thus restricting access in the former (i.e. Mg_3Ga-

        PW_{11}); higher stability may be due to grafting of the Keggin ion to the

        LDH layers via the octahedral vacancy.

The energy of activation for the dehydration of 2-propanol to propene has

previously been determined under similar conditions for a series of metal oxide

surfaces[97]; the values obtained were: Al_2O_3 (136.2 ± 2.5 kJmol^{-1}); Ga_2O_3 (146.5 ± 41.6 kJ

mol^{-1}); MgO (98.4 ± 7.8 $kJmol^{-1}$); WO_3 (104.5 ± 8.1 $kJmol^{-1}$); and ZnO (130.9 ± 48.3

$kJmol^{-1}$). Although there is considerable uncertainty in some of the above values, it is

apparent that the activation energy values in Table 5.3 for the LDH-POM catalysts agree

most closely with the value obtained for WO_3, and not with the metal oxides of the layer

cations in general. In addition, the unpillared LDH materials (i.e. LDH-CO_3) did not

exhibit any acidic character under the same experimental conditions. The only

conclusion that can be drawn is that it is highly unlikely that the mixed metal oxides

formed by LDH layer decomposition are providing the active sites for 2-propanol

decomposition.

5.6 Catalytic conversion of 2-propanol over LDH-POM activated at 550°C

The same procedure was carried out for LDH-POM catalysts activated at 550°C,

with the conversion, rate and selectivity data for the series appearing in Table 5.4. Note

that 250°C has been used as a representative reaction temperature in the case of catalysts

activated at 550°C (c.f. 200°C for catalysts activated at 200°C) in order to obtain

measurable conversion values for all LDH-POM catalyst samples. It is interesting to note

that the mixed metal oxide produced by the thermal decomposition of Mg_3Al-CO_3 and

Mg_3Ga-CO_3 did not catalyze dehydration or dehydrogenation of 2-propanol at 250°C,

whereas the Zn/Al mixed oxide achieved 27.3% conversion with 98% selectivity to

acetone. This result is consistent with a previous study which found that the rate of

formation of acetone was 35.5 times greater over ZnO than over MgO at 250°C[97].

The predominant reaction product produced over each LDH-POM was propene, with selectivity ranging from 79 – 100%. Both Zn/Al-POM catalysts also produced acetone, suggesting a contribution to the overall activity from the LDH layers. There is also apparently a contribution from the decomposed layers in the Mg/Ga-H_2W_{12} catalyst, however the remaining Mg^{2+} containing materials were 100% selective for the dehydration reaction.

Table 5.4: Conversion, selectivity and deactivation data for 2-propanol decomposition at 250°C (catalysts activated at 550°C under helium)

Sample	Total conversion (% after 2 h)	r_p (mmol h^{-1} m^{-2})	r_a (mmol h^{-1} m^{-2})	Selectivity to propene (%)	Selectivity to acetone (%)
$Mg_3Al-H_2W_{12}$	8.2	0.065	0	100	0
Mg_3Al-PW_{11}	14	0.095	0	100	0
$Mg_3Ga-H_2W_{12}$	40	0.35	0.023	94	6
Mg_3Ga-PW_{11}	8.7	0.15	0	100	0
$Zn_3Al-H_2W_{12}$	60	1.2	0.041	97	3
Zn_3Al-PW_{11}	33	0.39	0.10	79	21
Mg_3Al-CO_3	0	0	0	-	-
Mg_3Ga-CO_3	0	0	0	-	-
Zn_3Al-CO_3	27	0.004	0.26	2	98

Plots of the rate of formation of propene (r_p) or rate of formation of acetone (r_a) versus the reciprocal of the reaction temperature for catalysts activated at 550°C appear in Figs. 5.8 and 5.10, respectively, and the corresponding Arrhenius plots are presented in Figs. 5.9 and 5.11. An inspection of Figs. 5.8 and 5.9 reveals that the Zn/Al-POM catalysts are more active than the Mg^{2+} containing analogues for the dehydration of 2-propanol. Unlike the observation after 200°C activation, the pillar identity does not
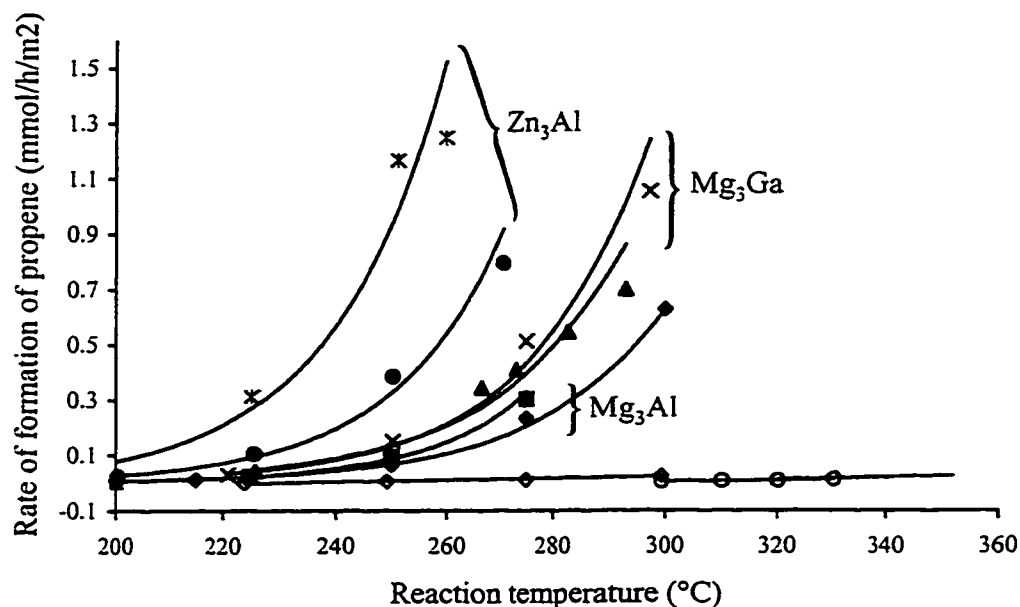
Fig. 5.8: Rate of formation of propene vs. reaction temperature for ▲Mg₃Ga-H₂W₁₂
✱ Zn₃Al-H₂W₁₂ ◆ Mg₃Al-H₂W₁₂ ✕ Mg₃Ga-PW₁₁ ● Zn₃Al-PW₁₁ ■ Mg₃Al-PW₁₁
△Mg₃Al-CO₃ ○ Mg₃Ga-CO₃ ◇ Zn₃Al-CO₃
(Activation temperature was 550°C).
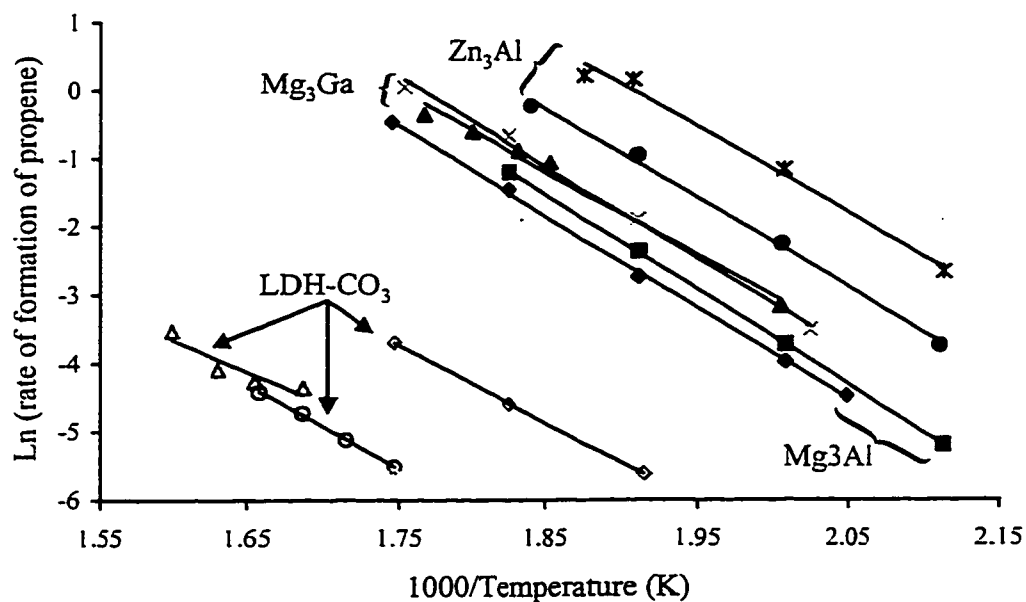
Fig. 5.9: Arrhenius plots for the decomposition of 2-propanol to propene for
▲ Mg₃Ga-H₂W₁₂ ✱ Zn₃Al-H₂W₁₂ ◆ Mg₃Al-H₂W₁₂ ✕ Mg₃Ga-PW₁₁
● Zn₃Al-PW₁₁ ■ Mg₃Al-PW₁₁ △ Mg₃Al-CO₃ ○ Mg₃Ga-CO₃ ◇ Zn₃Al-CO₃
(Activation temperature was 550°C).
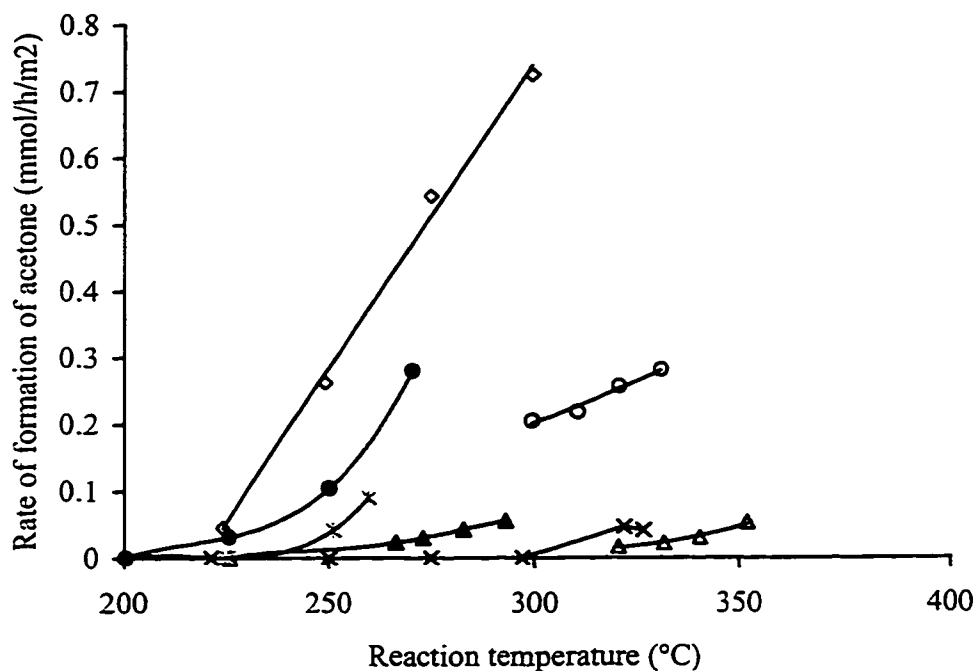
Fig. 5.10: Rate of formation of acetone vs. reaction temperature for ▲ $Mg_3Ga-H_2W_{12}$
✱ $Zn_3Al-H_2W_{12}$ ✕ Mg_3Ga-PW_{11} ● Zn_3Al-PW_{11} △ Mg_3Al-CO_3 ○ Mg_3Ga-CO_3
◇ Zn_3Al-CO_3 (Activation temperature was 550 °C).
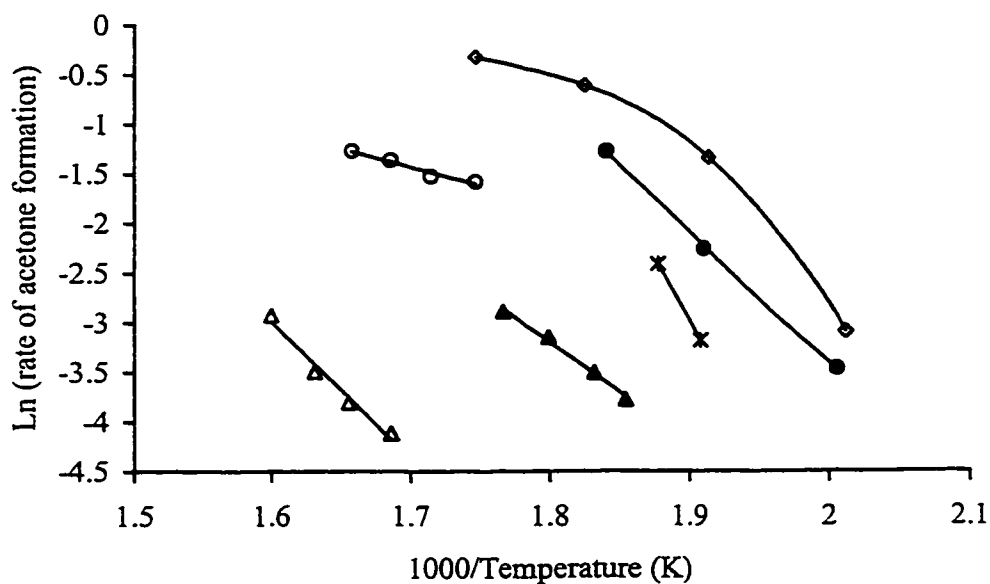
Fig. 5.11: Arrhenius plots for the decomposition of 2-propanol to acetone for
▲ $Mg_3Ga-H_2W_{12}$ ✱ $Zn_3Al-H_2W_{12}$ ● Zn_3Al-PW_{11} △ Mg_3Al-CO_3
○ Mg_3Ga-CO_3 ◇ Zn_3Al-CO_3 (Activation temperature was 550 C).

appear to exert a significant influence, and it is assumed that in each case the Keggin ion was decomposed during activation, leaving a residue supported on the mixed metal oxide matrix. The nature of the residue is not certain, however, the dark color of samples activated at high temperature indicates at least partial reduction of the tungsten, and it is likely that decomposition of either H_2W_{12} or PW_{11} will result in a very similar species supported on the mixed oxide. Thus, the major factor determining the acid strength of the catalyst, and thereby the rate of formation of propene, is the specific interaction between the tungsten containing residue and the mixed metal oxide. Based on this argument, the effect of replacing Mg^{2+} with Zn^{2+} in the initial LDH-CO_3 precursor is considerably greater than the effect of replacing Al^{3+} with Ga^{3+}. One possible explanation is that since the ZnO is much more basic than MgO (i.e. r_a is 35 times greater over ZnO than over MgO), then the interaction of the tungsten residue with ZnO results in a greater degree of strengthening of the acid sites compared to the interaction with MgO. The trivalent cations, on the other hand, do not form separate phases but instead occupy tetrahedral or octahedral positions in the $M^{2+}O$ matrix, thus modifying the basic character of the metal oxide, but having little influence over the overall acidity of the catalyst.

Attempting to quantify the above general observations by considering the energy of activation values tabulated in Table 5.5 below fails to provide an unambiguous answer. It is apparent that the values of E_p for the formation of propene are generally much larger than the E_a values for the formation of acetone, but there does not appear to be a definite trend with respect to the layer composition. It has previously been suggested that the

latter reaction requires less selective sites than the former, and that in fact the rate of

acetone formation is independent of the strength of both the acid and base sites[97]. If this

is true, then it is not possible to expand upon the general observations based on the data

that is currently available for the dehydrogenation reaction. An examination of r_a vs.

reaction temperature plots in Fig. 5.10 illustrates the greater uncertainty that exists in the

dehydrogenation data, due at least in part to the very low conversions in some cases. The

Arrhenius plots in Fig. 5.11 show pronounced deviation from linearity in some cases,

possibly reflecting a change in the rate-limiting step.

Table 5.5: Arrhenius parameters for 2-propanol decomposition over catalysts activated at 550°C under flowing helium

Sample	Reaction to propene		Reaction to acetone	
	ln A^a	E_p (kJ/mol)^b	ln A^a	E_a (kJ/mol)^b
Mg_3Al-H_2W_{12}	23	111 ± 2	-	-
Mg_3Al-PW_{11}	24	115	-	-
Mg_3Ga-H_2W_{12}	23	109 ± 5	16	90 ± 10
Mg_3Ga-PW_{11}	27	116 ± 11	-	-
Zn_3Al-H_2W_{12}	27	115 ± 2	169	169 ± 35
Zn_3Al-PW_{11}	24	109 ± 6	21	102 ± 12
Mg_3Al-CO_3	15	96 ± 20	23	134 ± 2
Mg_3Ga- CO_3	18	111 ± 3	9	52 ± 2
Zn_3Al- CO_3	16	93 ± 2	-	-

^{a} A expressed in mmol h^{-1} m^{-2}
^{b} errors were estimated based on the uncertainty of the slope of the Arrhenius plots

The data obtained for the dehydration of 2-propanol to propene, however resulted

in more linear Arrhenius plots as shown in Fig. 5.9. The lines corresponding to the

catalysts derived from the LDH-POM materials are all shifted up and to the right

compared to the catalysts derived from the LDH-CO_3 materials. Furthermore, within

each of these two groups of lines, the ones corresponding to ZnAl layer compositions are

shifted further, and the Mg/M^{3+} analogues are grouped tightly together. The ln A values

in Table 5.5 are grouped into pillared and non-pillared, and suggest that significantly

more acid sites are present on the LDH-POM materials than on the LDH-CO_3 materials.

5.7 Direct comparison of LDH-POM catalysts activated at 200 °C and at 550 °C

The discussion of the activity of catalysts activated at 550°C in Section 5.6 was

for a reaction temperature of 250°C, compared to a reaction temperature of only 200°C

for the catalysts activated at 200°C, in order to obtain reasonable conversion data for the

high temperature activation materials. In Section 5.6, the activity of the catalysts

activated at different temperatures will be compared at a common reaction temperature of

200°C. The r_p and r_a data presented in Table 5.6 for catalysts activated at 200°C are

simply reproduced from Table 5.2, whereas the corresponding data for catalysts activated

at 550°C were not presented in earlier tables.

As was previously stated in Section 5.6, the data obtained at a reaction

temperature of 200°C over catalysts activated at 550°C could not be used since some

catalysts did not display any activity at that temperature. Specifically, both catalysts

derived from Mg_3Ga-POM lost 100% of their activity for the dehydration of 2-propanol

at a reaction temperature of 200°C after activation at 550°C. This is in spite of the fact

that both the Mg_3Ga-H_2W_{12} and Mg_3Ga-PW_{11} samples displaying the highest rate of

formation of propene after activation at 200°C. Activation at 550°C also resulted in a significant decrease of r_p for both Mg_3Al-POM catalysts, by a factor of 23 for the H_2W_{12} containing material and by a factor of 10 for the PW_{11} containing material. In contrast, the decrease in the activity of the Zn/Al analogues was only by a factor of two, and the decrease was independent of the POM composition.

Table 5.6: r_p and r_a values for 2-propanol decomposition at a reaction temperature of 200°C for catalysts activated at 200°C or 550°C under helium

Sample	Activated at 200°C		Activated at 550°C	
	r_p (mmol h^{-1} m^{-2})	r_a (mmol h^{-1} m^{-2})	r_p (mmol h^{-1} m^{-2})	r_a (mmol h^{-1} m^{-2})
Mg_3Al-H_2W_{12}	0.14	0	0.006	0
Mg_3Al-PW_{11}	0.046	0	0.005	0
Mg_3Ga-H_2W_{12}	0.18	0	~ 0	-
Mg_3Ga-PW_{11}	0.061	0	~0	-
Zn_3Al-H_2W_{12}	0.14	0	0.069	0
Zn_3Al-PW_{11}	0.056	0	0.024	0
Mg_3Al-CO_3	0	0	0	0
Mg_3Ga- CO_3	0	0	0	0
Zn_3Al- CO_3	0	0.043	0	0

In summary, activation at 200°C followed by reaction at 200°C resulted in high activity for propene formation (Fig. 5.6), but activation at 550°C followed by reaction at 200°C resulted in substantially lower conversion rates (Fig. 5.8). It therefore seems likely that high temperature activation produces catalysts in which the strongest acid sites are either destroyed or simply never formed. One possibility is that the complete dehydration of the materials causes loss of Brønsted acid sites, two of which may combine and be evolved as water. The active sites in the catalysts activated at high temperature would

therefore be weaker Lewis acid sites, which are capable of catalyzing the dehydration only at higher temperature. In addition, the rate of formation of acetone at 200°C was zero for all catalysts activated at 550°C, which is not consistent with the fact that the LDH-POM materials should form basic mixed oxide solid solutions. It is possible that the final step of the mechanism, desorption of the adsorbed acetone molecule, is energetically unfavorable at 200°C, poisoning the surfaces toward further acetone formation. All of the r_a vs. reaction temperature plots in Fig. 5.10 appear to converge to a value of zero at a reaction temperature of approximately 220°C, which may be the minimum temperature required to desorb the product of dehydrogenation.

5.8 Summary of catalytic results

In this chapter the activity of a wide range of LDH-POM based catalysts encompassing a significantly wide range of compositions has been studied for the catalytic decomposition of 2-propanol. Catalysts activated at low temperature (200°C) displayed 100% selectivity toward the dehydration pathway, and the magnitude of the rate of formation of propene was determined primarily by the identity of the pillar. It was found that the energy of activation over catalysts with a particular layer composition was virtually the same regardless of whether H_2W_{12} or PW_{11} pillars were present. The observed trend that the rate of reaction is determined by the pillar identity was then rationalized on the basis that it is the number of active sites, and not the strength of the individual sites, that is crucial to the activity. Several factors, which might affect the

number of sites expected for each pillar type, were identified in Section 5.5. It was concluded that since the LDH layers are not catalytically active after low temperature activation, it is not possible to modify the acid-base properties of LDH-POM catalysts in which the original LDH structure has been retained. Therefore, in order to exploit the microporous LDH structure it is essential that POM pillars are utilized which will provide the desired activity after low temperature activation.

Several key differences were subsequently observed between the behavior of the same catalyst samples subjected to activation conditions of 550°C for 4 hours. Most significantly, it was found that replacing Mg^{2+} with Zn^{2+} in the LDH layers introduced basic character, while the predominant acidic nature of the catalyst was maintained. The effect of replacing Mg^{2+} with Zn^{2+} was significantly more pronounced than for replacing Al^{3+} with Ga^{3+}. In addition to forming surface base sites in catalysts of certain composition, high temperature activation also had the effect of drastically reducing the number of strong surface acid sites, with the consequence that propene formation was reduced virtually to zero at a reaction temperature of 200°C. It was necessary to increase the reaction temperature to between 220°C and 300°C to observe significant activity for the formation of propene via the dehydration pathway.

In summary, it is apparently possible to adjust the number, strength and even the nature of the active sites that are present in the final catalyst by varying the composition of the LDH-POM material and the activation temperature. This flexibility could provide a convenient means of obtaining a range of catalysts suitable for a variety of applications.

Chapter 6

Concluding Remarks

6.1 Summary of Results

The work carried out during this dissertation has provided additional insight into the physical and chemical properties of polyoxometalate-pillared layered double hydroxide materials. One of the original goals of the project was to develop an optimized synthesis method that is applicable to both acidic and basic LDH layer types; two separate approaches were investigated, which involved numerous syntheses that were carried out using mixed metal salt solutions of various compositions. The effects of several experimental parameters were examined, including: coprecipitation pH, rate of addition of the mixed-metal salt solution, aging period and aging temperature following complete addition, optimal excess of the various reagents to be used, sequence of addition of the reagents, etc. The main criterion for a synthesis attempt to be considered successful was the degree of retention of the initial $M^{2+}:M^{3+}$ ratio from the synthesis solution in the LDH layers, which were the final product. One aspect of this work included the first serious, systematic study of the synthetic requirements, physical characteristics and catalytic

activity of gallium containing layered double hydroxides[48]. Binary Mg/Ga LDH materials containing anions other than carbonate have been reported for the first time.

In Chapter 3, the results of a study of the utility of the organic anion synthesis method[8] for preparing LDH materials containing Mg^{2+}/Al^{3+}, Mg^{2+}/Ga^{3+} or Zn^{2+}/Al^{3+} in the brucite-like layers, and one of the Keggin ions $H_2W_{12}O_{40}^{6-}$ or $PW_{11}O_{39}^{7-}$ in the interlayer region are reported. For each cation pair, an attempt was made to synthesize a series of POM-pillared LDH materials in which the $M^{2+}:M^{3+}$ ratio within the layer was varied between 2:1 and 4:1. An extensive study was conducted in order to compare the structure and composition of the LDH-terephthalate precursors that were formed at various coprecipitation pH values. The samples were precipitated from mixed metal chloride salt solutions in the presence of terephthalate anions, resulting directly in organic anion containing materials in which the aromatic rings were orientated perpendicular to the layers. The properties of the resulting materials containing Mg^{2+} and either Al^{3+} or Ga^{3+} were found to be generally similar, with a few notable exceptions. In each case the initial $M^{2+}:M^{3+}$ ratio in the mixed metal salt solution was retained in the layers only when the synthesis was carried out at pH 10.0. It was further determined that the incorporation of terephthalate anions into the gallery region could occur only in high surface charge density LDH materials (i.e. $M^{2+}:M^{3+} \approx 2:1$). LDH materials in which the layer composition was 3:1 or 4:1 preferentially incorporated the chloride anion of the metal salts. It was suggested that a high layer charge density is necessary to create a continuous hydrophobic layer in which the aromatic rings of the terephthalate anions may exist.

Attempts to prepare LDH-TA precursors containing magnesium at coprecipitation

pH values lower than 10.0 resulted in the incomplete incorporation of Mg^{2+} cations into

the brucite-like layers. $Mg(OH)_2$ becomes appreciably more soluble below pH 10.0, and

therefore it is believed that true coprecipitation conditions did not exist when the

precursors were prepared at pH 8.6, 7.7 or 6.8. It is more likely that $Al(OH)_3$ formed

first, and then reacted with Mg^{2+} cations in solution. ICP-AES analysis indicated that

$Mg^{2+}:M^{3+}$ ratios as low as 0.20:1.00 were observed, which suggests that the dissolution of

Mg^{2+} was virtually complete; in such extreme cases, relatively pure α-GaO(OH)

appeared to have been formed, rather than a layered double hydroxide. More moderate

examples of Mg^{2+} loss were also observed, with $Mg^{2+}:M^{3+}$ ratios in the range 1.0:1.0 to

1.6:1.0 being typical values, which still lie considerably outside the range of values

expected for pure LDH phases, suggesting that another phase might be present.

Complementary experiments, in which the amount of carbon that was present as

terephthalate was determined, allowed an indirect measurement of the $Mg^{2+}:M^{3+}$ content

of the layers alone to be made (i.e. not including any non-layer impurity). It was

determined that in all $Mg^{2+}:M^{3+}$-TA precursors precipitated at pH 7.7 the layer

composition was $Mg^{2+}:M^{3+} = 2:1$, regardless of the initial solution composition, and that

a separate M^{3+}-rich phase was also present. For the Ga^{3+} series the separate phase was

relatively crystalline, and POXRD studies revealed that α-GaO(OH) was the likely

identity of the phase. In contrast, the POXRD patterns obtained for the Al^{3+} analogues

did not contain peaks associated with a similar phase, however, the presence of an Al^{3+}-rich impurity was inferred based on the similarity of the elemental analysis data to that of the Ga^{3+} materials.

POM anion exchange occurred smoothly for both the Mg^{2+}/M^{3+} LDH-TA series, resulting in well-ordered LDH-H_2W_{12} and LDH-PW_{11} materials. Despite the complete replacement of terephthalate anions by POM anions, the resulting products were not considered to be truly pillared materials since micropore size distribution and BET-N_2 surface area measurements indicated that all samples were non-porous. Thus after pretreatment at 125°C the gallery region was inaccessible to molecules at least the size of N_2. It was concluded that the products might still be viable catalysts, but only following high temperature activation, which would decompose the layered structure and provide improved accessibility to the interior active sites.

The organic anion precursor route was also screened for the synthesis of LDH layers known to be stable at lower pH values compared to the Mg^{2+} materials described above. Thus, Zn_RAl-terephthalate, Zn_RAl-benzoate and Zn_RAl-p-hydroxybenzoate precursors were prepared using experimental conditions that were slightly modified from those used to prepare the Mg_RAl- and Mg_RGa-terephthalate analogues. It was found that well ordered Zn_RAl precursors could be formed in which the above three organic anions were incorporated into the LDH structure. Subsequent attempts to exchange the organic anions with POM anions, however, revealed that the Zn_RAl-TA and Zn_RAl-BA precursors were extremely stable, and virtually inert towards anion exchange. The Zn_RAl-p-HyBA

precursor could be made to undergo anion exchange, but only after prolonged reaction times, usually up to several days; however several new reflections appeared in the POXRD pattern, indicating that phases in addition to the desired LDH-POM phase had been formed.

Despite the encouraging results obtained with the organic anion precursor route, it was decided that the physical and chemical properties of the final LDH-POM products could not be sufficiently well controlled to allow a systematic study of the catalytic properties. Therefore, a second synthesis screening study was undertaken in which the LDH-OH/LDH-adipate precursor route was examined. A comprehensive study of each of the precursors formed during the synthesis of $Mg_RAl-H_2W_{12}$ (R = 2, 3, 4) by this method was performed in order to identify any potentially problematic steps in the overall procedure. Chapter 4 provided a summary of the properties of the materials that were obtained using this method.

It was found that for each R value, the desired $Mg^{2+}:Al^{3+}$ ratio was obtained in the initially formed LDH-CO$_3$ precursor, and in fact the ratio appeared to be maintained up to the penultimate product. The lowering of the pH of the reaction mixture that occurred when the POM solution was added, however, resulted in the dissolution of some Mg^{2+} from the LDH layers during the final step of the synthesis. It is significant to note, however, that three $Mg_RAl-H_2W_{12}$ samples were obtained with R values ranging from 1.75 to 3.51, which represents the widest range of layer compositions obtained for POM-pillared LDH materials. In addition, the $Mg_RAl-H_2W_{12}$ products had specific surface

areas ranging from 110 to 140 m^2g^{-1}, and micropore volumes of up to 0.039 mLg^{-1}. The micropore size distribution plots obtained from argon adsorption isotherms indicate that the micropore diameters become smaller as the surface charge density of the LDH increases; variation of pore size with layer composition had not previously been reported. Thus, it was concluded that the products obtained by the LHD-OH/LDH-adipate precursor route were truly pillared materials, and should be suitable samples for use in the catalytic testing stage.

The true measure of the success of the LDH-OH/LDH-adipate precursor method, however, was based on the wide range of materials of different compositions that could be produced with only very minor modifications to the synthesis procedure. Thus Mg_RGa-POM and Zn_RAl-POM (POM = H_2W_{12} or PW_{11}) products were also prepared in order to demonstrate the widely applicable nature of the method. This represents the first time that the method was used to prepare acidic LDHs. Due to imperfect optimization of the synthesis conditions for some of the different layer types, the materials obtained in the Mg/Ga and Mg/Al series were generally characterized by somewhat lower $M^{2+}:M^{3+}$ ratios within the layers than were obtained in the Mg/Al series. Despite the M^{3+} enrichment of the layers, all materials displayed high specific surface areas and appreciable micropore volumes. Thus, the POM-pillared Mg/Al, Mg/Ga and Zn/Al LDH-POM materials prepared using the LDH-OH/LDH-adipate precursor route were used in the work described in Chapter 5 to study the catalytic decomposition of 2-propanol over LDH-POM materials.

The results of the study of the acid-base and catalytic properties of the pillared LDH materials were presented in Chapter 5. These studies include the first study of the catalytic properties of POM-pillared LDH materials containing gallium. The study was divided into two parts, involving activity over LDH-POM materials pretreated at low temperature (200°C) and at high temperature (550°C). After low temperature activation, the catalysts showed activity only for the acid catalyzed pathway, the dehydration of 2-propanol to propene. It was proposed that residual or generated protons associated with the POM pillars provided Brønsted acid sites. The energy of activation values for the dehydration process obtained by carrying out the reaction over a range of temperatures depended on the composition of the pillaring species. Thus it was suggested that the differing magnitude of the negative charge that was present on the terminal oxygen atoms of the two intact Keggin ions resulted in different acid strengths; this implies, of course, that the Keggin structure of the POM was retained after low temperature activation. The unpillared (carbonate containing) LDH materials did not show any activity under the same conditions at a reaction temperature of 200°C, indicating that the activity for dehydration was localized to the pillars and there was no contribution from the LDH layers.

Activation at high temperature, however, resulted (as expected) in significant decomposition of the LDH layer structure accompanied by at least partial decomposition of the Keggin structure of the POM pillars. Thus, it was argued that both types of POM pillar decomposed to form WO_3 crystallites that were supported on the mixed oxide

matrix of the decomposed LDH, resulting in similar types of acid sites being present in all decomposed pillared samples. The major influence affecting activity appears to be the interaction between the decomposed POM anions and the mixed oxide support, and it was found that similar activity was obtained over materials with the same layer composition. Furthermore, the substitution of Zn^{2+} for Mg^{2+} in the mixed metal oxide support had a dramatically larger effect on the dehydration rate than the replacement of Al^{3+} by Ga^{3+}.

Finally, it was also found that the layer composition of the LDH materials activated at 550°C had a large influence on the catalytic properties of the samples. In general, the Zn^{2+} containing catalysts displayed the highest activity for 2-propanol dehydration, whereas the incorporation of Ga^{3+} into the LDH materials introduced only a small amount of dehydrogenation activity. The point was made that ZnO is 35 times more active for dehydrogenation of 2-propanol under the reaction conditions used in the current study than MgO, which agrees well with the data obtained for the series of calcined LDH-POM materials. It was apparent that the strength and number of acid sites could be varied by changing the layer or pillar composition, or by using different activation conditions, suggesting that the LDH-OH/LDH-adipate precursor route offers a great deal of flexibility for synthesizing catalysts with modifiable activity. The results of the catalytic study provide the most comprehensive comparative study to date of the activity of POM-pillared LDH materials in terms of sample composition and activation conditions.

6.2 Future Work

Significantly more effort was required to synthesize layered double hydroxide materials pillared by polyoxometalate anions than was anticipated at the outset of the project. As the difficulties associated with maintaining simultaneous control over the compositional and microtextural properties of the hybrid material became increasingly obvious, it seemed natural to attempt to improve upon the results that had previously been published by other workers. Thus considerable time was dedicated to screening the various synthesis methods and attempting to optimize the conditions to suit a wider range of LDH-POM compositions, resulting in significant improvement for the $Mg_RAl-H_2W_{12}$ series. Further work is required in order to obtain similar compositional control and enhanced microtextural properties for the Mg/Ga and Zn/Al analogues. It would also be desirable to study the conditions that are necessary in order to scale up the size of each synthesis, since difficulties were encountered during larger scale reactions.

Furthermore, additional characterization of the various LDH-POM materials would also help to shed light upon the nature of the surface active sites that are present after activation at low temperature and after activation at high temperature. In particular, adsorption/desorption studies, possibly involving an IR study of the adsorbed species, to properly quantify the number, types and strengths of acid and base sites would be of interest. Additional pore size studies examining the mesopore size range in addition to the micropore size range would increase the understanding of the accessibility to the

interior of the materials. The effects of the microporous structure on the catalytic activity could then be probed more effectively.

Perhaps the greatest limitation to the commercial application of LDH-POM materials to industrially important reactions is the low thermal stability and poor mechanical characteristics of the hybrid materials. It is therefore of paramount importance to develop pillared LDH materials in which the pore structure remains stable following activation at temperatures above 200°C. The POM-pillared LDH materials studied in the current work generally appeared to lose their structural integrity at temperatures between 150 – 180°C. Incorporation of different types of inorganic pillars, possibly involving grafting to the LDH layers, could lead to more thermally stable catalysts. Furthermore, the small mesh size particles used in the catalytic work described in Chapter 5 were easily crushed into a fine powder with limited mechanical abrasion. This friability could make them impractical for use in commercial fixed bed reactors. Thus, alternative methods of forming the catalyst pellets or of otherwise supporting the pillared-LDH materials should also be explored.

Finally, the LDH-POM catalysts prepared using the LDH-OH/LDH-adipate precursor method have been tested only for the catalytic decomposition of 2-propanol. It would be interesting to extend the study to include other catalytic systems, possibly enabling the detection of possible size or shape selective effects. In addition, the POM-pillared materials may be more suitable for reactions with different acid strength requirements, or alternatively the effects of having both acid and base sites present on the

surface could be further explored. Future catalytic work should be carried out after the

additional physical and chemical characterization experiments have been completed, in

order to develop a more focused research plan.

References

1. Mitchell, I.V. (ed.) **Pillared Layered Structures: Current Trends and Applications**, Elsevier, New York, (1990).

2. Brindley, G.W.; Sempels, R.E. *Clay Miner.*, **12**, 229 (1977).

3. Pinnavaia, T.J. *Science*, **220**, 365 (1983).

4. Lagaly, G.; Beneke, K. *Colloid Polym. Sci.*, **269**, 1198 (1991).

5. Szostak, R.; Ingram, C. In **Catalysis by Microporous Materials**, Beyer, H.K.; Karge, H.G..; Kiricsi, I.; Nagy, J.B., eds., **Studies in Surface Science and Catalysis**, **94**, 13 (1995).

6. Clearfield, A.; Roberts, B.D. *Inorg. Chem.*, **27**, 3237 (1988).

7. Dimotakis, E.D.; Pinnavaia, T.J. *Inorg. Chem.*, **29**, 2393 (1990).

8. Drezdzon, M.A. *Inorg. Chem.*, **27**, 4628 (1988).

9. Kwon, T.; Pinnavaia, T.J. *Chem. Mater.*, **1**, 381 (1989).

10. Climent, M.J.; Corma, A.; Iborra, S.; Primo, J. *J. Catal.*, **151**, 60 (1995).

11. Cavani, F.; Trifirò, F.; Vaccari, A. *Catal. Today*, **11**, 173 (1991).

12. Radoslovich, E.W. *Am. Miner.*, **3**, 3 (1963).

13. Taylor, H.F.W. *Miner. Magazine*, **39**, 377 (1973).

14. Allmann, R. *Acta Cryst.*, **B24**, 972 (1968)

15. De Roy, A.; Forano, C.; El Malki, K.; Besse, J.-P. In **Synthesis of Microporous Materials, Anionic Clays: Trends in Pillaring Chemistry**,

16. Bellotto, M.; Rebours, B.; Clause, O.; Lynch, J.; Bazin, D.; Elkaïm, E. *J. Phys. Chem.*, **100**, 8527 (1996).

17. Gherardi, P.; Ruggeri, O.; Trifiro, F.; Vaccari, A. In *Preparation of Catalysts III*; Poncelet, G.; Grange, P.; Jacobs, P.A. eds., Elsevier: Amsterdam, (1983).

18. Nunan, J.G.; Himelfarb, P.B.; Herman, R.G.; Klier, K.; Bogdan, C.E.; Simmons, G.W. *Inorg. Chem.*, **28**, 3868 (1989).

19. Narita, E.; Kaviratna, P.D.; Pinnavaia, T.J. *J. Chem. Soc., Chem. Commun.*, 60 (1993).

20. Hu, C.; He, Q.; Zhang, Y.; Wang, E.; Okuhara, T.; Misono, M. *Catal. Today*, **30**, 141 (1996).

21. Hofmeister, W.; von Platen, H. *Cryst. Rev.*, **3**, 3 (1992).

22. Hernandez-Moreno, M.J.H.; Ulibarri, M.A.; Rendon, J.L.; Serna, C.J. *Phys. Chem. Miner.*, **12**, 34 (1985).

23. Serna, C.J.; White, J.L.; Hem, S.L. *Clays Clay Miner.*, **25**, 384 (1977).

24. Serna, C.J.; Rendon, J.L.; Iglesias, J.E. *Clays Clay Miner.*, **30**, 180 (1982).

25. Malherbe, F.; Forano, C.; Besse, J.-P. *Microporous Materials*, **10**, 67 (1997).

26. Miyata, S. *Clays Clay Miner.*, **31**, 305 (1983).

27. Bish, D.L. *Bull. Minéral.*, **103**, 170 (1980).

28. Reichle, W.T. *Solid State Ionics*, **22**, 135 (1986).

29. Kukkadapu, R.K.; Witkowski, M.S.; Amonette, J.E. *Chem. Mater.*, **9**, 417 (1997).

30. Yun, S.K.; Pinnavaia, T.J. *Inorg. Chem.*, **35**, 6853 (1996).

31. McKenzie, A.L.; Fishel, C.T.; Davis, R.J. *J. Catal.*, **138**, 547 (1992).

32. Fishel, C.T.; Davis, R.J. *Langmuir*, **10**, 159 (1994).

33. Constantino, V.R.L.; Pinnavaia, T.J. *Inorg. Chem.*, **34**, 883 (1995).

34. Kagunya, W.; Hassan, Z.; Jones, W. *Inorg. Chem.*, **35**, 5970 (1996).

35. López-Salinas, E.; García-Sanchez, M.; Llanos-Serrano, M.E.; Navarrete-Bolañoz, J. *J. Phys. Chem. B*, **101**, 5112 (1997).

36. Reichle, W.T. *Chemtech*, 58 (1986).

37. Reichle, W.T.; Kang, S.Y.; Everhardt, D.S. *J. Catal.*, **101**, 352 (1986).

38. Bellotto, M.; Rebours, B.; Clause, O.; Lynch, J.; Bazin, D.; Elkaïm, E. *J. Phys. Chem.*, **100**, 8535 (1996).

39. Reichle, W.T. *J. Catal.*, **94**, 547 (1985).

40. Brindley, G.W.; Kikkawa, S. *Clays Clay Miner.*, **28**, 87 (1980).

41. Corma, A.; Fornés, V.; Rey, F. *J. Catal.*, **148**, 205 (1994).

42. Kohjiya, S.; Sato, T.; Nakayama, T.; Yamashita, S. *Makromol. Chem., Rapid Commun.*, **2**, 231 (1981).

43. Nakatsuka, T.; Kawasaki, H.; Yamashita, S.; Kohjiya, S. *Bull. Chem. Soc. Jap.*, **52**, 2449 (1979).

44. Hibino, T.; Yamashita, Y.; Kosuge, K.; Tsunashima, A. *Clays Clay Miner.*, **43**, 427 (1995).

45. Sato, T.; Wakabayashi, T.; Shimadu, M. *Ind. Eng. Chem. Prod. Res. Dev.*, **25**, 89 (1986).

46. Miyata, S. *Clays Clay Miner.*, **23**, 369 (1975).

47. Kooli, F.; Chisem, I.C.; Vucelic, M.; Jones, W. *Chem. Mater.*, **8**, 1969 (1996).

48. Weir, M.R.; Moore, J.; Kydd, R.A. *Chem. Mater.*, **9**, 1686 (1997).

49. Kooli, F.; Jones, W. *Inorg. Chem.*, **34**, 6237 (1995).

50. Evans, J.; Pillinger, M.; Zhang, J. *J. Chem. Soc., Dalton Trans.*, 2963 (1996).

51. Wang, J.; Tian, Y.; Wang, R.-C.; Colón, J.L.; Clearfield, A. *Mat. Res. Soc. Symp. Proc.*, **233**, 63 (1991).

52. Wang, J.; Tian, Y.; Wang, R.-C.; Clearfield, A. *Chem. Mater.*, **4**, 1276 (1992).

53. Twu, J.; Dutta, P.K. *J. Catal.*, **124**, 503 (1990).

54. Liu, Y.; Hu, C.; Wang, Z.; Jiyu, Z.; Wang, E. *Science in China B*, **39**, 86 (1996).

55. Narita, E.; Kaviratna, P.; Pinnavaia, T.J. *Chem. Lett.*, 805 (1991).

56. Miyata, S.; Kumura, T.; Hattori, H.; Tanabe, K. *J. Chem. Soc. Jpn.*, **92**, 514 (1971).

57. Derouane, E.G.; Jullien-Lardot, V.; Davis, R.J.; Blom, N.; Höjlund-Nielsen, P.E. *Prep. X Inter. Congr. Catal., Budapest*, **B**, 1031 (1993).

58. Asakura, K.; Iwasawa, Y. *Mater. Chem. Phys.*, **18**, 499 (1988).

59. Pope, M.T. "Heteropoly and Isopoly Oxometalates", Springer-Verlag, New York (1983).

60. Signer, R.; Gross, H. *Helv. Chim. Acta*, **17**, 1076 (1934).

61. Illingworth, J.W.; Keggin, J.G. *J. Chem. Soc.*, 575 (1935).

62. Wu, H. *J. Biol. Chem.*, **43**, 189 (1920).

63. Geisinger, K.R.; Batsakis, J.G.; Bauer, R.C. *Am. J. Clin. Path.*, **72**, 330 (1979).

64. Negin, A. *Clin. Chem.*, **15**, 829 (1969).

65. Sharpless, N.E.; Munday, J.S. *Anal. Chem.*, **29**, 1619 (1957).

66. Rocchiccioli-Deltcheff, C.; Thouvenot, R.; Franck, R. *Spectrochimica Acta*, **32A**, 587 (1976).

67. Thouvenot, R.; Fournier, M.; Franck, R.; Rocchiccioli-Deltcheff, C. *Inorg. Chem.*, **23**, 598 (1984).

68. Lyhamn, L.; Pettersson, L. *Chemica Scripta*, **12**, 142 (1977).

69. Kasprzak, M.S.; Crouch, S.R.; Leroi, G.E. *Appl. Spectrosc.*, **32**, 537 (1978).

70. Kasprzak, M.S.; Leroi, G.E.; Crouch, S.R. *Appl. Spectrosc.*, **36**, 285 (1982).

71. Murata, K.; Ikeda, S. *Polyhedron*, **8**, 1681 (1987).

72. Massart, R.; Contant, R.; Fruchart, J.-M.; Ciabrini, J.-P.; Fournier, M. *Inorg. Chem.*, **16**, 2916 (1977).

73. McGarvey, G.B.; Moffat, J.B. *J. Mol. Catal.*, **69**, 137 (1991).

74. Souchay, P. *Talanta*, **12**, 1187 (1965).

75. Smith, D.P.; Pope, M.T. *Inorg. Chem.*, **12**, 331 (1973).

76. Pope, M.T.; Varga, Jr. G.M. *Inorg. Chem.*, **5**, 1249 (1966).

77. Keggin, J.F. *Nature*, **131**, 908 (1933).

78. Keggin, J.F. *Proc. Roy. Soc. A*, **144**, 75 (1934).

79. Tsigdinos, G.A. "Heteropoly Compounds of Molybdenum and Tungsten", Springer-Verlag, New York (1978.

80. Albonetti, S.; Cavani, F.; Trifirò, F.; Gazzano, M.; Koutyrev, M.; Aissi, F.C.; Aboukais, A.; Guelton, M. *J. Catal.*, **146**, 491 (1994).

81. Moffat, J.B.; Kasztelan, S. *J Catal.*, **109**, 206 (1988).

82. West, S.F.; Audrieth, L.F. *J. Phys. Chem.*, **59**, 1069 (1955).

83. Hayashi, H.; Moffat, J.B. *J. Catal.*, **77**, 473 (1982).

84. Mooney, R.W.; Chiola, V.; Hoffman, C.W.W.; Vanderpool, C.D. *J. Electrochem. Soc.*, **109**, 1179 (1962).

85. Mizuno, N.; Misono, M. *J. Mol. Catal.*, **86**, 319 (1994).

86. Mizuno, N.; Misono, M. *Current Opinion in Solid State and Materials Science*, **2**, 84 (1997).

87. Rocchiccioli-Deltcheff, C.; Fournier, M. *J. Chem. Soc. Faraday Trans.*, **87**, 3913 (1991).

88. Bradley, A.J.; Illingsworth, J.W. *Proc. R. Soc. (London)* **A157**, 113 (1936).

89. Moffat, J.B.; McGarvey, G.B.; McMonagle, J.B.; Nayak, V.; Nishi, H. **Zeolitic Heteropoly Oxometalates**, Barthomeuf, D. et al. eds., **Guidelines for Mastering the Properties of Molecular Sieves**, Plenum Press, New York, 193 (1990).

90. Tatsumi, T.; Yamamoto, K.; Tajima, H.; Tominga, H. *Chem. Lett.*, 815 (1992).

91. Yun, S.K.; Constantino, V.R.L.; Pinnavaia, T.J. *Microporous Materials*, **4**, 21 (1995).

92. Kwon, T.; Tsigdinos, G.A.; Pinnavaia, T.J. *J. Am. Chem. Soc.*, **110**, 3653 (1988).
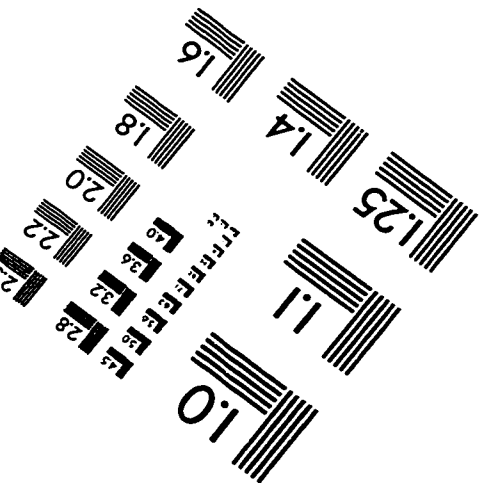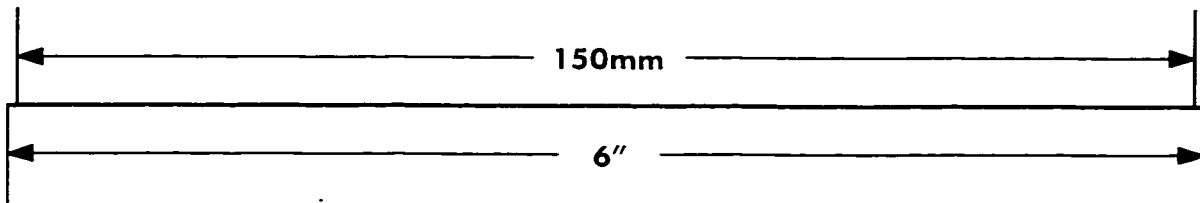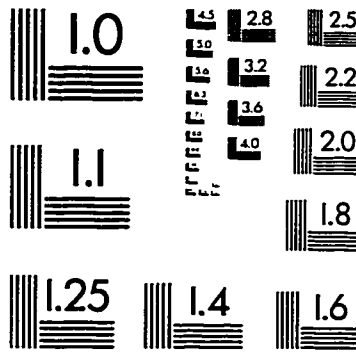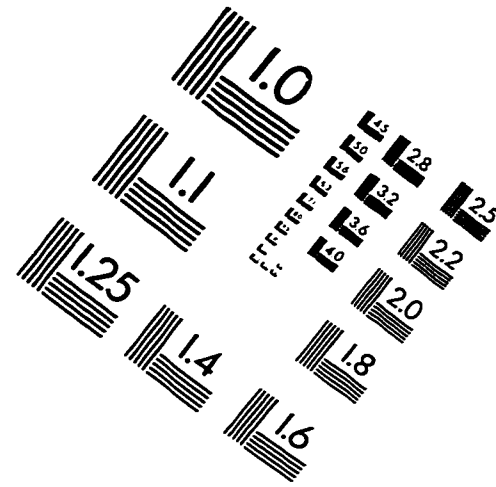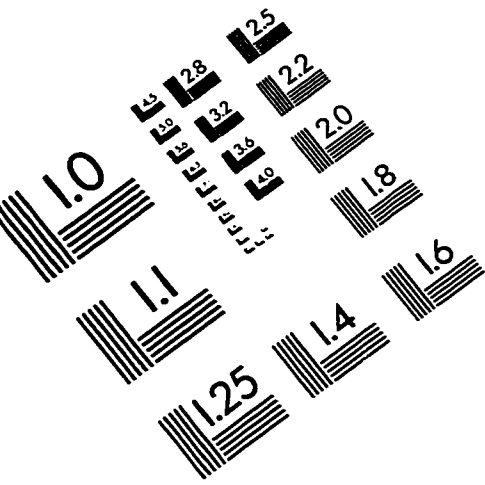
93. Guo, J.; Jiao, Q.Z.; Shen, J.P.; Jiang, D.Z.; Yang, G.H.; Min, E.Z. *Catal. Lett.*, **40**, 43 (1996).

94. Gardner, E.; Pinnavaia, T.J. *Appl. Catal. A: General*, **167**, 65 (1998).

95. López Nieto, J.M.; Dejoz, A.; Vazquez, M.I. *Appl. Chem. A: General*, **132**, 41 (1995).

96. Saito, A.; Foley, H.C. *AIChE Journal*, **37**, 429 (1991).

97. Gervasini, A.; Auroux, A. *J. Catal.*, **131**, 190 (1991).

98. Ai, M., *Bull. Chem. Soc. Jpn.*, **50**, 2579 (1977).

99. Dietz, W.A. *J. of G. C.*, 68 (1967).

100. Woltermann, G.M. U.S. Patent 4454 244 (to Ashland Oil, Inc.), June 12, 1984.

101. Kikkawa, S.; Koizumi, M. *Mater. Res. Bull.*, **17**, 191 (1982).

102. Aramendía, M.A.; Borau, V.; Jiménez, C.; Marinas, J.M.; Romero, F.R.; Ruiz, J.R. *J. Solid State Chem.*, **131**, 78 (1997).

103. Seddon, D. *Catal. Today*, **6**, 351 (1990).

104. Bellaloui, A.; Plee, D.; Meriaudequ, P. *Appl. Catal.*, **63**, L7 (1990).

105. Moore, D.M.; Reynolds, R.C. "X-Ray Diffraction and the Identification and Analysis of Clay Minerals", Oxford University Press (1989).

106. Gastuche, M.C.; Brown, G.; Mortland, M. *Clay Minerals*, **7**, 177 (1967).

107. Brindley, G.W.; Kikkawa, S. *Am. Miner.*, **64**, 836 (1979).

108. Drits, A.; Sokolovaa, T.N.; Sokolova, G.V.; Cherkashin, V.I. *Clays Clay Miner.*, **35**, 401 (1987).

109. Bradley, S. Ph.D. Thesis, University of Calgary, Canada, 1992.

110. Labajos, F.M.; Rives, V.; Ulibarri, M.A. *J. Mater. Sci.*, **27**, 1546 (1992).

111. Joint Committee for Powder Diffraction Standards (JCPDS) file number 6-180.

112. Foster, L.M.; Stumpf, H.C. *J. Am. Chem. Soc.*, **73**, 1590 (1951).

113. Roy, R.; Hill, V.G.; Osborn, E.F. *J. Am. Chem. Soc.*, **74**, 719 (1952).

114. Frondel, C. *Am. Mineral.*, **26**, 295 (1941).

115. Allmann, R.; Jepsen, H.P. *Neues Jahrb. Mineral. Monatsh.*, **11**, 544 (1969).

116. Brunauer, S.; Deming, L.S.; Deming, W.S.; Teller, E. *J. Am. Chem. Soc.*, **62**, 1723 (1940).

117. Sato, T.; Kato, K.; Endo, T.; Shimada, M. *React. Solids*, **2**, 253 (1986).

118. Sato, T.; Fujita, H.; Endo, T.; Shimada, M. *React. Solids*, **5**, 219 (1988).

119. Joint Committee for Powder Diffraction Standards (JCPDS) file number 30-0794.

120. Velu, S.; Ramkumar, V.; Narayanan, A.; Swamy, C.S. *J. Mater. Sci.*, **32**, 957 (1997).

121. Joint Committee for Powder Diffraction Standards (JCPDS) file number 36-1451.

122. Kooli, F.; Depege, C.; Ennaqadi, A.; deRoy, A.; Besse, J.P. *Clays Clay Miner.*, **45**, 92 (1997).

123. Ai, M. *J. Catal.*, **40**, 318 (1975).

124. Ai, M. *J. Catal.*, **40**, 327 (1975).

125. Ai, M. *Bull. Chem. Soc. Jpn.*, **49**, 1328 (1976).

126. Ai, M.; Suzuki, S. *Bull. Chem. Soc. Jpn.*, **47**, 3074 (1974).

127. Ai, M.; Suzuki, S. *Bull. Chem. Soc. Jpn.*, **46**, 1208 (1973).

128. Ai, M.; Suzuki, S. *J. Catal.*, **30**, 362 (1973).

129. Ai, M.; Ikawa, T. *J. Catal.*, **40**, 203 (1975).

130. Kelkar, C.P.; Schutz, A.; Marcelin, G. *in* "Perspectives in Molecular Sieve Science" (Flank, W.H.; Whyte, T.E. Eds.) ACS Symp. Series, **368**, Washington D.C. p. 324 (1988).

131. Drezdzon, M.A. *in* "Novel Materials in Heterogeneous Catalysis" (Baker, R.T.K.; Murrel, L.L. eds.) ACS Symp. Series, **437**, Washington D.C. p.140 (1990).

132. Okuhara, T.; Kasai, A.; Hayakawa, N.; Misono, M.; Yoneda, Y. *Chem. Lett.*, 391 (1981).

133. McMonagle, J.B.; Moffat, J.B. *J. Catal.*, **91**, 132 (1985).

134. Hayashi, H.; Moffat, J.B. *J. Catal.*, **81**, 61 (1983).

135. Highfield, J.G.; Moffat, J.B. *J. Catal.*, **88**, 177 (1984).

136. Highfield, J.G.; Moffat, J.B. *J. Catal.*, **89**, 185 (1984).

137. Baba, T.; Watanabe, H.; Ono, Y. *J. Phys. Chem.*, **87**, 2406 (1983).

138. Akimoto, M.; Tsuchida, Y.; Sato, K.; Echigoya, E. *J. Catal.*, **72**, 83 (1981).

139. Koga, O.; Onishi, T.; Tamaru, K. *J. Chem. Soc., Faraday Trans 1*, **76**, 19 (1980).

IMAGE EVALUATION
TEST TARGET (QA-3)

1.0

1.1

1.25

1.4

1.6

1.8

2.0

2.2

2.5

2.8

3.2

3.6

4.0

150mm

6"